

# Characteristics and Mobility of Zero-Valent Nano-Iron in Porous Media

a Laboratory Assessment Study

Cjestmir de Boer

*cjestmir.deboer@cjestmir.com*

University of Utrecht

Faculty of Geosciences, Department of Earth Sciences

Environmental Hydrogeology Group

*Supervisor: Dr. Ruud Schotting, schotting@geo.uu.nl*

Research Performed at: Universität Stuttgart

Institute of Hydraulic Engineering

Research Facility for Subsurface Remediation (VEGAS)

*Supervisors: Dr.-Ing. Norbert Klaas, norbert.klaas@iws.uni-stuttgart.de*

*Juergen Braun, PhD, juergen.braun@iws.uni-stuttgart.de*

September 26, 2007

# CONTENTS

1. <i>Introduction</i> . . . . .	1
1.1 Background . . . . .	1
1.2 Current Remediation Methods . . . . .	1
1.3 Zero-Valent Iron for In-Situ Remediation . . . . .	3
1.4 Previous Research on Zero-Valent Nano-Iron . . . . .	5
1.5 Determination of Nano-Iron Injection Extend . . . . .	6
1.6 Project Goals and Strategy . . . . .	7
1.7 About this Thesis . . . . .	8
2. <i>Preliminary Research</i> . . . . .	9
2.1 Introduction . . . . .	9
2.2 2-D Experiments: Numerical Simulations . . . . .	9
2.2.1 Methods . . . . .	9
2.2.2 Results & Discussion . . . . .	10
2.3 2-D Experiments: Physical Model, Reproduction of 2003 experiment with new colloids . . . . .	11
2.3.1 Methods . . . . .	11
2.3.2 Results & Discussion . . . . .	13
2.4 Settlement/Attachment experiment . . . . .	15
2.4.1 Methods . . . . .	15
2.4.2 Results & Discussion . . . . .	16
2.5 Drag velocity . . . . .	17
2.5.1 Methods . . . . .	17
2.5.2 Results & Discussion . . . . .	18
2.6 Testing the Iron Determination with the ICP-OES . . . . .	21
2.6.1 Methods . . . . .	21
2.6.2 Results & Discussion . . . . .	21
2.7 In-Situ Determination of Iron Occurrence . . . . .	23
2.7.1 Methods - Hobby Metal Detector . . . . .	23
2.7.2 Methods - Commercially Available Metal Detector . . . . .	24
2.8 Conductance measurement of the Nano-Iron . . . . .	25
2.8.1 Methods . . . . .	25
2.8.2 Results & Discussion . . . . .	25
2.9 Stirred vs. Disperged and Stirred Nano-Iron Suspensions . . . . .	26
2.9.1 Transport in a Horizontal Capillary Tube . . . . .	27

---

2.9.2	Transport in a Horizontal Column . . . . .	28
2.9.3	Sedimentation Rate . . . . .	31
2.9.4	Reactivity . . . . .	33
2.10	Summary . . . . .	36
3.	<i>1-D Transport Experiments</i> . . . . .	37
3.1	Introduction . . . . .	37
3.2	Methods . . . . .	38
3.2.1	Setup . . . . .	38
3.2.2	Initial and Boundary Conditions . . . . .	41
3.2.3	(A) Nano-iron Suspension Concentration - Dorsilit Sand . . . . .	43
3.2.4	(B) Pore Velocity - Dorsilit Sand . . . . .	43
3.2.5	(C) Pore Velocity - Rhine-Valley Sand . . . . .	43
3.2.6	(D) Grain Size Distribution / Hydraulic Conductivity - Different Sand Types . . . . .	44
3.2.7	Nano-Iron Detection . . . . .	44
3.2.8	Signal Analysis . . . . .	44
3.2.9	Calibration . . . . .	45
3.3	Results & Discussion . . . . .	46
3.3.1	Signal Analysis . . . . .	46
3.3.2	Calibration . . . . .	46
3.3.3	About the Metal Detector . . . . .	47
3.3.4	Conditions used for the 1-D flow experiments . . . . .	49
3.3.5	Characteristics of 1-D flow experiments . . . . .	49
3.3.6	Measurement Results Overview . . . . .	51
3.3.7	(A) Nano-iron Suspension Concentration - Dorsilit Sand . . . . .	52
3.3.8	(B) Pore Velocity - Dorsilit Sand . . . . .	56
3.3.9	(C) Pore Velocity - Rhine-Valley Sand . . . . .	60
3.3.10	(D) Grain Size Distribution / Hydraulic Conductivity - Different Sand Types . . . . .	63
3.3.11	Homogeneous Packing . . . . .	65
3.3.12	Retardation . . . . .	65
3.4	Summary . . . . .	68
4.	<i>Discussion</i> . . . . .	69
4.1	2-D Experiments . . . . .	69
4.2	Small Scale Experiments . . . . .	70
4.2.1	Minimum Velocity and Drag Force . . . . .	70
4.2.2	Chemical Detection of Nano-Iron . . . . .	71
4.2.3	Disperged Nano-Iron . . . . .	71
4.3	The use of a Metal Detector for Nano-Iron detection . . . . .	72
4.4	Column Experiments . . . . .	73
4.4.1	Pump Location . . . . .	74

4.4.2	Theory and Practice . . . . .	74
4.4.3	Base-Case . . . . .	75
4.4.4	Influence of Injection Concentration - About the Results . . . . .	75
4.4.5	Stages of Movement - About the Results . . . . .	75
4.4.6	Influence of Pore Velocity - About the Results . . . . .	75
4.5	Obstacle for Further Research? . . . . .	76
5.	<i>Conclusions</i> . . . . .	77
6.	<i>Outlook</i> . . . . .	79
7.	<i>Acknowledgements</i> . . . . .	82
	 <i>Appendix</i>	 86
A.	<i>Comments on 1-D Transport Experiments</i> . . . . .	87
A.1	(A) Nano-iron Suspension Concentration - Dorsilit Sand . . . . .	87
A.2	(B) Pore Velocity - Dorsilit Sand . . . . .	89
A.3	(C) Pore Velocity - Rhine-Valley Sand . . . . .	91
A.4	(D) Grain Size Distribution / Hydraulic Conductivity - Different Sand Types . . . . .	93
B.	<i>Extra Figures</i> . . . . .	96
B.1	Continued Injection of Experiment # 2 . . . . .	96
B.2	Continued Injection of Experiment # 4 . . . . .	97
B.3	Experiments with Errors - B # 8 & C # 12 . . . . .	98
B.4	Experiments with Errors - D #'s 14, 15 & 16 . . . . .	100
C.	<i>Signal Processing Code</i> . . . . .	101

## LIST OF FIGURES

1.1	A Permeable Reactive Barrier . . . . .	2
1.2	Schematic in-situ reactive barrier . . . . .	6
2.1	Setup of the 2D numerical simulations . . . . .	10
2.2	Flow paths simulated with PMPATH . . . . .	12
2.3	Injection, extraction with dye tracer test . . . . .	12
2.4	Schematic presentation of several injection and extraction wells on a line . . . . .	13
2.5	Setup of the 2D experiments . . . . .	14
2.6	Settling experiment . . . . .	16
2.7	Effluent filtration . . . . .	17
2.8	Setup to test at which velocity nano-iron settles and is being re-mobilized . . . . .	19
2.9	Forces that act on a particle deposited on the surface of a pore . . . . .	20
2.10	Transport of nano-iron in a glass tube, using a peristaltic pump . . . . .	21
2.11	Transport of nano-iron in a glass tube, using a syringe pump . . . . .	21
2.12	Zeta potential of RNIP . . . . .	22
2.13	Transport of nano-iron in a glass tube, dispersed and non-dispersed . . . . .	28
2.14	Laminar velocity profile in a pipe . . . . .	29
2.15	Disperger setup . . . . .	29
2.16	Schematic disperser setup . . . . .	30
2.17	Rotor and Stator of the disperger . . . . .	30
2.18	Transport of dispersed nano-iron in a horizontal column . . . . .	31
2.19	Concentration change due to sedimentation of the nano-iron . . . . .	34
2.20	Decrease in sedimentation bedding height with time . . . . .	34
2.21	Change of Concentration of PCE during the batch experiment . . . . .	35
2.22	Chemical analyse of the batch experiment after 48 hours . . . . .	35
3.1	Inlet-Outlet column plugs . . . . .	40
3.2	Sand-packing mouthpiece . . . . .	40
3.3	Setup overview of the 1-D experiments . . . . .	40
3.4	Calibration setup of the metal detector and the recorded frequency response . . . . .	47
3.5	Calibration curve of the metal detector . . . . .	48
3.6	Nano-iron content distribution in the column . . . . .	50
3.7	Nano-iron content distribution in the column . . . . .	53
3.8	Transport distance characteristics. Explanation is given in section 3.3.5 . . . . .	53
3.9	Relative transport distance characteristics. Explanation is given in section 3.3.5 . . . . .	53

---

3.10 Nano-iron content per 1 mm of column length for different flow velocities in Dorsilit 1/8 sand . . . . .	57
3.11 Transport distance characteristics. Explanation is given in section 3.3.5 . . . . .	57
3.12 Relative transport distance characteristics. Explanation is given in section 3.3.5 . . . . .	57
3.13 Nano-iron content per 1 mm of column length for different pore velocities in Rhine-Valley sand . . . . .	61
3.14 Transport distance characteristics. Explanation is given in section 3.3.5 . . . . .	61
3.15 Relative transport distance characteristics. Explanation is given in section 3.3.5 . . . . .	61
3.16 Nano-iron content per 1 mm of column length for sand types with different K-values . . . . .	64
3.17 Transport distance characteristics . . . . .	64
3.18 Relative transport distance for sand types with different K-values . . . . .	64
3.19 Heterogeneities in a column . . . . .	66
3.20 Preferential flow paths in a column . . . . .	66
B.1 0.1 g/l injection continued for an extra 464 min after 240 min . . . . .	96
B.2 10 g/l injection continued for 290 min . . . . .	97
B.3 Nano-iron content per 1 mm of column length for different velocities in Rhine-Valley sand, experiments with errors . . . . .	99
B.4 Nano-iron content per 1 mm of column length for sand types with different K-values, experiments with errors . . . . .	100
B.5 Transport distance characteristics . . . . .	100
B.6 Relative transport distance for sand types with different K-values . . . . .	100

## LIST OF TABLES

1.1	Pollutants that can be remediated by zero-valent nano-iron . . . . .	3
1.2	Specific surface of three types of zero-valent iron . . . . .	3
2.1	Boundary and Initial conditions for the 2D simulations . . . . .	11
2.2	Transport in a glass tube . . . . .	19
2.3	ICP results of iron determination . . . . .	22
2.4	Conductivity Measurements . . . . .	26
3.1	Comparison Table . . . . .	43
3.2	Conditions used for the concentration dependent 1-D flow experiments . . . . .	52
3.3	Characteristics of concentration dependent 1-D flow experiments . . . . .	52
3.4	Overview of the total injected mass and the measured total mass of nano-iron . . . . .	52
3.5	Conditions of the 1-D flow experiments in Dorsilit 1/8 sand, with different pore velocities	56
3.6	Characteristics of 1-D flow experiments in Dorsilit 1/8 sand with different pore velocities	56
3.7	Overview of the total injected mass and the measured total mass of nano-iron . . . . .	56
3.8	Conditions used for the 1-D flow experiments in Rhine-Valley sand with different pore velocities . . . . .	60
3.9	Characteristic of 1-D flow experiments in Rhine-Valley sand with different pore velocities. († present exp. where an unknown part of iron left the system through the outlet). Explanation is given in section 3.3.5 . . . . .	60
3.10	Overview of the total injected mass and the measured total mass of nano-iron . . . . .	60
3.11	Conditions used in the 1-D flow experiments for dependencies on the grain size and grain distribution . . . . .	63
3.12	Characteristics of sand dependent 1-D flow experiments . . . . .	63
3.13	Overview of the total injected mass and the measured total mass of nano-iron . . . . .	63

## ABSTRACT

Aquifers contaminated with chlorinated solvents promises to be very effectively remediated with reactive nano-iron. The large specific surface of nano-iron results in extremely fast reaction rates. Due to the small size, the particles are thought of to be able to be injected into the aquifer and reach the contaminants through simple injection wells. So far, very little is known about the exact transport capacity of nano-iron. In the literature the claims toward this differ greatly.

In this research project, systematic experiments were conducted to get a better understanding of the mobility and characteristics of nano-iron. It was shown that the transport distance of nano-iron particles was affected by the age (and with that the aggregation stage) of the particles, by the discharge and the concentration of the suspension during injection, by the grain size distribution, as well as the permeability and heterogeneity of the porous media. There was no significant change in the retardation of nano-iron at different velocities. Apart from the experiments, a technology to accurately and non-destructively measure the concentration distribution of nano-iron in a column was developed.

## **Nederlandse Samenvatting**

De sanering van gechlloreerde koolwaterstof verontreinigingen in watervoerende lagen met reactief nano-ijzer, belooft een snelle en effectieve afbraak. Door het grote specifieke oppervlak van de nano-ijzer deeltjes ontstaat een grote reactiviteit. De veronderstelling is, dat de deeltjes eenvoudig en voordelig in de ondergrond geïnjecteerd kunnen worden, waardoor het eenvoudig bij de verontreiniging gebracht kan worden. Tot nu toe is echter zeer weinig bekend over de exacte transport eigenschappen, en wordt onderling in de literatuur een groot verschil in uitbreiding beschreven.

In dit onderzoek zijn systematische experimenten uitgevoerd om meer over de transport eigenschappen van nano-ijzer te weten te komen. Aan de hand van batch, 1-D en 2-D experimenten kon aangetoond worden dat de transport afstand van nano-ijzer in suspensie beïnvloed werden door de ouderdom (en daarmee het aggregatieniveau van de deeltjes), de volume stroom en de concentratie van de suspensie tijdens de injectie, de korrel grootte verdeling en de heterogeniteit in het poreuze medium. Er was geen significant verschil in de retardatie van nano-ijzer te zien bij een verhoging van de stroomsnelheid. Daarnaast was een meetmethode ontwikkeld om de verdeling van nano-ijzer in een zuil-experiment nauwkeurig en destructie vrij te bepalen.

### **Deutsche Kurzfassung**

Die Sanierung von CKW-Schadenfällen mittels Nanoeiseninjectionen verspricht schnelle Abbauraten auf Grund der großen spezifischen Oberfläche sowie eine kostengünstige Anwendung, da die Eisenpartikel in Form einer Suspension gezielt in den kontaminierten Aquifer eingebracht werden können. Über die Transporteigenschaften von Nanoeisen in porösen Medien, insbesondere bei der Injektion einer Nanoeisen-Suspension, ist bisher wenig bekannt.

Im vorliegenden Forschungsvorhaben wurden systematische Versuche zur Ausbreitung, verbunden mit der Entwicklung einer entsprechenden Messtechnik, durchgeführt. Es konnte nachgewiesen werden, dass die Transportentfernung von Nanopartikeln im Untergrund vom Alter und damit dem Aggregationsgrad der Suspension, der Injektionsgeschwindigkeit und -konzentration, der Korngrößenverteilung, der Durchlässigkeit sowie der Heterogenität des Aquifers abhängt. Es wurde gezeigt, dass bei einer Änderung der Fließgeschwindigkeit kein signifikanter Unterschied in Retardierung stattfindet. Weiterhin wurde ein Messverfahren zur zerstörungsfreien Bestimmung der Ausbreitung des Nanoeisens in einer Säule entwickelt.

# 1. INTRODUCTION

## *1.1 Background*

For a long time the danger of pollution in the subsurface has been unknown or ignored. Since the pollution is located under the surface, it is invisible and can stay unnoticed for a long time. The presence of flowing groundwater in the subsurface result in spreading of the pollution. In this way the pollution can also reach drinking water wells and be a threat for human health. The awareness of the dangers of contaminated sites and the resulting contamination in groundwater has been increasing for the last 15 years. The number of sites that need to be treated is rising to large amounts. For example, only in Germany 350 000 sites are potentially contaminated and are a danger for the environment and the groundwater [Hahn, 2006]. Of these sites 35% are contaminated with chlorinated hydrocarbons (CHC's). CHC's were used in many industrial areas, where it was mainly used for degreasing metal. It was also applied in many dry-cleaning facilities, which are often situated in urban areas.

## *1.2 Current Remediation Methods*

At present, many different types of remediation techniques exist. For near surface pollution sites often excavation, also called ex-situ remediation techniques, are the most effective. This technique is rather expensive and ecologically ineffective due to the high energy consumption for excavation, transport and off-site treatment. Furthermore this technique is rather unsuitable for residential areas and saturated aquifers. Fetter [1999]

In that case a pump-and-treat remediation might work. With pump-and-treat the groundwater together with the contaminant is pumped out of the ground and remediated at the surface. With this technique it often takes many years or even decades to remediate a site. Fetter [1999]

If the contaminants are mainly located in the unsaturated zone as a residual contaminant or in gas phase, they can be removed by applying Soil Vapor Extraction (SVE). With SVE the air in the soil is extracted by applying a vacuum on a well. This way air from outside the contaminated area is attracted and lead through the contaminated soil. The residual contaminants can be mainly evaporated, then the air cleaned above ground (e.g. with activated carbon). [Fetter, 1999]

New remediation methods are still being developed and older techniques are combined to get better results. A recent and good working method is Vacuum-Enhanced Recovery (VER) [Solc, 2006]. With this method the soil vapor and the groundwater are being pumped out of a well by creating a vacuum above the water table and pumping the water below the water table inside the well. With this technique the free (pure), dissolved and gas phase products are extracted. This is suitable for sites where residual and free phase contaminants exists. Which is often the case when a light non-aqueous phase liquid

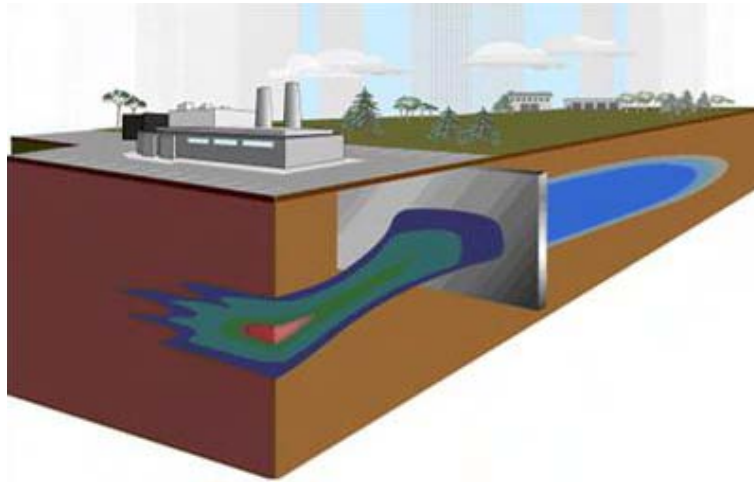


Fig. 1.1: A Permeable Reactive Barrier (from: Environmental Technologies)

(LNAPL, with a density less than that of water) is present in the unsaturated to saturated transition zone.

At the surface the pumped mixture is separated on site. For small polluted sites this technique is often suitable and will be able to clean the site in one to three years to the regulatory or environmentally acceptable risk-based limits. It is more effective than the traditional Pump and Treat or SVE methods alone, and will take less time. [Solc, 2006]

Often when a contaminated site is older, most of the pollution will no longer be in the source zone as a free phase, but as a residual phase. Fluctuations in the groundwater table can smear a LNAPL over a large area as a residual phase in the unsaturated zone.

Dense non-aqueous phase liquids (DNAPL) are another type of contaminants, which have a larger density than water and will sink to lower levels in the aquifer until a less permeable area holds it from moving further. The contaminant (either LNAPL or DNAPL) dissolves in passing groundwater, a plume of contaminated groundwater is then created. This polluted groundwater plume is a lot larger than the original source zone. Gillham and O'Hannesin [1992] developed a system called the permeable reactive barrier (PRB). These barriers are slugs in the soil where sand is mixed with reactive material (the exact chemical substance differs for each pollution origin). The mixed material is still permeable for passing groundwater (see fig. 1.1). When the polluted groundwater flows through a PRB, the chemicals react with the pollutants and will transform them into environmental benign products [Gillham and O'Hannesin, 1992].

One of the materials often used in these PRB's is zero-valent iron (also denoted as 'elementary iron' or ' $Fe^0$ '). Zero-valent iron is able to remediate plumes polluted with several pollutants (table 1.1). Common pollutants in plumes are the chlorinated hydrocarbons (CHC's). Most of these can be degraded by zero-valent iron. Zero-valent iron is applied in PRB's as granular or micro scale particles.

Tab. 1.1: Pollutants that can be remediated by zero-valent nano-iron [Zhang, 2003, Müller et al., 2006a]

<i>Chlorinated methanes</i>	<i>Chlorinated benzenes</i>	<i>Pesticides</i>
Carbon tetrachloride ( $CCl_4$ )	Hexachlorobenzene ( $C_6Cl_6$ )	DDT ( $C_{14}H_9Cl_5$ )
Chloroform ( $CHCl_3$ )	Pentachlorobenzene ( $C_6HCl_5$ )	Lindane ( $C_6H_6Cl_6$ )
Dichloromethane ( $CH_2Cl_2$ )	Tetrachlorobenzenes ( $C_6H_2Cl_4$ )	Organic dyes
Chloromethane ( $CH_3Cl$ )	Trichlorobenzenes ( $C_6H_3Cl_3$ )	Orange II ( $C_{16}H_{11}N_2NaO_4S$ )
	Dichlorobenzenes ( $C_6H_4Cl_2$ )	Chrysoidine ( $C_{12}H_{13}ClN_4$ )
	Chlorobenzene ( $C_6H_5Cl$ )	Tropaeolin O ( $C_{12}H_9N_2NaO_5S$ )
		Acid Orange
		Acid Red
<i>Heavy metal ions</i>	<i>Trihalomethanes</i>	<i>Chlorinated ethenes</i>
Mercury ( $Hg^{2+}$ )	Bromoform ( $CHBr_3$ )	Tetrachloroethene ( $C_2Cl_4$ )
Nickel ( $Ni^{2+}$ )	Dibromochloromethane ( $CHBr_2Cl$ )	Trichloroethene ( $C_2HCl_3$ )
Silver ( $Ag^+$ )	Dichlorobromomethane ( $CHBrCl_2$ )	cis-Dichloroethene ( $C_2H_2Cl_2$ )
Cadmium ( $Cd^{2+}$ )		trans-Dichloroethene ( $C_2H_2Cl_2$ )
Cobalt ( $Co^{2+}$ )		1,1-Dichloroethene ( $C_2H_2Cl_2$ )
Tin ( $Sn^{2+}$ )		Vinyl chloride ( $C_2H_3Cl$ )
Lead ( $Pb^{2+}$ )		
Copper ( $Cu^{2+}$ )		
<i>Polychlorinated hydrocarbons</i>	<i>Other organic contaminants</i>	<i>Inorganic anions</i>
PCB's	N-nitrosodimethylamine (NDMA)	Dichromate ( $Cr_2O_7^{2-}$ )
Dioxins	( $C_4H_{10}N_2O$ )	Arsenic ( $AsO_4^{3-}$ )
Pentachlorophenol ( $C_6HCl_5O$ )	TNT ( $C_7H_5N_3O_6$ )	Perchlorate ( $ClO_4^-$ )
		Nitrate ( $NO_3^-$ )

Tab. 1.2: Specific surface of three types of zero-valent iron

	Nano-iron <sup>a</sup>	Micro-iron <sup>b</sup>	Granular-iron <sup>c</sup>
Particle diameter (nm)	10 - 100	150 000	500 000
Specific surface (m <sup>2</sup> /g)	30	0.1 - 1	0.04

<sup>a</sup>Nurmi et al. [2005]<sup>b</sup>Nurmi et al. [2005]<sup>c</sup>Huang et al. [2003]

### 1.3 Zero-Valent Iron for In-Situ Remediation

As an alternative for the classic permeable reactive barriers an in-situ method is developed by the injection of zero-valent iron into an aquifer [Cantrell and Kaplan, 1997]. Cantrell and Kaplan [1997] used iron of micrometer scale in diameter. These particles were rather heavy and gravitational settling occurred during injection, limiting the transport. At present it is possible to create particles of nanometers. Some of the commercial available zero-valent nano-iron particles are between 10 and 100 nm in diameter (e.g. RNIP, Toda Kogyo). The zero-valent nano-iron (further called *nano-iron*) can be suspended in water or an other delivery fluid (see for other delivery fluids e.g. Schrick et al. [2004], Quinn et al. [2005]). The particles are small enough to be transported through the finer pore spaces of the porous media [Elliott and Zhang, 2001]. Common aquifer pore diameters vary approximately from 100.000 nm for a gravel aquifer to 200 nm in a silty aquifer. Nano-sized particles can enter those pores where micro sized

particles can not. Due to the small size, the chance of clogging the aquifer is reduced. The particles will have a lower settling velocity due to their small size (eqn. 2.2), which should make it possible to get them further transported. Though, Tratnyek and Johnson [2006] describes that still the transport distance in an aquifer is expected to be limited.

Nano-sized particles further have the big advantage of a large specific surface. The specific surface increases with a reducing diameter (see table 1.2), simultaneously the reactivity of the zero-valent iron particles increases. The reactivity is mainly controlled by the specific surface of the particle.

Because of these advantages of nano-iron, this technology is preferable above micro- and granular-iron technology.

In theory the use of nano-iron looks promising. Still in practice there appears to be some difficulties. The delivery of the particles to the desired location often was unsuccessful or disputable [Schrick et al., 2004] or the transported distance was very small which resulted in a narrow grid of boreholes needed for the injection (e.g. Müller et al. [2006b]). In several cases the used nano-iron suspension was chemically instable and lost most of the reactivity before it was injected. Possibly this is due to oxidation of the particles or chemical reactions with elements in the applied water for suspending the nano-iron (reducing the reactivity).

The nano-iron can react with dissolved oxygen as given in equation 1.1 as well to some extent with water itself as given in equation 1.2. Because of this the nano-iron particles developed for remediation techniques are now produced with a thin layer that shields the zero-valent iron from direct contact with water. The particles developed by Wang and Zhang [1997] are produced with a palladium acetate ( $[Pd](C_2H_3O_2)_2$ )<sub>3</sub> that reacts with a small outer part of the zero-valent iron particle and creates a small shield (see equation 1.4). Other materials used by other researchers to shield the particles are for example platinum ( $Fe/Pt$ ), silver ( $Fe/Ag$ ), nickel ( $Fe/Ni$ ), cobalt ( $Fe/Co$ ), copper ( $Fe/Cu$ ), and the particles of Toda Kogyo are shielded with crystalline magnetite ( $Fe_3O_4$ ) ( $Fe/Fe$ ) [Wang and Zhang, 1997].

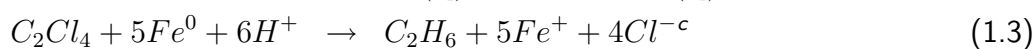
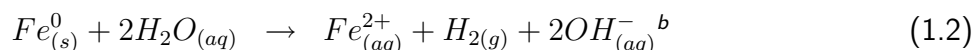
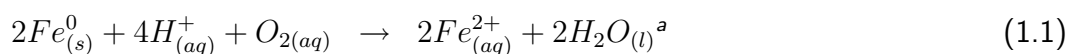
The chemical reaction that takes place between a CHC like tetrachloroethene (PCE,  $C_2Cl_4$ ) and zero-valent iron follows a reduction reaction into ethene given by equation 1.3. If insufficient zero-valent iron is available, the chemical abiotic reduction of the CHC's (e.g. TCE) might not be complete. The reduction can follow several pathways of  $\beta$ -elimination [Liu et al., 2005]:

$TCE \rightarrow chloracetylene \rightarrow acetylene \rightarrow ethene$ ;

$TCE \rightarrow cis-1,2-DCE \rightarrow acetylene \rightarrow ethene$  or

$TCE \rightarrow cis-1,2-DCE \rightarrow VC \rightarrow ethene$ .

Ethene can at the end also be changed into *ethane*. The end product though can also be *cis-1,2-DCE* or *VC* which are poisonous. Thus if the reduction was incomplete one CHC has only been changed into an other CHC.




---

<sup>a</sup>Zhang [2003]

<sup>b</sup>Bartzas et al. [2006]

<sup>c</sup>Lien and Zhang [2001]

<sup>d</sup>Lien and Zhang [2001]

The particles tend to aggregate and adhere to soil particles. One of the mechanisms responsible for this is the electrical force between particles, which can be described by the zeta-potential. The electrically charged cloud around the nano-iron particles results in a strong attraction to negatively charged soil particles. During infiltration in the soil, the zeta-potential of the suspension can be adjusted by changing the pH of the suspension to decrease this effect. The particle also tend to aggregate due to magnetic forces between the particles. Especially the uncoated and unshielded particles suffer from this. The aggregation and gelation (building of a network of aggregates) can result in pore plugging, gravity settling and thus reduced transportability [Saleh et al., 2006].

#### 1.4 Previous Research on Zero-Valent Nano-Iron

In 2003 the first experiments with nano-iron where performed at the VEGAS institute by Eugen Ruzin from Forschungszentrum Karlsruhe (FZK) [Ruzin, 2003]. These experiments showed that the nano-iron at moment developed by the FZK was too reactive, instable and highly immobile.

Several other research institutes have been working on the use of reactive iron in remediation techniques. Two of these are: Wei-Xian Zhang and co-workers at Lehigh University, Bethlehem, USA; Dahmke and co-workers at Christian-Albrechts-Universität, Kiel, Germany Several pilot field tests with nano-iron have been performed in cooperation with these institutes.

In a field test in North Carolina the nano-iron produced at Lehigh University (as described in the article of Wang and Zhang [1997] nano-iron with a palladium outer shield) is used to remediate a mixture of CHC's (mainly TCE, PCE and DCE). Since zero-valent iron can be used to remediate each of the contaminants found, it was thought of to be a suitable remediation technique. In this field test most of the contaminants in the source zone had been removed by excavation. Contaminants still occurred with an average concentration of 14 000  $\mu g/l$  in the groundwater, indicating that the remediation was not complete. The nano-iron was mixed with potable water to a concentration of 1.9  $g Fe^0/l$  and injected in the contaminated zone. Within the first few weeks, about 90% of the contamination was reduced to environmental benign ethanes and ethenes (as described by Glazier et al. [2003], Zhang [2003]).

At the Naval Air Station in Jacksonville [Gavaskar et al., 2005], nano-iron has been used in a pilot test to remediate the site with various CHC's, of which: TCE, 1,1,1-TCA and cis-1,2-DCE. These leaked out of a waste solvents storage tank. Previous remediation with Chemical Oxidation has been unsuccessful. After each treatment a re-bounce in the concentration was measured, indicating that contaminants where still left behind. In the source zone a large amount of water mixed with nano-iron was injected.

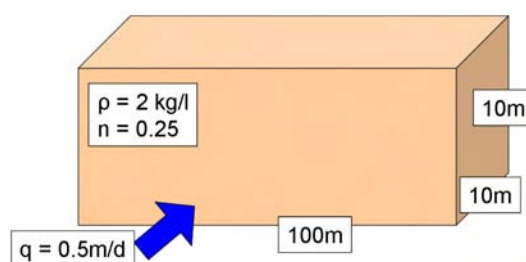


Fig. 1.2: Schematic in-situ reactive barrier

The water used was not degassed (de-oxidized) before use, and thus contained dissolved oxygen (DO). This most likely has caused the nano-iron to react with the DO and in some extent with the water itself. Especially when the particles were kept for a longer period in suspension with water, the nano-iron could have reacted with the water (setting  $H_2$ -gas free). By reacting with DO and water, the nano-iron lost most of the reactivity even before it was injected in the source zone. This hypothesis is supported by the creation of large amounts of cis-1,2-DCE after the injection. Another cause for the low amount of nano-iron available for the reaction can be a small spreading radius, or off-site migration by preferential flow paths.

In Germany a field test was performed by ALSTOM [Müller et al., 2006a,b]. In Europe, some more field tests are currently performed with RNIP of Toda Kogyo in Czech Republic, Italy and Germany. Of these tests no reports or publications are available yet.

### 1.5 Determination of Nano-Iron Injection Extend

To be able to use the nano-iron for an in-situ remediation, it is necessary to know the extend of the injection. For a source zone remediation the nano-iron needs to be delivered in the right amount over the whole zone. Thus it is important to know where the nano-iron is exactly going to during the injection. If the nano-iron is used to create an in-situ permeable reactive barrier, the distribution of the iron in the barrier must be continuous. Otherwise in parts of the wall the contaminants can pass without interaction with the nano-iron. Also the hydraulic permeability is not allowed to change significant since then the groundwater flow will follow an easier path around the barrier.

CHC's like PCE often occur in a plume with a concentration between 200 & 15 000  $\mu\text{g/l}$ . In weight, the amount of nano-iron needed for full reduction of PCE into ethene is stoichiometric equal to the weight of PCE present. In practice the nano-iron will also react with other substances in the groundwater. D'Andrea et al. [2005] describe experiments to investigate the influence of inorganics in the groundwater on the reductive dechlorination of TCE. They conclude that the composition of the groundwater strongly influences the ability of zero-valent iron to degrade TCE. This will also hold for other contaminants like PCE or DCE. Because of this, the weight of the nano-iron should at least be ten times that of CHC present. This weight factor is being used by several consulting companies in the pilot field tests, and is advised by the producers of the nano-iron. In several researches the lifetime of nano-iron has been tested. In general it is accepted that the material can be reactive for at least half a year [Liu et al., 2005].

As an example the situation presented in figure 1.2 demonstrates a PRB of  $100 \times 10 \times 10$  meter. Contaminated groundwater with a concentration of  $200 \mu\text{g}/\text{l}$  flows with a velocity of  $0.5 \text{ m}/\text{d}$  through the barrier. The total weight of nano-iron needed to remediate the contaminants passing through this volume over a period of 200 days can be calculated as following.

The total amount of porevolume (assuming a porosity of 25%) in this barrier is  $100 \cdot 10 \cdot 10 \cdot 0.25 = 2\,500 \text{ m}^3$ . The time for the groundwater to fill this volume with the flow rate of  $0.5 \text{ m}/\text{d}$  is 20 days, within these 20 days the nano-iron can dechlorinate the contaminant present. The concentration is  $200 \mu\text{g}/\text{l}$ , per volume this is  $50 \text{ g}$ . The efficiency of the nano-iron is assumed to be 10 %, resulting in ten times the weight of nano-iron needed ( $50 \times 10 = 500 \text{ g}$ ) and a total lifetime of 200 days, this comes to  $10 \text{ kg Fe}^0$  that is needed. Per kilogram of sand this is approximately  $0.5 \text{ mg}$ .

With these low concentrations of nano-iron it is hard to determine the extend of the nano-iron injection. The geogenic amount of iron in sand usually varies between  $5 \text{ mg}/\text{g}$  and  $45 \text{ g}/\text{kg}$  (there is an average of 4.5% of iron in the earth's crust, aquifers with higher or lower iron content can also be found). Chemical determination techniques are not able to distinguish between the elementary nano-iron and the natural occurring dissolved iron and iron oxides (see section 2.6.2). Because of this problem a different technique to determine the change of iron content has been developed in this research. By using a highly sensitive metal detector it was possible to measure the exact amount of iron present before and after the injection. The difference of these two measurements gives the amount of iron added by the injection of the nano-iron. A detailed description of the technique is given in chapter 3

## 1.6 Project Goals and Strategy

This research was set up as a feasibility study for the use of nano-iron as an in-situ remediation technique for chlorinated hydrocarbons. It was supported by the Ministry of Environment of Baden-Württemberg, Germany as a BW-Plus project. The project was setup such that the chemical part would be done by FZK and the physical application at VEGAS. Goal of the research was to test if the technique is suitable for remediation of a plume by creating an in-situ reactive barrier through the injection of nano-iron in the subsurface.

Various types of injections would be tested, e.g. different ordering of injection and extraction wells or injection under a magnetic gradient, which could help direct the nano-iron into a preferred direction, like a spreading perpendicular to the direction of natural groundwaterflow. The efficiency of the nano-iron to reduce a PCE or TCE contamination in 2-D and column experiments was to be tested. Also an upscaling into small 3-D experiments (app.  $1 \text{ m}^3$ ) would be done, to see if a homogeneous coverage of nano-iron can be created in a 3-D situation. From this an efficiency prognose and an economical feasibility was to be calculated for application in a field situation.

The effects of injecting nano-iron in the subsurface, like the change in pH or the permeability would be characterized through column experiments. From these the occurrence of endproducts and their possible dangers for the soil and groundwater would be analyzed.

The nano-iron as developed by FZK in 2003 would be further developed to improve the injection of the particles. The suspension needed to be electrostatically stabilized, the size of the particles would have to be further reduced and the aggregation of the particles needed to be limited. Stabilisation by

adding surfactants during the synthesis should create more separate particles, improving the migration of the suspension in a porous media. A chemical stabilization of the particles that reduce the reactivity of the nano-iron was necessary, otherwise the nano-iron would get oxidized before the injection. An upscaling of the synthesis of nano-iron was needed, to be able to create the amount of nano-iron needed in a field situation.

2-D and column experiments as done by Ruzin [2003] at VEGAS would be performed to test the improved nano-iron suspension of FZK.

At the end it should have been possible to decide if the technique is ready for application in a field situation or if further research and a larger project (e.g. large-scale 3-D experiment) will be needed.

### 1.7 About this Thesis

During the experiments in the beginning of the research, expected as well as new problems were found. A change in the goals and strategy of the research was needed and was based on the results of the preliminary research. From the preliminary research it was decided to develop an experimental method and setting that focuses on the transport behaviour of the nano-iron in porous media. With a special focus on the injection period when the nano-iron needs to be delivered to the desired location. It was used to investigate the transport of the nano-iron in such a way that the initial and boundary conditions were all known.

The conditions that were expected to be of influence on the transport were adjusted to find their relation to the transport. They were (I) the age of the nano-iron prior to injection, (II) the pore velocity, (III) the input concentration, (IV) the permeability and (V) the heterogeneity of the porous media.

A new method to measure and visualize the concentration distribution of nano-iron in a column was developed. This new method based on a metal detector, has given good results plus it made it possible to get a non-destructive measurement of the distribution of nano-iron injected in a column.

A disperger was used to partly reverse the process of aggregation by applying high shear forces on the suspension.

The five described conditions were indeed found to be of influence on the transportability. (I) The age, and with that the stage of agglomeration of the particles, reduces the transportability. The dispersing of the nano-iron suspension improved the transport. (II) At very high velocities the transport appeared to be very good, at lower stages of velocities (pore velocities between  $1.325 \cdot 10^{-5} m/s$  and  $1.06 \cdot 10^{-4} m/s$ ), the relative retardation of the nano-iron did not change. (III) With an increasing input concentration a reduced retardation was observed. (IV) In highly permeable porous media, nano-iron was capable of moving to the lowest point due to the gravitation force acting on the particles. In low permeable porous media the nano-iron could not even be removed or further transported when at high velocities the column was flushed with fresh water. (V) Heterogeneities could work in favour of the transport due to preferential flow paths through which the nano-iron could be easily transported.

## 2. PRELIMINARY RESEARCH

### *2.1 Introduction*

Several small, relatively quick, experiments were conducted in order to get a better understanding of the behaviour of the nano-iron in different situations. During these experiments and based on their results, a final experimental set-up was constructed to compare several factors that could be of influence on the transport behaviour of nano-iron.

In 2003, 2-D experiments with nano-iron, produced by the FZK [Ruzin, 2003], were carried out at VEGAS. The conclusion was that the nano-iron particles were highly reactive and incapable of transport in porous media. The particles were uncoated and untreated which resulted in direct oxidation as soon as contact with oxygen occurred.

The particles have been further developed by FZK in 2005. To test whether their transport capabilities had been improved the same 2-D experiments were carried out with the new nano-iron particles.

During the summer of 2005 the consulting company ALSTOM carried out a field test [Müller et al., 2006a] with nano-iron produced by Toda Kogyo (Reactive Nano Iron Particles RNIP). A sample of this was provided by ALSTOM to compare it's behaviour with that of the FZK particles. After these first experiments with the two different nano-iron types the rest of the experiments were done with RNIP of Toda Kogyo. Since FZK was not yet able to provide sufficient amounts of nano-iron needed for the rest of the experiments.

The preliminary experiments were mainly a result of each other. Many were experiments to test hypothesis and questions raised in a previous one. For this reason the experiments will be presented in chronological order.

### *2.2 2-D Experiments: Numerical Simulations*

#### *2.2.1 Methods*

To test the two particle types, a 2-D setting was thought of to create a barrier of nano-iron within a one layer system. By placing wells in a confined aquifer with a constant groundwater flow, a flow system that will spread the nano-iron particles in an area perpendicular to the background flow field would be created. In this way a permeable reactive barrier (PRB) would be constructed within the layer.

Before physically running the 2-D experiment, a numerical simulation was performed. This way a better understanding of the hydraulics was created. As well as the possibility to easily adjust parameters and test several scenarios. The physical experiment will be described in section 2.3.1

The used numerical code to calculate the flow paths was MODFLOW 2000 [Harbaugh et al., 2000] and the software package PMPATH [Chiang and Kinzelbach, 1993] was used to simulate the transport

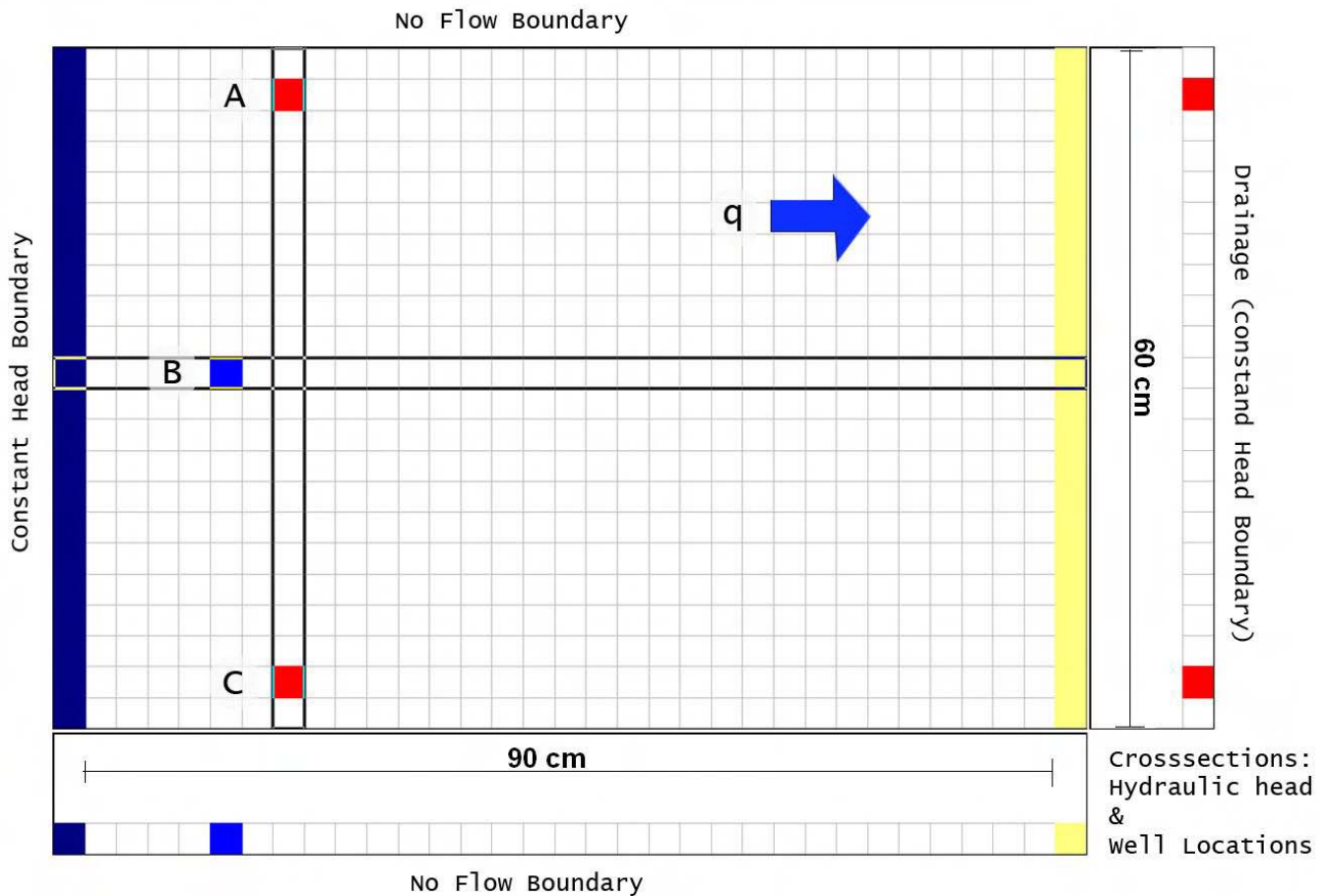


Fig. 2.1: Setup of the 2D numerical simulations. A,C: Extraction wells, B: Injection well, q: background groundwater flow

of a conservative tracer. To simulate the 2-D experiment, which was vertical oriented in the physical experiment, a horizontal one layer setting was constructed. Because only a conservative tracer was simulated, gravity effects played no role and the choice of a horizontal one layer system was valid.

A graphical presentation including the boundary conditions of the model is showed in figure 2.1. A constant background flow was created by applying a constant hydraulic head boundary on the left side and a maximum head level (overflow drain) at the right side. This way only water from the left and no water from the right entered the system during the pump tests. The top, bottom (both facing the paper), upper and lower boundaries were designed as impermeable no-flow barriers. Three wells were implemented, the upper (A) and lower (C) were extraction wells, the one in the middle (B) an injection well. They were fully penetrating the depth of the layer and over the whole length screened.

Several scenarios were ran. The simulated injection rates and flow velocities within the model were partly based on the data from the field test of ALSTOM [Müller et al., 2006a].

### 2.2.2 Results & Discussion

The resulting flow field is presented in figure 2.2, the velocities of the field test and the capacities of the used pumps for the 2-D physical experiments were taken into account. The used boundary and initial conditions are given in table 2.1. The  $100 \text{ cm}^3/\text{min}$  discharge difference was the maximum that

Tab. 2.1: Boundary and Initial conditions for the 2D simulations

Condition	Value
Constant Head (BC)	68 cm
Drainage level (BC)	65 cm
Upper well discharge	$-150 \text{ cm}^3/\text{min}$
Middle well discharge	$100 \text{ cm}^3/\text{min}$
Lower well discharge	$-150 \text{ cm}^3/\text{min}$
Hydraulic conductivity ( $K$ )	$1.5 \text{ cm}/\text{min} = 0.025 \text{ m}/\text{s}$
Transmissivity	$T = K \cdot d = 1.5 \text{ cm}/\text{min} \cdot 12 \text{ cm} = 18 \text{ cm}/\text{min}$
Background flow velocity	$2 \text{ m}/\text{s}$
Porosity ( $n$ )	0.33
Grain size bandwidth	0 – 4 mm Rhine-valley sand

the pump could deliver for the constant head boundary in the physical experiments. If the amount of water extracted from the system through the extractions wells was above the maximum delivery capacity, the right hand side of the container was drained and the hydraulic head drops on that side below the drainage level. In a natural situation the amount of water that can be extracted might be higher. Then the water from larger distances can be attracted to provide the needed amounts of water. In the first numerical runs this more natural situation with a constant head on the right hand side was modelled. This situation though was not representable for the physical experiments and thus the fixed hydraulic head on the right was replaced by an overflow drainage. A drainage can only remove the excess of water and can not add water from outside to the simulated model area.

The chosen conditions were partly based on the field test of ALSTOM as described by Müller et al. [2006a]. By adapting the test-field data and slightly correcting the pump rates to establish the flow fields as wished in the 2-D physical experiment, the data as presented in table 2.1 were set.

A barrier perpendicular to the background flow direction was created. In a real field situation (or a larger experimental setup) several wells would be placed on a line. Each set of three wells could then be used as a injection-extraction set. The extraction wells could also be used as injection wells, and the injection wells as extraction wells (see figure 2.4).

### 2.3 2-D Experiments: Physical Model, Reproduction of 2003 experiment with new colloids

#### 2.3.1 Methods

In the setup a configuration of three wells in a sand-box container was chosen such that the wells were on a line perpendicular to the flow direction. In this way the creation of a in-situ PRB system was imitated.

The spreading of nano-sized iron colloids in the setup of the sand-box experiment was first determined by visual observation. Later the sandbox was excavated block wise and from some of these blocks a mix-probe was taken. For each probe the total iron content could be determined by dissolving all iron in the probe with a strong acid. The iron content could then be determined with an ICP-OES (Inductively

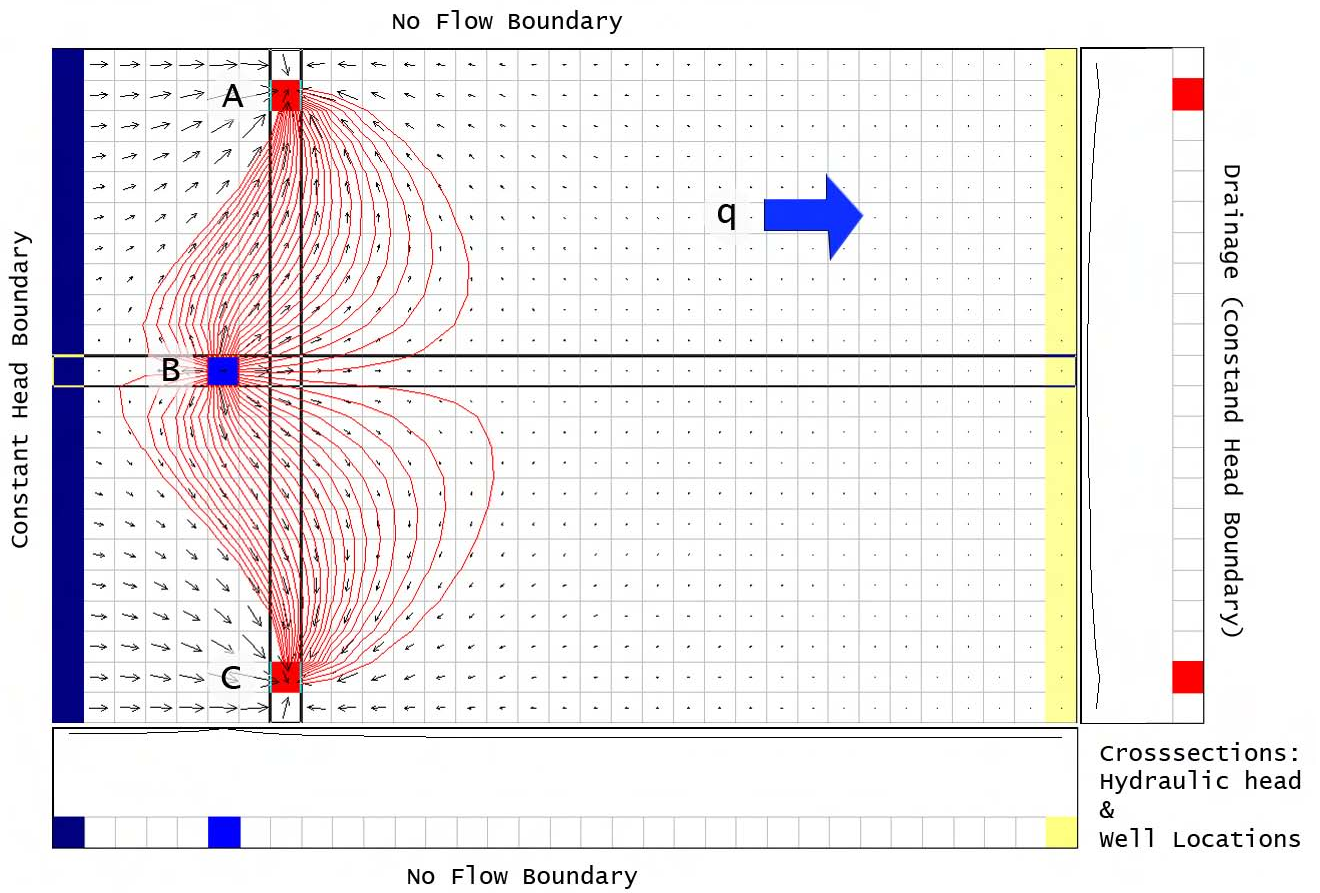


Fig. 2.2: Flow paths simulated with PMPATH. Cross sections are scaled with factor 0.25



Fig. 2.3: Injection, extraction with dye tracer test

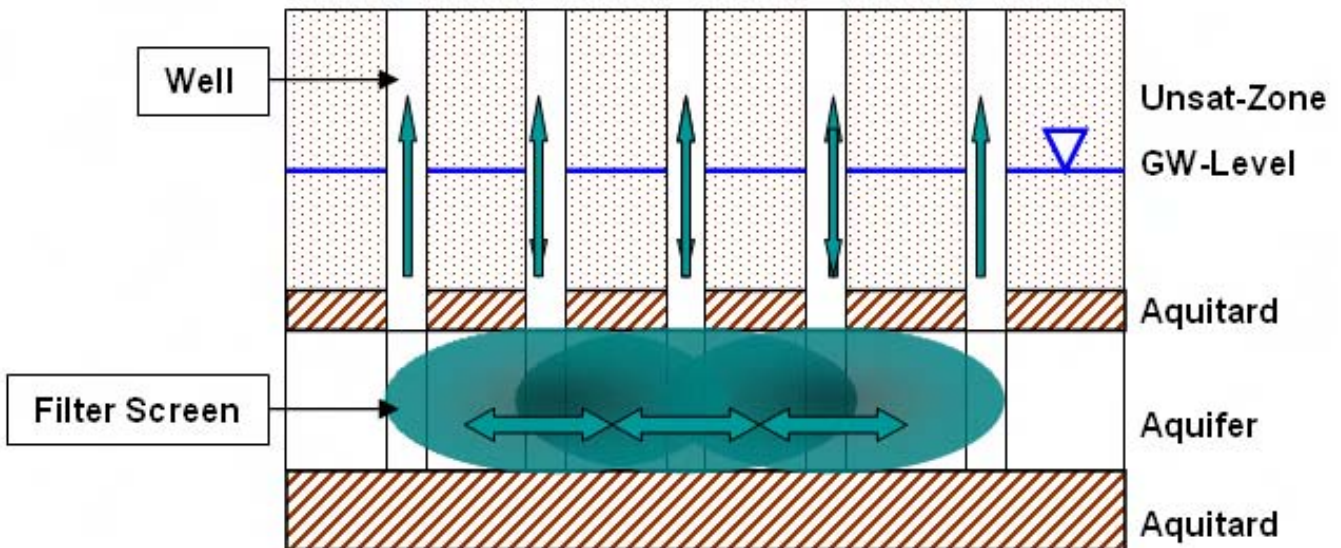


Fig. 2.4: Several injection and extraction wells on a line. Each injection well can also be used as an extraction well, creating an overlapping nano-iron injected reactive barrier

Coupled Plasma Optical Emission Spectrometer). Before all the probes were tested, this detection method was tested for applicability, this test is described in section 2.6.

The sand was packed wet in the container. In this way the wide distribution of sand grain sizes (0 – 4 mm Rhine valley Sand) would stay together and could be packed in the container with a reduced amount of vertical sorting. The water level in the container was raised each time a new layer of sand was placed. This way, the sand stayed wet and no air could enter the pores. At the top a layer of 3 cm very fine sand (0.003 - 0.2 mm Dorsilit 2500,  $K \approx 4 \cdot 10^{-6} \text{ m/s}$ ) was placed to create an impermeable layer. The flow in the sand-box container was created by a constant head level on one side and an overflow (drainage) on the other side. The outflow level was set below the constant head level. This head-difference creates a flow inside the container (convention is to create a flow from left to right). See figure 2.5 for a graphical presentation of the setup. The container used was 1 m wide, 70 cm high and 12 cm deep.

To compare the spreading of the nano-iron of FZK with that of ALSTOM, the same experiment setting was build again. The same type of sand was used and the wells are positioned in the same location as the first experiment. The colloids of ALSTOM were supplied as a suspension with a concentration of 200 g/l, this was diluted to make a suspension of 10 g/l, which equals the concentration of the suspension of FZK.

For both experiments the head levels and the pump rates used were based on the results of the numerical model outcome. The first setup was first used to calibrate the numerical model. The outcome of the numerical model was calibrated and verified by using a green dye (Uranine,  $C_{20}H_{10}O_5Na_2$ ) instead of the nano-iron. Uranine is a conservative tracer and can thus show the flow paths within the container.

### 2.3.2 Results & Discussion

Before the nano-iron injection was performed, a conservative tracer (Uranine  $C_{20}H_{10}O_5Na_2$  which gives a green solution) was used to verify the flow field in the container with that of the numerical simulations.

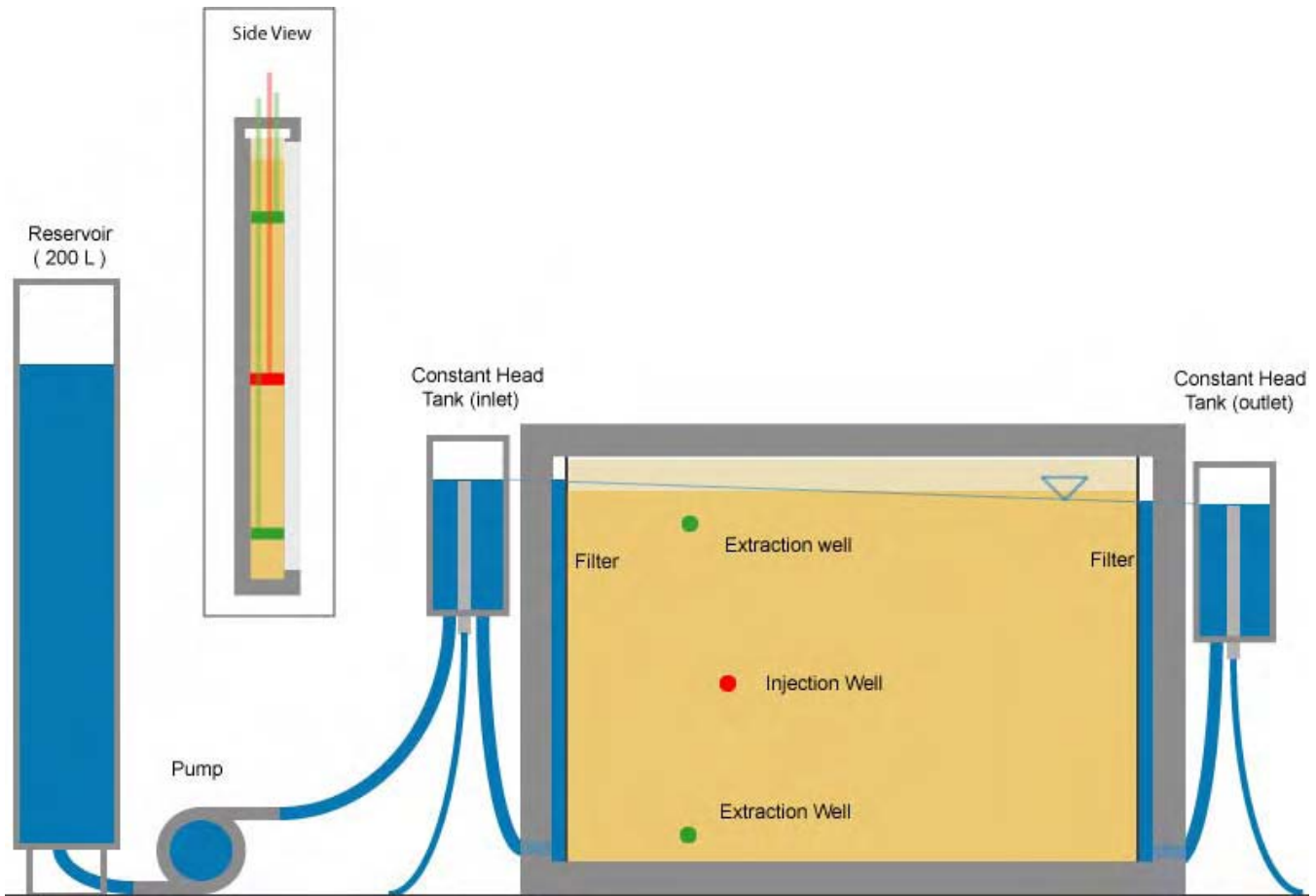


Fig. 2.5: Setup of the 2D experiments. The pump keeps the constant head on the left, the overflow level at the right is set such that a background flow is created. The Side view shows a vertical cross section to show the location and position of the wells

Several runs were performed in the first setup. The first was used to calibrate the numerical model to the experimental setup. The hydraulic conductivity and the horizontal anisotropy needed to be adjusted in the numerical model to fit the experimental setup. The resulting dye spreading closely resembled the calculations of the numerical model (fig. 2.3). The boundary conditions used for the physical 2-D simulations were chosen as given in table 2.1.

The spreading of the FZK nano-iron was very limited. A maximum distance of 3 *cm* was achieved. This distance was determined by visual observation. The nano-iron was black and well visible against the glass. Further on other detection techniques of the nano-iron will be discussed (e.g. paragraph 2.6.2). Though it was assumed that the spreading was fully 2-dimensional, there was still a depth component of 12 *cm*. This means that some 3-dimensional differences would remain present. After the injection of the nano-iron the container was emptied and the distance obtained from the iron at the glass side appeared to be representative for the spreading inside. The differences in the third dimension are not significant and thus the assumption of a 2-dimensional experiment was validated for this case.

After rebuilding the set-up, the nano-iron of ALSTOM was injected under the same conditions (table 2.1). The maximum distance the particles traveled was 6 *cm*. This was a larger spreading than the FZK particles achieved. Though the spreading was also not as large as would be expected. Compared to the results from field tests, the spreading under these conditions should reach over 1 *m* (e.g. Müller

et al. [2006a], Elliott and Zhang [2001]). In this case the spreading inside the container was also observed and the spreading as visualized on the glass seemed representable for the spreading over the whole depth of the container.

The maximum traveled distance of the particles showed a sharp front around the well. Around the injection well, the velocity profile is radial (see equation 2.1). The velocities are thus decreasing hyperbolic with distance  $r$  from the well. A possible explanation for the sharp boundary is the existence of a minimum flow velocity to carry the nano-iron particles, or in other words: to keep them in suspension. To test this hypothesis the drag velocity experiment was performed (see paragraph 2.5).

Radial flow around a well in a confined aquifer:

Assuming that an aquifer is homogeneous and that the medium is isotropic, then the hydraulic conductivity  $K$  is constant. The velocity decrease with distance  $r$  from the well can then be determined with the following relation:

$$\mathbf{v} = \frac{\mathbf{Q}}{2\pi r b n} \quad (2.1)$$

where  $\mathbf{v}$  is the flow velocity ( $m/s$ ),  $\mathbf{Q}$  the total discharge ( $m^3/s$ , negative for extraction, positive for injection),  $r$  the radius from the well ( $m$ ),  $b$  the thickness of the aquifer ( $m$ ) and  $n$  the porosity ( $-$ ) [Schwartz and Zhang, 2003]

## 2.4 Settlement/Attachment experiment

### 2.4.1 Methods

Nano-iron can attach to sand grains through electrostatics and Van der Waals forces between the nano-iron particles and sand grains. Nano-iron particles are positively charged, the charge of the sand grains is controlled by the pH of the suspension and can be indicated with the zeta potential. To test if the nano-iron colloids attach to the sand, a batch experiment was done. In a beaker the nano-iron colloid suspension was mixed with sand. The whole was shaken to get an optimal mixing effect, and then put to rest to let the suspension settle.

If the nano-iron would be attached to the sand, the sedimented suspension would be homogeneous black from the nano-iron colloids that surround the sand grains.

If they would not be attached to the sand, they would settle separately.

The nano-iron colloids were assumed to be small, but had a much higher density as sand grains (app.  $7000 \text{ kg/m}^3$  for iron against app.  $2500 \text{ kg/m}^3$  for sand). Due to this, depending on the size and shape of the individual colloids they would sink faster, slower or equally fast compared to a sand grain. Thus it could also form a homogeneous mixed suspension of sand and nano-iron without attachment. It can only be shown by a separated settling of the sand and the nano-iron particles whether the particles attach or not.

Both the colloid suspensions of ALSTOM and FZK were tested.

### 2.4.2 Results & Discussion

For the ALSTOM colloids the sediment was mixed with the colloids by shaking it over head by hand several times. After the vessel was placed to rest, most of the colloids settled much slower than the sand. It could be concluded that the colloids were not attached to the grain surface. The FZK colloids settled much faster. Probably because they were already aggregated resulting in heavier particles. The sand still settled much faster and thus a sharp interface was seen between the iron and the sand bedding (see fig. 2.6).

To get an other impression about the attraction between the iron colloids and the sand grains as well as the size of the colloids, the suspensions were filtered (see fig. 2.7). The water that came through the filter from the FZK nano-iron was yellow and contained no black particles. This indicated that some iron was dissolved in the water and that the particles were aggregated to such large particles that they could not pass through the filter. The water flowing through the filter from the ALSTOM nano-iron was colorless except for a significant amount of nano-iron. Indicating that those particles were a lot smaller and could thus pass through the filter and that the reactivity of the ALSTOM particles was lower due to a coating compared to the uncoated particles from FZK.

Afterwards the mix of sand and nano-iron left behind in the filters was washed out with water (normal potable water). The nano-iron could be completely washed out and the sand was clean again. In loose sand it was thus possible to simply separate the two from each other. Indicating that the nano-iron did not strongly bind to the sand. Which corresponded to the observed settling difference between the sand and nano-iron.

It should be noted that the suspension of FZK was getting old and started to aggregate and corrode, due to this it probably wasn't able to give optimal results.

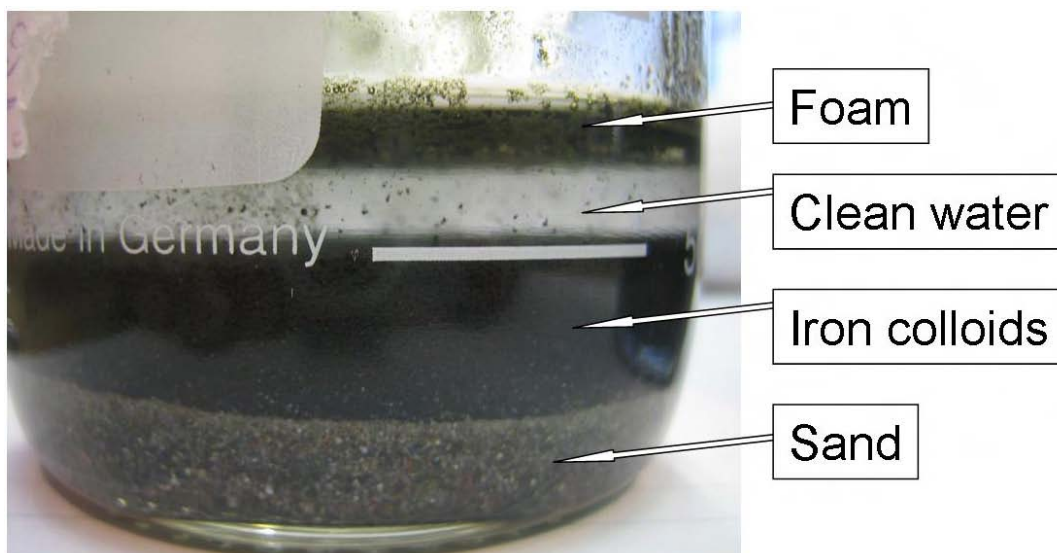


Fig. 2.6: Vessel containing the nano-iron of FZK and the sand after it has been set to rest and the mixture settled. Almost no iron settled together with the sand, it mainly settled in a layer on top of the sand

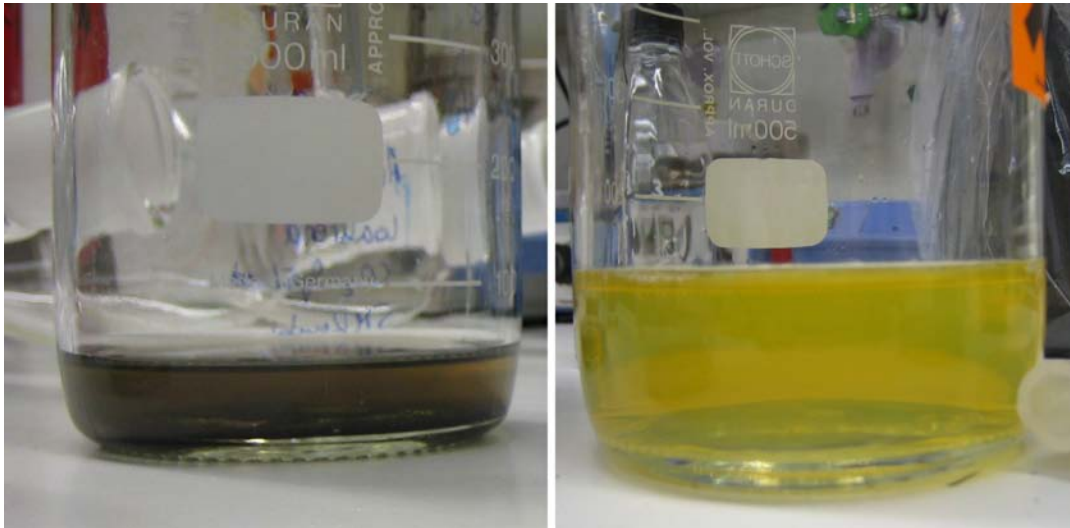


Fig. 2.7: Filtration effluent of the nano-iron mixtures. On the right the mixture of FZK is seen, the left one is from the ALSTOM mixture

## 2.5 Drag velocity

Assuming there is a minimal velocity from which on the nano-iron particles are able to be transported within the porous media, there should be a minimum velocity from which on they are being dragged with the flow of water. From that velocity on, the particles will no longer settle to the lowest point by gravity forces or stay at that position if they were already settled.

The drag-force of the flowing water should be at least so strong to prevent the gravitational force pulling on the nano-iron particles from settling the particles before transported to the desired distance. If the flowing water needs to pick up the particles from the bottom, it will also need to counteract the attracting forces (probably mainly electric and magnetic forces that coagulate the particles in the bedding) between the particles and the frictional forces.

### 2.5.1 Methods

To test this hypothesis a setup was created in which a glass pipe of 1.5 m length and an inner diameter of 3.6 mm was used. A peristaltic pump (Watson Marlow, 323), and later a 50 ml syringe pump (Harvard Apparatus Pump '44') was connected on the outlet side, on the inlet side a nano-iron reservoir was connected. The reservoir was equipped with a mixer in order to keep the nano-iron in suspension during the experiments. The reservoir contained 250 ml of nano-iron suspension with a concentration of 20 g Fe<sup>0</sup>/l (See figure 2.8).

First a laboratory magnetic mix plate was used (KMO2 IKA), this resulted in large aggregates of magnetized particles in the glass pipe. Also a large portion of the iron got attached to the magnet. Due to this problem a mixer made of PVC and rubber was constructed and used (see fig 2.8). The mixer was equipped with a small electro motor and the velocity of the rotation could be varied with a adjustable power supply.

The syringe pump could be accurately set to a certain discharge. This way, by knowing the diameter of the glass pipe, the average velocity inside the pipe could be controlled and would be constant from

the beginning to the end of the pipe. The average velocity in the pipe was varied between 1.5 mm/s and 280 mm/s. The flow could be assumed laminar since the Reynolds number was between 5.5 and 1026.7 (see eqn. 2.4). The flow field in this glass pipe was parabolic (see fig. 2.14) at the applied velocities.

For these velocities a settling velocity was calculated with Newtons equation for terminal settling velocity (eqn. 2.2). Assuming a particle diameter of 100 nm, the settling velocities would be approximately  $3.67 \cdot 10^{-3}$  m/s or in other dimensions: 3.67 mm/s (the used constants were:  $g = 9.81$  m/s,  $\rho_p = 6150$  kg/m<sup>3</sup>,  $\rho_l = 998$  kg/m<sup>3</sup>,  $D = 1 \cdot 10^{-7}$  m,  $C_d = 0.5$ ).

Particle Settling in flowing water:

Particle settling, or sedimentation, may be described for a single particle by the Newton equation for terminal settling velocity of a spherical particle. The rate at which discrete particles settle in a fluid of constant temperature is given by

$$v = \sqrt{\frac{4g(\rho_p - \rho_l)D}{3C_d\rho_l}} \quad (2.2)$$

where  $v$  is the settling velocity,  $g$  the gravitational acceleration,  $\rho_p$  the density of the particle,  $\rho_l$  the density of the liquid,  $D$  the diameter of the particle and  $C_d$  the coefficient of drag [EPA, 1999].

The coefficient of drag can be derived for low Reynolds numbers ( $< 1$ ) from Stokes' Law (eqn. 2.10):

$$\begin{aligned} \mathbf{F}_{drag} &= 3\pi\eta v D \\ \mathbf{F}_{drag} &= \frac{24}{\rho_l v D / \eta} \frac{\pi D^2}{4} \frac{\rho_l v^2}{2} \\ \mathbf{F}_{drag} &= \frac{24}{Re} A \frac{\rho_l v^2}{2} \\ \mathbf{F}_{drag} &= C_d A \frac{\rho_l v^2}{2} \\ C_d &= \frac{24}{Re} \end{aligned} \quad (2.3)$$

where  $\mathbf{F}_{drag}$  is the drag force,  $v$  the flow velocity,  $D$  is the diameter of the particle,  $\rho_l$  is the density of the liquid,  $\eta$  the viscosity of the liquid,  $Re$  Reynolds number,  $A$  the frontal surface of the particle,  $C_d$  the drag coefficient.

In laminar flow ( $1 < Re < 2300$ ) a drag coefficient of 0.5 can be used for spherical particles. In turbulent flow ( $Re > 2300$ ) the drag coefficient is 0.2 [Çengel and Cimbala, 2006].

### 2.5.2 Results & Discussion

For each of the velocities in the glass tube the approximated travelled distance of the nano-iron and a short description is given in table 2.2. A visual observation of the behaviour of the particles during the transport was also possible in the tube (see fig. 2.11). From these observations it was expected that the gravity acting on the particles played a large role in the transport distance. In the capillary tube at small velocities a grouping of the particles could be seen when the peristaltic pump was used (see fig. 2.10). The peristaltic pump created a non-continuous (pulsed) flow inside the tube. Using the syringe pump,

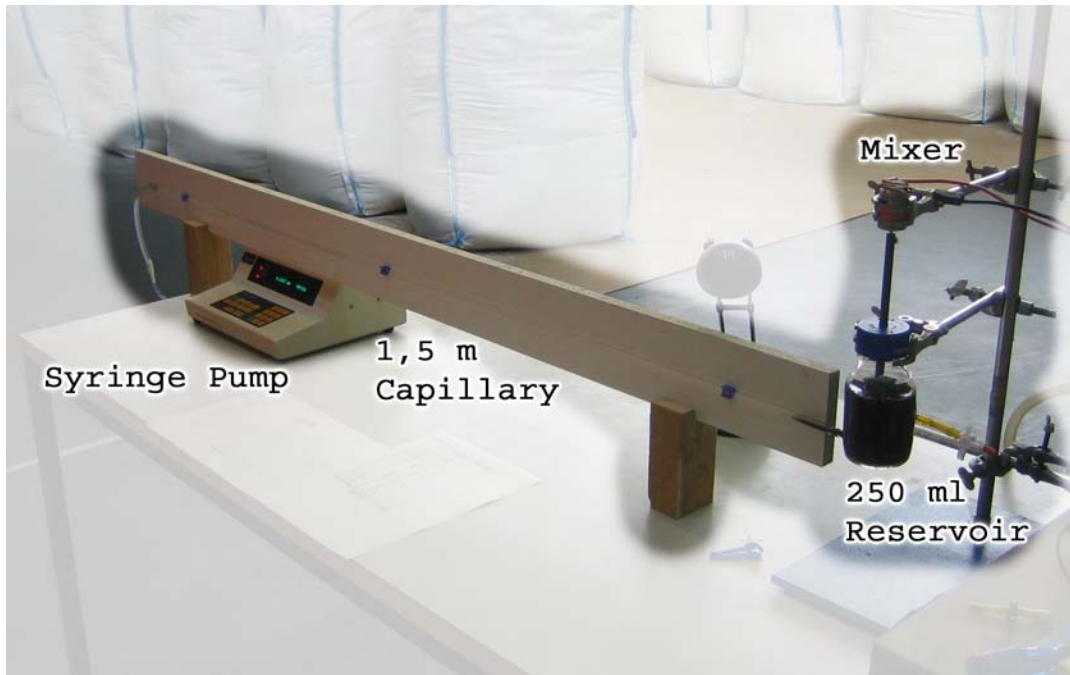


Fig. 2.8: Setup to test at which velocity nano-iron settles and is being re-mobilized

the grouping was not observed, the particles though were attached to each other. At low velocities, the particles accumulated (or gelled) to form even larger groups.

Tab. 2.2: Transport in a glass tube with a  $3.7 \text{ mm}$  inner diameter and  $1.5 \text{ m}$  length.  $\dagger$  presents the total distance over which transport at the whole cross section was seen

Flow Velocity ( $\text{mm}/\text{sec}$ )	Distance $\dagger$	Comments
1.5	7 cm	max transport for some particles was 30 cm in the lower region
15.5	30 cm	max transport for some particles was 80 cm in the lower region
50	1.5 m	some particles settled, accumulated and rolled over the bottom
97	1.5 m	more in suspension, still some rolling at the bottom
280	1.5 m	All is in suspension, fully black suspension, no differences in the regions were seen

During this experiment, particles were seen and had various shapes and sizes. The nano-iron though should have a diameter of less than  $100 \text{ nm}$ , which makes it only visible with the aid of a microscope. This indicates that almost all nano-iron used in this experiment was aggregating to form larger particles, which were visible even without the use of a microscope.

At the end of the tube, some iron was visually deposited, transport of the nano-iron in this part of the tube though was not seen. This could indicate that some particles were much more stable and consisted of a much smaller size, resulting in a larger transport distance. When they settled on the glass surface, they became visible.

The calculated settling velocity was approximately  $3.67 \cdot 10^{-3} \text{ m}/\text{s}$ . From the observed transport distance the settling velocity was between  $7.83 \cdot 10^{-5} \text{ m}/\text{s}$  and  $0.50 \cdot 10^{-3} \text{ m}/\text{s}$  on average over the cross section of the glass pipe.

The calculation of the settling velocities was probably not completely representable for this situation. The flow was laminar, but not in the whole pipe the same velocity was present, the velocity profile was

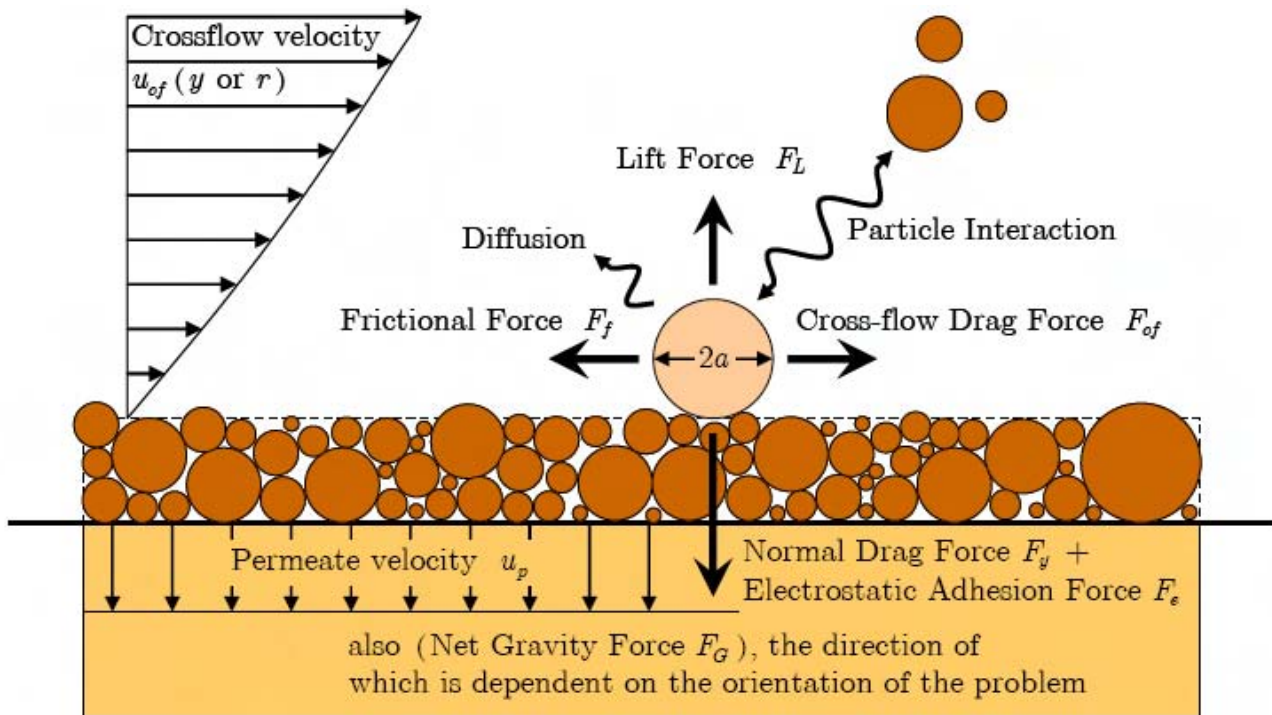


Fig. 2.9: Presentation of the forces that act on a particle deposited on the surface of a pore [Al-Abduwani et al., 2005]

parabolic. The particles in the upper part of the pipe would thus settle to the faster flow regime in the middle, where they would stay longer in suspension. From lower parts the particles would settle due to the low velocity and create a sedimentation bed. In the pipe, shear forces and particle interaction would have to be taken into account next to the drag and gravitational force. Since the sedimentation on the bottom would reduce the diameter of the pipe, the velocity profile changed with time, giving a non-linear system. It should be possible to create a mathematic and computer model that can describe the particle transport in the pipe. Within this project this was not performed.

Phenrat et al. [2006] showed that magnetic attraction is a main mechanism in the accumulation. If an tube experiment in an alternating magnetic field would be done, it might be possible to see if this positively influences the transport due to less aggregation of the nano-iron particles.

The change of the Zeta potential of the nano-iron of ALSTOM with a changing pH value is given in figure 2.12, which was determined by FZK. An acidic suspension will thus give a higher Zeta potential, which means that less aggregation would occur in acidic suspensions. During the experiments some pH measurements were done, the pH of nano-iron suspension was approximately 10.5. From the curve in figure 2.12 it is clear that a base solution is actually not preferable and would increase the aggregation of the colloids.

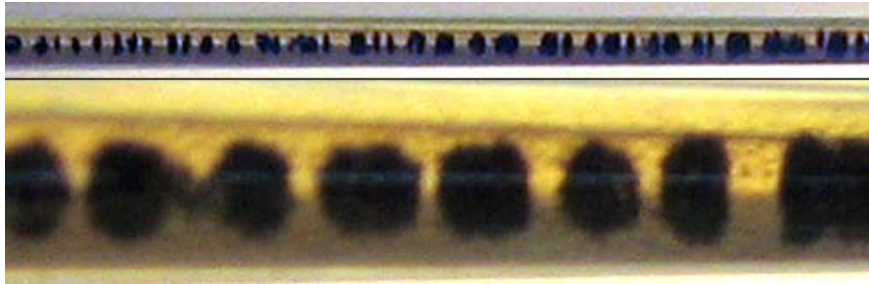


Fig. 2.10: Transport of nano-iron in a glass tube by using a peristaltic pump. Inner diameter of the glass tube is 3.6 mm. The bottom picture is a detail of the top picture

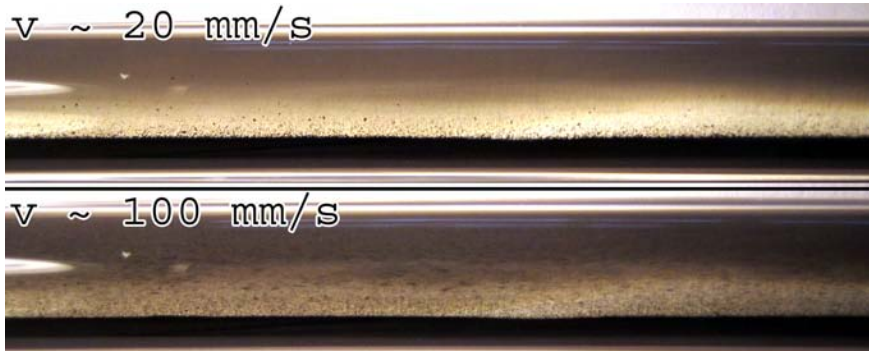


Fig. 2.11: Transport of nano-iron in a glass tube by using a syringe pump. Top: 20 mm/s, almost no transport of particles visible. Bottom: 100 mm/s, transport of iron particles is well visible

## 2.6 Testing the Iron Determination with the ICP-OES

### 2.6.1 Methods

To find out how far the iron colloids were being transported in the 2-D experiments a reliable technique was needed. With the use of an ICP-OES (Inductively Coupled Plasma Optical Emission Spectrometry) measuring device the total amount of iron could be accurately determined in a solution. The iron in several samples taken at different distances from the injection well in the 2-D container experiment, were to be dissolved. Each sample would then give its own iron content, based on these data it should be possible to construct a breakthrough curve of the nano-iron. The dissolving is often done by using a 1 molar  $H_2SO_4$  solution, else wise it is dissolved using a diluted or concentrated  $HCl$  solution.

To see how large the background iron content of the sand was, first two sand samples of 10 g each were prepared. The iron in the sand samples was dissolved with the pure  $HCl$  which was stirred for 1 day on a laboratory magnetic stirrer (KMO2 IKA). The filtered solution was diluted 100 times in order to make it analyzable with the ICP device. At the same time, 100  $\mu l$  of nano-iron suspension (RNIP 200 g/l) was completely dissolved, diluted by a factor 100 and analyzed with the ICP.

### 2.6.2 Results & Discussion

To see if  $H_2SO_4$  was an appropriate agent to determine nano-iron, the pure nano-iron colloid suspension was taken and mixed with a 1 molar  $H_2SO_4$  solution. It did not dissolve very rapidly and not all

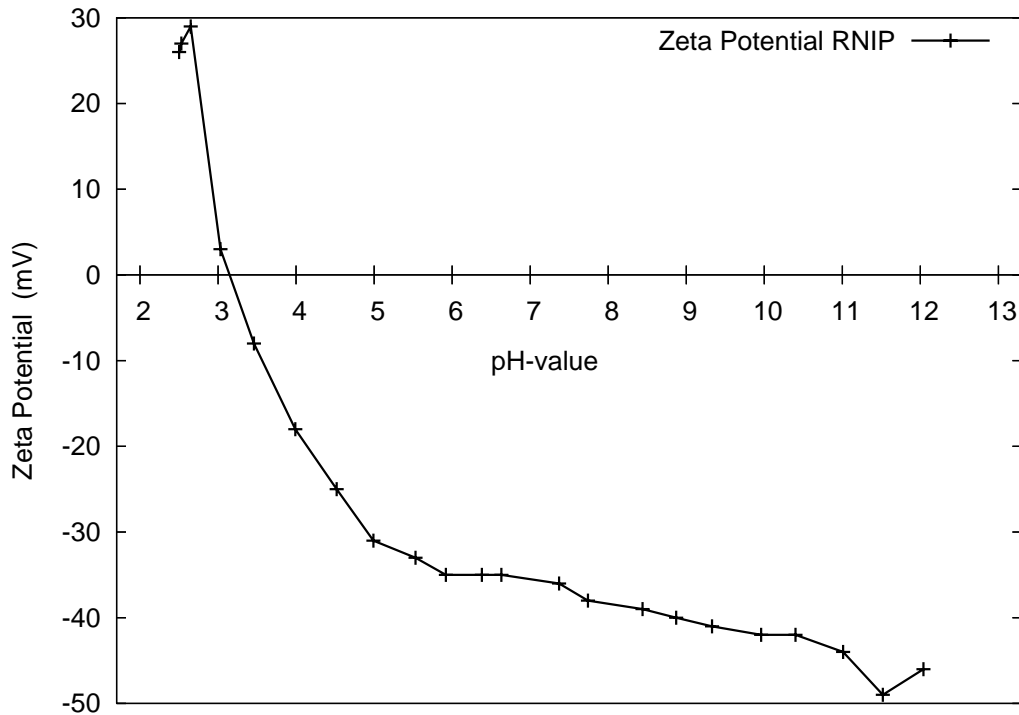


Fig. 2.12: Curve showing the change of the Zeta potential due to the change in pH of the suspension of the nano-iron of ALSTOM (RNIP, Toda Kogyo), measured by FZK

nano-iron could be dissolved. Also 50 ml of a diluted  $HCl$  solution (3.2%) was not able to dissolve 100  $\mu l$  (200 g  $Fe^0/l$ ) iron colloids as quickly as expected. A pure solution of  $HCl$  (32%) was able to do this. All the nano-iron was dissolved and the colour of the solution changed to yellowish. The samples of the nano-iron that were measured are labeled A and B in table 2.3. This solution was diluted to a 100th of its original concentration, a solution of approximately 4 mg/l iron should now have been established. The determined concentration of the nano-iron solution was approximately 2 mg/l, instead of 4 mg/l as was expected. This had most likely to do with the small amount of nano-iron that was taken from the large bottle. The nano-iron in suspension might not have been equally spread within the bottle. The total amount of suspension in the bottle had a concentration of 200 g/l, this settled and accumulated at the bottom of the bottle. Even when a bottle was emptied some iron was still left behind in the bottle. It was thus not known exactly which concentration of nano-iron was to be measured.

Tab. 2.3: ICP results of iron determination

Sample	Iron Content ( $\frac{mg}{l}$ )
A	1.93
B	2.05
C	11.60
D	11.00

The two sand samples without nano-iron from which the naturally occurring iron was dissolved, are labeled C and D in table 2.3.

From these results it can be seen that the concentration of naturally occurring iron in the soil was far

larger than the extra iron concentration that would be needed to be injected as nano-iron. The difference would be measurable, but a very accurate determination of the natural occurring iron content would then be necessary. This is impossible in a natural situation and almost impossible for an experimental setup. The iron content differs too much between different samples taken even close to each other. In an experiment an approximate average iron content can be estimated before injecting the nano-iron. The concentration after the injection will though be mainly influenced by the background iron content at that specific location and not by the nano-iron.

Due to this large background concentration the chemical detection was decided unsuitable for the low iron concentrations that were needed for the experiments.

Because of the poor capability of this method to distinguish between  $Fe^0$ ,  $Fe^{II}$  and  $Fe^{III}$  in the samples, and the high geogenic iron content in the soil samples, it was decided that the block samples of the 2D experiments would not be further analyzed.

## 2.7 *In-Situ Determination of Iron Occurrence*

A metal detector generally uses electromagnetic induction to detect metal. In basics, it consists of an oscillator producing an alternating current that passes through a coil producing an alternating magnetic field. If a piece of metal, which is electrically conductive, is close to the coil eddy currents will be induced in the metal, and this produces an alternating magnetic field of its own. Another coil is used to measure the magnetic field the change in the magnetic field due to the metallic object can be detected (after Wikipedia [jan. 2007]).

### 2.7.1 *Methods - Hobby Metal Detector*

A simple metal detector was build, with a coil that exactly fits around a column (4 cm outer diameter and 1 m long), it could be moved along the length of the column. When the iron content changed, the metal detector would give a change in the audio signal produced. This audio signal could be recorded with an analog-to-digital converter. For this the audio card of a laptop was used. After processing the signal with a Fourier transformation, a single frequency peak that indicates the iron presence could be visualized.

For this test the column was filled with sand. The iron content in the sand was different for each quarter of the filling. The different iron contents were created by (I) flushing the sand with a 32% HCl solution, (II) doing nothing with the sand, (III) mixing the sand with a small amount of nano iron colloids in suspension and (IV) mixing the sand with a large amount of nano iron colloids. This large amount was expected to be much bigger than necessary for remediation in a PRB, but might be needed to clean up a pool of NAPL.

The impedance of a coil was influenced by iron and even stronger by magnetized iron within the coil. It was tested if the colloids could be magnetized after injection and if the metal detector would then give a different signal. A magnetic field was constructed with a coil and a heavy power supply. The coil was able to withstand 10 Ampères and creates a strong magnetic field within the pipe, parallel to the length direction. The residual magnetism of the nano-iron could be visualized by sliding a compass along the

pipe.

### 2.7.1.1 Results & Discussion - Hobby Metal Detector

The signal produced by the metal detector was recorded and after a Fourier transformation the frequency peaks that indicated the presence of iron could be seen. This frequency changed with time. Most likely due to the low quality of the used components of the simple metal detector. But also the change of electromagnetic radiation around the setting could have been partly responsible for the change. In the lab many electronic devices as well as a lot of metal could be found, activity in the lab could influence the metal detector. The shift in the peak frequency was too big to identify small changes in nano-iron occurrence. The part where a high concentration was present was visible as a peak in the measurement, as well as audibly recognizable. Though a quantitative nano-iron concentration determination was not possible due to the shift of the peak frequency with time.

Within the high concentration section, 5 *cm* of column length were magnetized. The needle of the compass changes approximately two to three degrees at the magnetized area, which indicated that residual magnetism was present. When moving the metal detector over this part, a change in the frequency signal was produced. Based on this result, in later researches the magnetization might be of help to identify low concentrations of nano-iron or improve the signal.

The first results of the metal detector showed that the principle works. Unfortunately the signal that was produced by the metal detector device was very unstable. And from the measured frequencies no quantitative relation to the amount of iron in each part of the pipe was found, but qualitatively the location of the nano-iron could be distinguished.

### 2.7.2 Methods - Commercially Available Metal Detector

Several metal detector producers were contacted about the possible applicability of their devices for this research. Institute Dr. Foerster (Reutlingen, Germany) offered to test one of their devices on the nano-iron.

To let the research and development department of Institute Dr. Foerster test the applicability and suitability of some of their metal detectors, two probes were sent. Two Plexiglas pipes of 40 *cm* length and 4 *cm* outer diameter were packed with sand of 1.6 – 2.5 *mm* in diameter (GRANUCOL 1/5G, this sand has a very low natural iron content). One pipe was filled in three sections, the sand was premixed with water and nano-iron to get a concentration of '5 *g Fe/kg sand*', '0.5 *g Fe/kg sand*' and one section had no nano-iron mixed. The other pipe was filled with sand and water only.

#### 2.7.2.1 Results & Discussion - Commercially Available Metal Detector

After the pipe with the nano-iron was filled, the nano-iron was moving freely through the porous media. By gravity forces alone it settled to the bottom of the pipe. By tapping the pipe it moved faster. The iron settled completely at the bottom of the pipe (which was placed horizontal). This high mobility was likely to be caused by the coarse grain size distribution and large pore connectivity. Because of the movement of the nano-iron the provided concentrations were no longer valid. It was only visible that at

the outer ends of the pipe (where no nano-iron was added) the concentration was much lower than in the middle.

The first measurements were not yet able to give quantitative results, though they were able to present clear visual readings that indicated the presence of iron. Higher and lower concentrations were distinguishable. The first results of the prepared pipes with nano-iron were promising. From the detector an almost raw signal with minimum filtering could be recorded. This signal might need to be analyzed by geophysical filtering methods (e.g. Böttcher et al. [2005]) to identify the nano-iron. Due to these promising results it was decided that the detector of Foerster would also be used in the 1-D flow experiments.

## 2.8 Conductance measurement of the Nano-Iron

### 2.8.1 Methods

To find a good way of determining the distance travelled by the nano-iron, another method was tested. If the electric conductance of water changes by the presence of the nano-iron, then this might be a suitable way of visualizing the nano-iron presence. To test whether the nano-iron solution changes its conductance, this was tested in a laboratory glass of 250 ml. The electrical conductance was first measured in the nano-iron suspension. Next the iron particles were filtered out of the suspension and the electric conductance was measured again. The filter used was a syringe glass-fiber filter (Glasfaser Membran Filter Gelb, PP  $\varnothing$  25 mm, CM 0.45  $\mu$ m). The electrical conductance was measured with a WTW LF 325-A (Wissenschaftlich-Technische Werkstätten, Germany).

First the RNIP suspension was measured in the delivered concentration of 200 g/l, next the suspension was filtered and the remaining liquid was measured. The iron filtered out was resuspended in de-ionized water and this suspension was measured. The same was done for the nano-iron of FZK.

### 2.8.2 Results & Discussion

Both the suspensions of FZK and ALSTOM were tested in this experiment. The suspension of FZK was already coloured brown due to oxidized and dissolved iron. The liquid phase of the suspension of ALSTOM was still colourless, this was visible as soon as the iron settled.

The measured electric conductivities are given in table 2.4.

There was a large difference in the conductance of both types of suspensions. This was due to the surfactants which were present in the ALSTOM suspension. Filtering the ALSTOM suspension gave an even higher reading, suggesting that this difference should have been within the measurement error.

For the FZK suspension, the difference between the original and filtered suspension was small. The dissolved concentration did not change by filtering the sample. Due to the dissolved iron in the sample, the measured conductance was as high before and after the filtering.

For comparison, deionized and tap water were also measured. Also the filtered iron of RNIP was re-injected into deionized water to see whether this would change the conductance. There was a slightly higher conductance measured, which was thought to be within the measurement error, and might also have been due to a small amount of surfactants that were perhaps injected together with the iron.

From these measurements it could be seen that the surfactants had a much larger effect on the electric conductance than the nano-iron itself. There might only be a large change due to the iron if the particles would be connected to each other. As long as they exist as free colloids, do not touch each other and are available in relatively low concentrations, there will be no change in the electric conductance due to the nano-iron. If in a field test the electric conductivity is measured when using reactive nano-iron of Toda Kogyo, this will give a good estimation of the injection extend. And thus can tell where the front of the injection is. This will though give no information about the spreading of the nano-iron itself. The nano-iron is transported at a much slower velocity and most likely will have a maximum transport distance as was seen in the previous experiments.

Tab. 2.4: Conductivity Measurements. (Device: WTW LF 325-A; Used settings: Tref 25deg; nLF 0.475; TP; ARng)

Sample	Electric Conductivity ( $\frac{\mu S}{cm}$ )
FZK suspension	387
FZK susp. without iron	291
RNIP suspension	8360
RNIP suspension without iron	8900
RNIP filtered, susp. in de-ionized water	8.9
de-ionized water	2.8
tap water	314

## 2.9 Stirred vs. Disperged and Stirred Nano-Iron Suspensions

It was seen in the previous experiments that the nano-iron particles tend to aggregate. Especially the older suspensions appeared to have build large aggregates. It was expected that this is an important factor limiting the transportability.

A disperger is a device that breaks up agglomerations and creates a well mixed suspension. The disperger contains of a rotor and a stator (see fig 2.17), the rotor rotates at velocities up to 15 000 *rpm* within the stator. The shear forces that are exercised on the suspension break down the aggregates. The velocity, and with that the shear force, can be set accurately on a digital control box. The disperger can circulate the nano-iron suspension through a container (see fig 2.16).

To test whether the disperging would improve the transportability of nano-iron, a horizontal capillary tube and column experiment were done, sedimentation curves of disperged and non-disperged suspensions were created, and a batch experiment to test whether the disperging creates a change in reactivity on PCE was performed. The disperger used was a Megatron MTG 36/4 produced by Kinematica AG. (Littau-Lucerne, Swiss), which has been developed in cooperation with the ETH Zürich (Swiss).

### 2.9.1 Transport in a Horizontal Capillary Tube

#### 2.9.1.1 Methods

As a first experiment, a horizontal capillary tube experiment was performed. In this experiment a capillary glass tube of 1.5 m length and a inner diameter of 3.6 mm was used. A 50 ml syringe pump (Harvard Apparatus Pump '44') was connected on the outlet side, at the inlet side the nano-iron reservoir was connected. The reservoir was equipped with a mixer in order to keep the nano-iron in suspension during the experiments. The reservoir contained 7 liters of nano-iron suspension with a concentration of 20 g Fe<sup>0</sup>/l, the suspension could be disperged by turning on the disperger (See figure 2.15). The syringe pump could be accurately set to a certain discharge. This way, by knowing the diameter of the capillary tube, the average velocity could be controlled and would be constant. The transport of nano iron was simulated with one pore volume of the capillary tube, the average velocity used was 1 mm/s = 3.6 m/h. The flow could be assumed laminar since the Reynolds number was 3.7 (also see eqn 2.4)

First the non-disperged suspension was injected in the capillary tube. Next the suspension was disperged, the tube was cleaned and the disperged suspension was injected.

Reynolds Number (Re):

a dimensionless indicator for the type of flow. In a pipe, Re needs to be below 2300 for laminar flow, above this value, the flow is Turbulent. Re is calculated by

$$Re = \frac{\rho_l V_{avg} D}{\mu} \quad (2.4)$$

where  $\rho_l$  is the fluid density (kg/m<sup>3</sup>),  $V_{avg}$  the average flow velocity (m/s),  $D$  the pipe diameter (m) and  $\mu$  the dynamic viscosity (kg/m·s) [Çengel and Cimbala, 2006]

#### 2.9.1.2 Results & Discussion

Within the capillary tube the maximum distance of nano-iron transport before complete settlement was observed. It was seen that the nano-iron was further transported at higher velocities (fig. 2.13). Thus the velocity of the water needed to be high enough to keep the nano-iron particles in suspension. From a certain velocity on the horizontal drag force will be large enough to completely compensate for the vertical gravity component acting on the nano-iron particles within the length of the column. This confirms the hypothesis stated in the 2-D container experiments, where a maximum transport distance was observed as well. Since the velocity decreases parabolic with the distance from the well, this minimum velocity bounded the transport distance. (This velocity is further investigated in section 2.9.3.)

Within a pipe the velocity profile is parabolic (see fig. 2.14), at the boundaries the velocity is zero and in the center it is approximately twice the average velocity. The nano-iron is kept in suspension from a certain minimum velocity. Close to the boundaries the flow is thus unable to keep the nano-iron in suspension. This will create a sedimentation of the nano-iron. In a horizontal flow the nano-iron at the bottom will create a sedimentation bed. The particles in the upper part will fall downward and will reach the high velocity regime and will thus be kept in suspension in that part.

In the capillary experiment it was visible that this three region transport distribution was present. From a certain distance on all the particles, that were in suspension in the beginning, were sedimented. No transport of nano-iron was observable from that distance on. Further away from the inlet, the amount of nano-iron in suspension was reducing significant. Only the most stable (probably the smallest) particles stayed longer in suspension. The nano-iron thus tended to sediment rapidly at small velocities. At higher velocities the drag force was strong enough and it could keep more particles in suspension over a larger distance. This indicated that the gravity played a role in the transport.

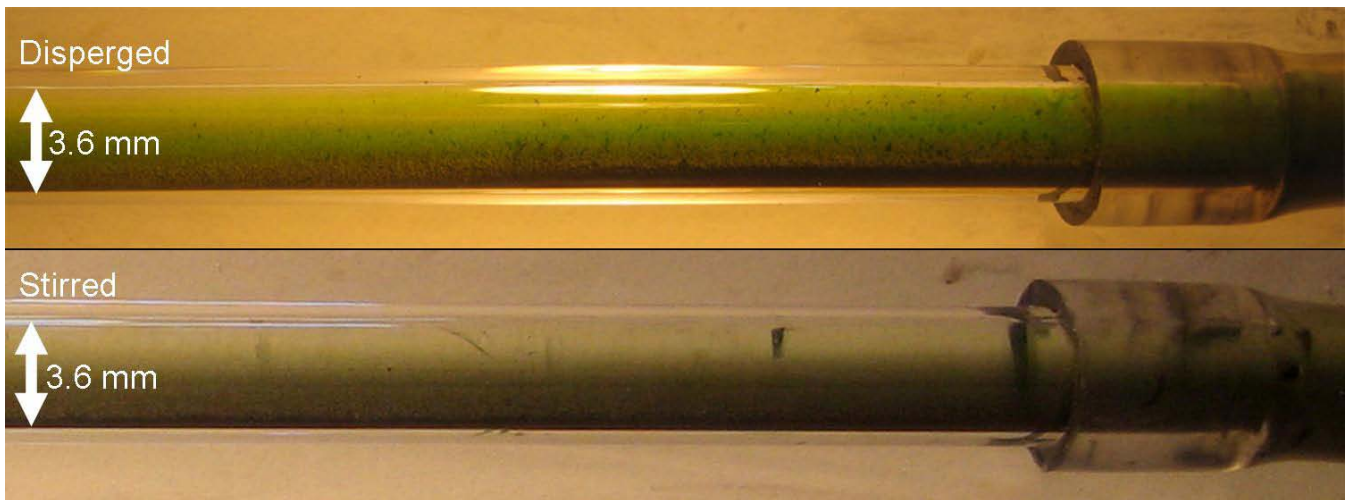


Fig. 2.13: Top: Transport of disperged nano-iron. Bottom: Transport of non-disperged nano-iron. Both suspensions are continuously stirred in a container to keep the nano-iron in suspension before injection

## 2.9.2 Transport in a Horizontal Column

### 2.9.2.1 Methods

The second experiment was done with a pipe with an inner diameter of 36 mm and a length of 1.2 m. The pipe was vertically filled with coarse sand (Dorsilit #7 0.6 - 1.2 mm). The filling was done with dry sand which was lightly compacted by tapping the pipe with wood clogs during filling, which afterwards was flooded with three pore volumes of  $CO_2$  gas to remove all air in the column. After this the degassed water was injected. Most of the  $CO_2$  gas was pushed out, the remaining  $CO_2$  gas dissolved in the water, resulting in a fully saturated filling. In total two columns were filled this way, one for a non-disperged suspension and one for a disperged suspension.

The hydraulic conductivity of the porous media was determined by applying hydraulic gradient of 5.6 cm over the column. For a period of at least 1 hour the water that flowed through was captured and weighted afterwards. By applying Darcy's Law (also see eqn. 2.5), the hydraulic conductivity was calculated.

The transport experiment was done in a horizontal setting, this was thought of to minimize the influence of gravity on the transport.

Within the columns the transport behaviour of the nano-iron could be observed. Both experiments were done with degassed water as carrier for the nano-iron. The pH value of the suspension of nano-iron

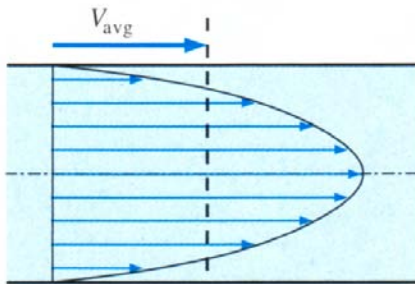


Fig. 2.14: Laminar velocity profile in a pipe. From Çengel and Cimbala [2006]



Fig. 2.15: Disperger setup

in degassed water was approximately 10.5, at a concentration of 20 g  $Fe^0/l$   $H_2O$ .

The pump rate was set such that the velocity in the pores would be on average 1 mm/s.

#### Darcy's Law:

Darcy's equation is valid for flow as long as the flow is laminar (eqn. 2.4). The Darcy equation (2.5) assumes flow to occur over the entire surface area of a soil column. The actual velocity in the pore space is greater than the Darcy velocity. It is called the pore velocity ( $v$ ) and is defined as the volumetric flow rate per unit interconnected pore space.

$$Q = qA = AK \frac{dh}{dx} \quad (2.5)$$

$$v = \frac{q}{n_e} \quad (2.6)$$

Symbols:  $Q$  the total discharge ( $m^3/s$ ),  $q$  the Darcy velocity ( $m/s$ ),  $A$  the total cross-sectional area ( $m^2$ ),  $K$  the hydraulic conductivity ( $m/s$ ),  $\frac{dh}{dx}$  the hydraulic gradient ( $m/m$ ),  $v$  the pore velocity ( $m/s$ ) and  $n_e$  the effective porosity [Darcy, 1856, Schwartz and Zhang, 2003]

### 2.9.2.2 Results & Discussion

To get the velocity of 1 mm/s a pump rate of 0.45  $cm^3/s$  was applied. The untreated nano-iron spreaded unequal through the column. In the bottom the transport was faster, gradually going to a slower transport in the top part. The accumulation of the nano-iron in the bottom part was most likely due to the gravity acting on it.

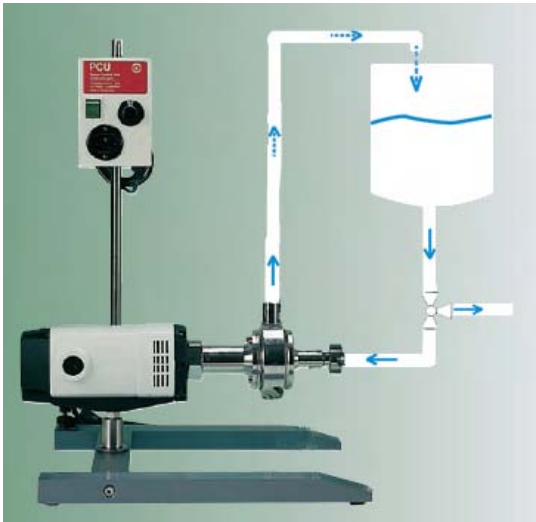


Fig. 2.16: Disperser setup [Kin, 2005]

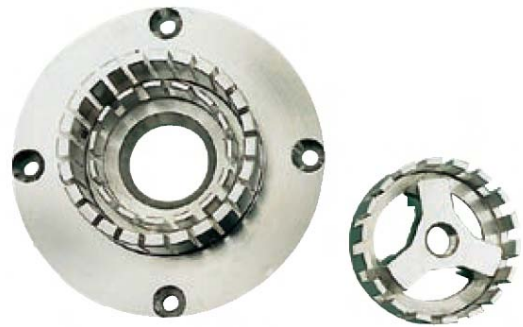


Fig. 2.17: Rotor and Stator used in the MTG 36-48 [Kin, 2005]

The dispersed nano-iron showed a much steeper slope, indicating less difference between the transport in the top and bottom part of the column. Thus the assumption could be made that the influence of gravity declines when the material is dispersed.

In these horizontal columns there was a void space between the inlet and the gaze where the sand was packed upon (app. 3 cm). In this void space the flow velocity was much lower, thus creating time for the nano-iron to settle. There would likely have been no (or only little) nano-iron entering the top part of the column. Therefore the gradient as seen in the pictures was a response to the concentration gradient at the inlet, as well as to the gravity settling during the transport in the porous media.

During the injection the nano-iron traveled significantly slower through the column than the water-front. In the non-dispersed case the concentration of the dye was too low to make it visible (as can be seen in fig. 2.18), for the determination of the breakthrough at the end of the column the concentration was still high enough. The dye broke through at 17.5 min at 120 cm, the nano-iron was at moment at 28 cm. The dispersed nano-iron was at 17.5 min at 39 cm. For the dispersed suspension a higher concentration of the dye was used, explaining the difference in colour between the two pictures.

In these two experiments, the gravity still played a role. But likely not as large as if the column would have been placed vertical, as was done in column experiments performed by others (e.g. Lecoanet et al. [2004], Schrick et al. [2004]).

In the dispersed suspension a large amount of small gas bubbles was present. This originated from the dispersing not from gas building from the reactive iron. During the circulation and mixing of the suspension in the container air was introduced in the suspension. This was dispersed and set into tiny gas bubbles. This might also have obstructed the transport through the top part of the column.

To minimize the amount of air getting trapped in the suspension, in later experiments the outlet of the disperser should be below the surface table of the suspension in the container during the dispersing. The volume of suspension in the container decreased during the injection and thus the disperser output would get below the surface table at some moment. The dispersing should thus be done only before the injection. Whether a non-continuous dispersing will be enough for breaking up the aggregates and whether the suspension will stay dispersed for longer time will be tested and described in the next section.

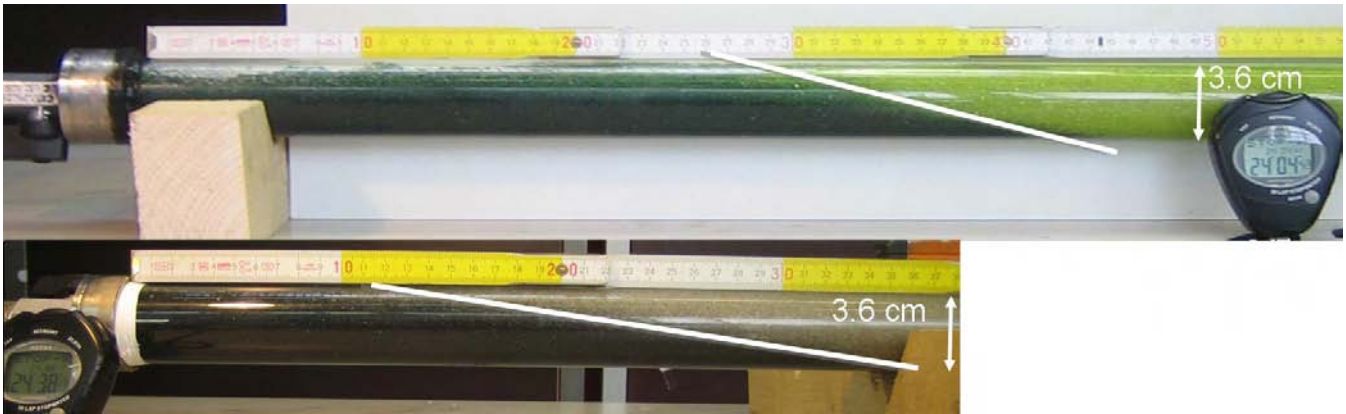


Fig. 2.18: Top: spreading of dispersed nano-iron, at 24 min. Bottom: spreading of nano-iron without being dispersed, at 24 min

### 2.9.3 Sedimentation Rate

#### 2.9.3.1 Methods

With the use of a hydrometer (also called a Bouyoucos hydrometer) the sedimentation rate was determined. This was based on the density of the fluid which changes during the sedimentation period. Water containing material in suspension has a greater density than pure water. The more material in suspension, the greater the density. The method of Dunford and Lorentz [see 1994, chap. 3.3] was used as guide to determine this.

The hydrometer (VWR NFB 35511, BS 718, ISO 649) was used to measure the density of the suspension. The higher the hydrometer floats, the lower the density of the suspension. The glass vessel used was 0.5 l with a diameter of 50 mm and a height of 250 mm.

During the experiment at different stages of the sedimentation, the density was measured. By plotting the density against the time, a sedimentation curve could be constructed. During the experiment the observed sedimentation was recorded with a digital camera. Both the undispersed and the dispersed suspensions were measured.

The calculated settling velocity (or terminal velocity) follows from Stokes' Law (eqn. 2.10). The settling velocity calculated is:  $2.81 \cdot 10^{-8} \text{ m/s}$  for a nano-iron particle of 100 nm, used constants:  $g = 9.81 \text{ m/s}^2$ ,  $\rho_p = 6150 \text{ kg/m}^3$ ,  $\rho_l = 998 \text{ kg/m}^3$ ,  $\eta = 1 \cdot 10^{-3} \text{ kg/m} \cdot \text{s}$  and  $D = 1 \cdot 10^{-7} \text{ m}$ .

Stokes' Law:

George Gabriel Stokes derived an expression for the frictional force exerted on spherical objects with very small Reynolds numbers (e.g., very small particles) in a continuous viscous fluid.

The forces action on a spherical particle are equated to determine the relationship between the settling velocity and the particle diameter.

$$\mathbf{F}_{friction} = \mathbf{F}_{down} - \mathbf{F}_{up} \quad (2.7)$$

The downward force on the particle due to its weight in water is:

$$\begin{aligned} \mathbf{F}_{down} &= \rho_p V_p g \\ \mathbf{F}_{down} &= \frac{4}{3\pi} \frac{D^3}{8} \cdot (\rho_p - \rho_l) g \end{aligned} \quad (2.8)$$

where  $\rho_p$  is the density of the particle,  $\rho_l$  is the density of the liquid,  $V_p$  is the volume of the particle,  $g$  is the gravitational acceleration,  $D$  is the diameter of the particle.

The opposing force due to viscous resistance is

$$\mathbf{F}_{up} = 3\pi D\eta v \quad (2.9)$$

where  $\eta$  is the fluid viscosity and  $v$  is the velocity of fall.

Equating these forces yields the fall velocity in terms of the particle diameter and properties of the solid and liquid.

$$v = \frac{g(\rho_p - \rho_l)}{18\eta} D^2 \quad (2.10)$$

Equation 2.10 is Stokes' Law. Stokes' Law assumes that: (I) The terminal velocity is attained as soon as settling begins, (II) Settling and resistance are entirely due to viscosity of the fluid, (III) Particles are smooth and spherical and (IV) There is no interaction between individual particles in the solution [Dunford and Lorentz, 1994, Çengel and Cimbala, 2006].

### 2.9.3.2 Results & Discussion

Both suspensions had an initial concentration of approximately 40 g/l. From the measurements of the density the ratio of measured concentration over initial concentration could be calculated. The curve given in figure 2.19 could then be constructed from this. The concentration of the untreated nano-iron decreased very rapid. Within 20 minutes almost all the nano-iron was settled. The disperged nano-iron took almost 2 hours to get to a minimum value, which was even then still above the minimum of the non-disperged nano-iron. Comparable sedimentation curves were also presented by Saleh et al. [2006].

The volume of water that holds the nano-iron decreased with time. The particles in suspension settle, leaving clear water in the upper part. The height of the particles in suspension in the vessel is plotted in figure 2.20 for both suspensions. During the settling it was seen that there was a volume of water on top that contained no nano-iron. This volume increased with time, the volume of water containing the nano-iron decreased. Though this did not give a quantitative relation of the sedimentation, the two curves could be qualitatively compared to each other.

The curves show that the non-disperged suspension settled much faster. The final sedimented bed

thickness of the dispersed suspension was larger. Because both the suspensions contained an equal initial concentration, the density in the dispersed suspension should have been less.

The settling velocity calculated was:  $2.81 \cdot 10^{-8} \text{ m/s}$  for a nano-iron particle of  $100 \text{ nm}$ . The hindered velocity (eqn. 2.11) would be in this case  $v_h = 2.74 \cdot 10^{-8} \text{ m/s}$  (with  $C_v = 5 \cdot 10^{-3}$ ), which shows that this difference is minimal and insignificant in the used concentration.

#### Hindered Settling Velocity:

Hindered settling occur when high densities of particles in suspension result in an interaction of particles. The displacement of water produced by the settling of one particle affects the relative velocities of its neighbours. A correction for hindered settling can be calculated by using this equation

$$v_h = v \cdot (1 - C_v)^{4.65} \quad (2.11)$$

where  $v_h$  is the hindered velocity ( $\text{m/s}$ ),  $v$  the free settling velocity ( $\text{m/s}$ ),  $C_v$  the volume of particles divided by the total volume of the suspension (-) [EPA, 1999].

The observed settling velocity for the non-dispersed suspension was approximately  $v_{obs,non-disp} \approx 1.1 \cdot 10^{-4} \text{ m/s}$  and for the dispersed suspension  $v_{obs,disp} \approx 2.7 \cdot 10^{-5} \text{ m/s}$ . These velocities are not even close to the calculated settling velocity. From this it can be assumed that the particles were aggregated and thus no longer of nano-scale size. From the determined settling velocity an approximation of the particle size can be made. The determined velocity is then used as the settling velocity in Stokes' Law, giving the diameter of the particle. For the non-dispersed suspension this is:  $D_{non-disp} \approx 6.2 \cdot 10^{-6} \text{ m} = 6.2 \text{ }\mu\text{m}$ , and for the dispersed suspension:  $D_{disp} \approx 3.1 \cdot 10^{-6} \text{ m} = 3.1 \text{ }\mu\text{m}$ . This would mean that the aggregates are approximately 50 times larger than the assumed diameter of the individual particles.

## 2.9.4 Reactivity

### 2.9.4.1 Methods

To test whether the reactivity of the dispersed nano-iron was altered by dispersing the material, a batch experiment was set up.

Two solutions of 1 liter degassed tap water (without further treatment) with a PCE concentration of  $1.5 \text{ mg/l}$  were mixed with  $0.2 \text{ g Fe}^0$  stirred nano-iron and dispersed nano-iron each. With a HPLC-UV device (High Performance Liquid Chromatography) the concentration of PCE was determined over a 48 hour period. During this period the mix was shaken regularly to keep the nano-iron in suspension, at the larger interval periods the vessels were placed in a rotational shaker to mix the suspensions.

### 2.9.4.2 Results & Discussion

The PCE concentrations for both the dispersed and original suspension were measured with the HPLC-UV and are presented in the graph in figure 2.21. From the results of this batch experiment no significant difference between both suspensions could be observed for the short term reactivity. Most of the chemical

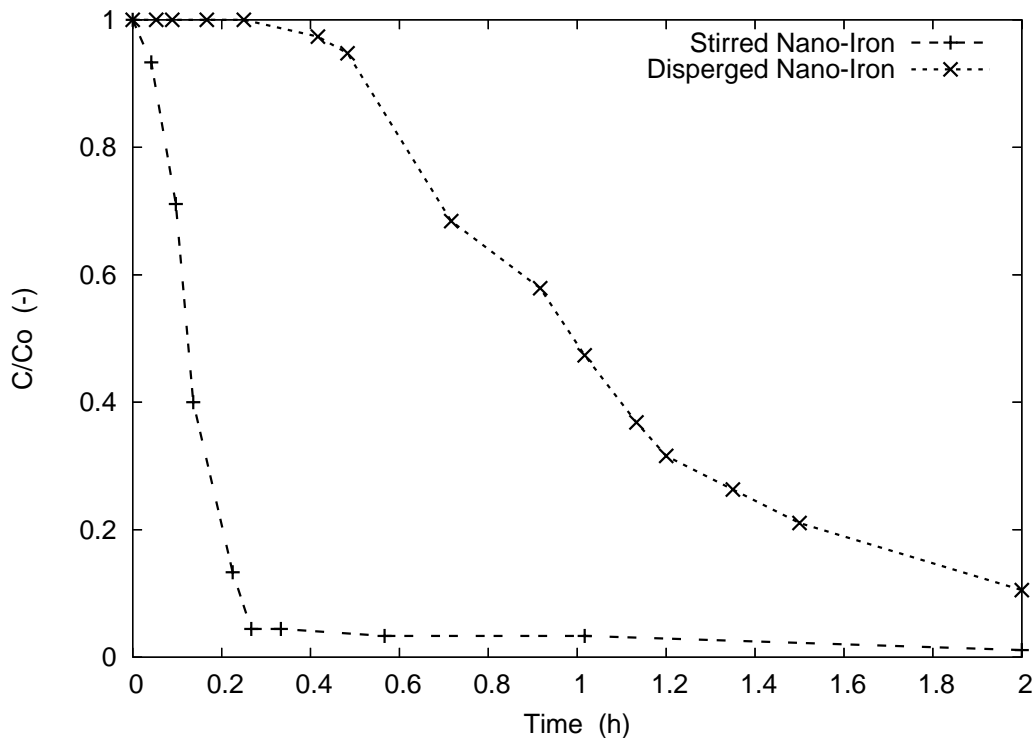


Fig. 2.19: Concentration change due to sedimentation of the nano-iron. Both suspensions had an initial concentration of 40 g/l

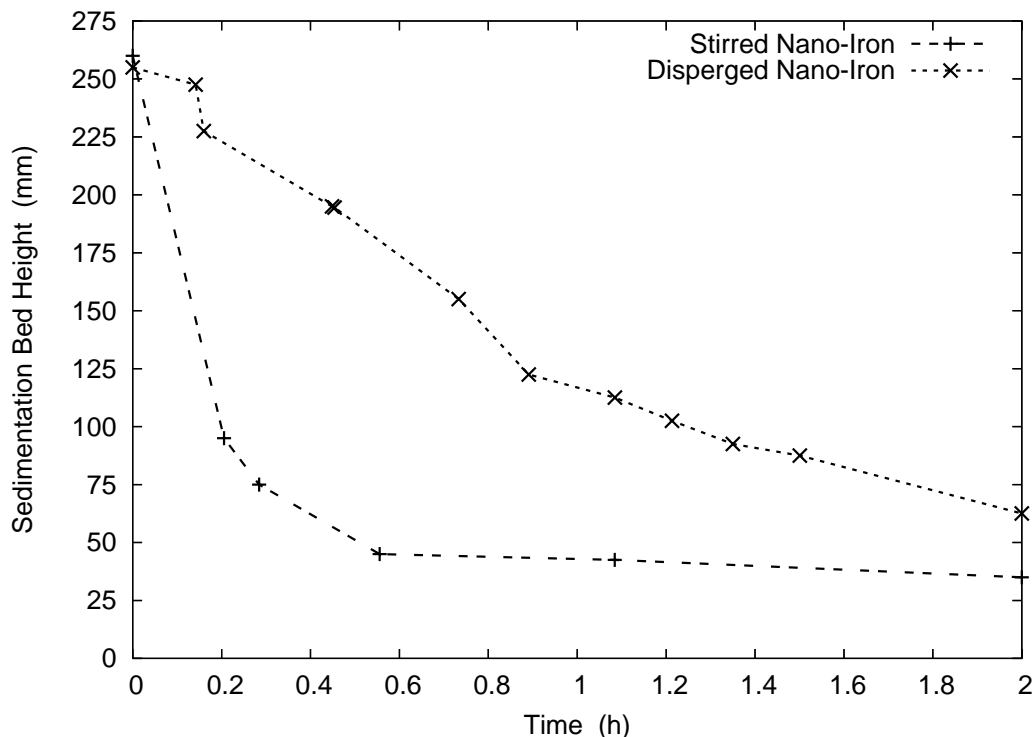


Fig. 2.20: Plot showing the decrease in sedimentation bedding height with time. Based on visual observation

reaction occurs in the first few minutes for both suspensions. During the experiment both suspensions coloured brownish. Indicating the oxidation and solution of iron. Due to the rotational shaking, the oxygen in the air in the vessels was mixed through the water and the water could no longer be assumed degassed. Due to this, the nano-iron could also react with oxygen. As can be seen in the figure, both

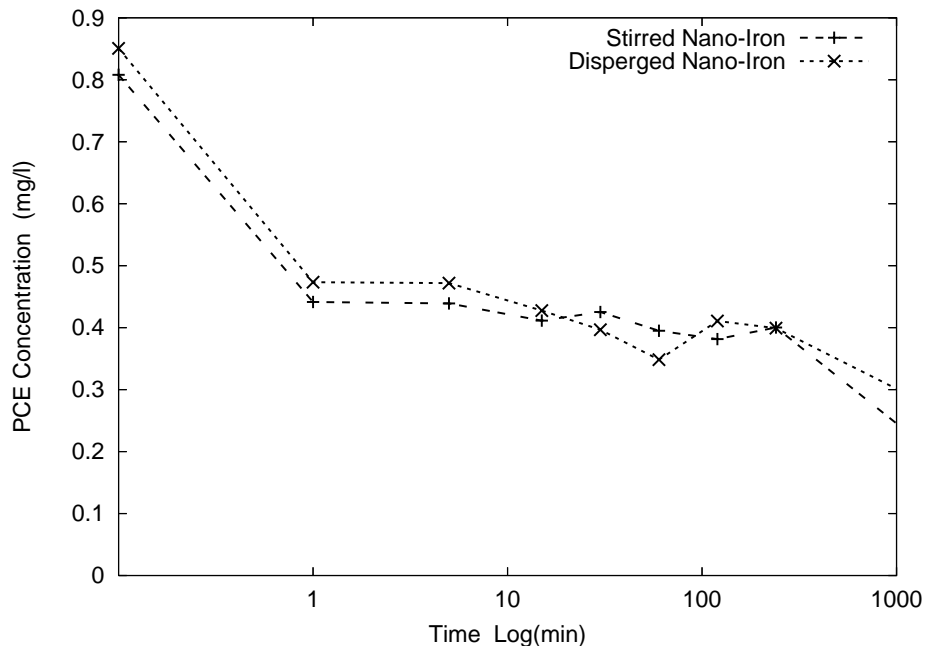


Fig. 2.21: Change of Concentration of PCE during the batch experiment. The initial concentration for the non-disperged nano-iron suspension was slightly higher. Time is in log scale, last measurement at 48 hours

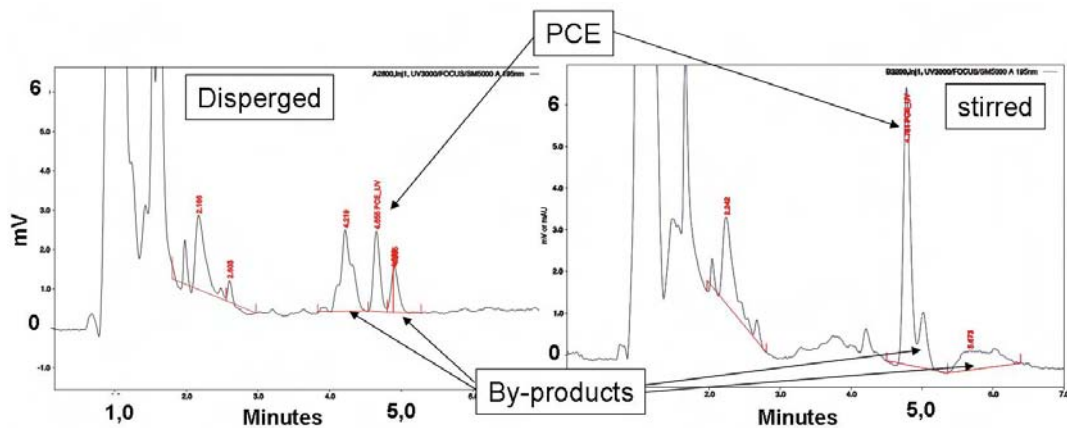


Fig. 2.22: Chemical analyse of the batch experiment after 48 hours

suspensions behaved almost identically in the first 48 hours. Whether this also counts for long term reactivity of several months could not be concluded from these batch experiments. In the chromatograms side-products around PCE were observed. In both suspensions these side-products developed differently. The side-products were not further identified. They might have been unwanted products like cis-1,2-DCE, but might also have been harmless products. These side-products should be identified in future research for the reactivity. To be able to state whether the dispersing influences reactivity, the effectiveness or completeness of dechlorination, more batch experiments should be done. The experiments should be performed twice to make sure that the results are fully reliable and the amount of oxygen introduced in the system should be minimized. The amount of oxygen can be minimized by using Argon as a head space gas and by working in a anoxic glove box, as described by Liu et al. [2005].

## 2.10 Summary

2-D experiments were performed and showed that the transport of two types of nano-iron was highly limited. There were too many unknown variable conditions to be able to identify the cause of the limited spreading. Several small scale experiments were performed to get a better understanding of the behaviour and the characteristics of nano-iron.

For horizontal column experiments the void space between the input tube and the inlet gaze should be as small as possible. Then a vertical concentration gradient at the inlet might be avoided.

A simple metal detector was build to test the possibility of using a metal detector to identify nano-iron against a large natural background iron content. This was not possible with chemical detection techniques. The first results showed that the nano-iron could be seen, but not quantified and the detector was too instable to be used for column experiments. A professional metal detector was also tested and the results of this device were promising. It was decided that this device would be used in the following 1-D experiments.

Several measurements during and after an injection can give information about the radius of influence and the spreading of the injected suspension.

It was shown that the electric conductivity of the nano-iron suspension was much higher than normal water, also after the nano-iron particles were filtered out. An electric conductivity measurement of the water flowing through observation wells, a conservative dye or a calculation based on the hydraulic permeability of the aquifer material could be used to determine the spreading extend of the injection plume. Nevertheless, this can not be used to determine the spreading of the nano-iron, since there is not yet a known relation between the injection extend and the spreading of the nano-iron particles.

In the experiments it was shown that the gravitation played a large role in the transport of nano-iron. The particles settled much faster than was expected for nano-particles, which was most likely the result of nano-particles forming micro-sized aggregates. Further it was shown that a horizontal orientation of a column was the best position to minimize the influence of the gravitation and to simulate a more natural situation, where the injection is also expected to take mainly place in a horizontal direction.

Disperged nano-iron was able to be further transported. It settled slower and thus stayed longer in suspension during transport. The large shear stresses break down the aggregated particles into smaller aggregates or single colloids. It was possible to keep the nano-iron for a long time in suspension by gently stirring the suspension after it had been disperged. From the behaviour of the disperged material it can be carefully concluded that it behaves like a fresh nano-iron suspension.

In a batch-experiment the reactivity of a disperged nano-iron suspension was compared with a non-disperged suspension. This showed that both suspension were equally fast and effective in removing PCE at a short time scale.

From the described experiments an idea for a setup was developed to make it possible to systematically investigate the factors of influence on the mobility of nano-iron.

## 3. 1-D TRANSPORT EXPERIMENTS

### 3.1 Introduction

In chapter 2, many questions raised from the preliminary experiments about the transportability of the nano-iron during the injection. A well known propagation of the nano-iron in the subsurface is necessary for the remediation technique to be successful.

The results of the preliminary experiments suggested that the limited transport of nano-iron depended on

- the age (and with that the aggregation stage) of the particles
- the discharge and with that the pore velocity during injection
- the concentration of the suspension during injection
- the grain size distribution as well as the permeability and heterogeneity of the porous media

To investigate in which way the above mentioned factors influence the transport of nano-iron in porous media, a series of column experiments were performed. The experiment constructed consisted of

- a transparent column with a length of  $2\text{ m}$  (to ensure that transport can be observed)
- the column was placed horizontal and had a small inner diameter ( $3.6\text{ mm}$ ) (gravity effects were minimized due to this diameter in combination with the horizontal orientation)
- a constant flow was created with a peristaltic pump at the outlet side
- a reservoir containing the nano-iron suspension was connected to the inlet side (to prevent settling of nano-iron in the tubing)

When the method is to be used for a permeable reactive barrier (section 1.2), only a low concentration of nano-iron is necessary. Low concentrations of nano-iron are difficult to identify in the subsurface due to the natural occurrence of iron (also see section 1.5). Iron is measurable with several techniques, but it is difficult to distinguish between the injected nano-iron and the natural occurring iron.

In field situations, often chemical detection of iron is used, which is unreliable due to the geogenic iron occurrence. Also the chemical change of the groundwater, like a lowered CHC concentration, which should be a result of the nano-iron reaction, is used as a detection method. This can also be an effect of the injection fluid spread (e.g. dilution or mobilization) instead of the nano-iron itself.

To get a quantitative and reliable determination of the nano-iron concentration in the 1-D flow experiments a new detection technique was developed. The new method consisted of a metal detector that could move along the column and register the iron content due to the electromagnetic induction that is induced by the presence of iron. A high accuracy could be reached and geogenic iron occurrences could be removed by using the difference of a measurement before and after the injection of nano-iron.

In the preliminary experiments, it was also shown that the nano-iron transport was significantly delayed and appeared to have a maximum injection extend. The 1-D transport experiments were thought of to quantify these effects.

In the original setup of the experiments one base case was thought of as a starting point. From this setting each time one variable was to be varied. Then it should have been possible to compare each one with the base case.

Due to time shortage and difficulties to keep all variables constant except for one, this comparison could not be made for each experiment. Three sets of experiments were performed where each time one variable was changed and between the sets more variables were changed. This way the effect of one variable could be individually investigated. Because more than one variable was changed between the sets, it was not yet possible to quantitatively compare the changes of one set of experiments with another. Within a set of experiments the effect of one altered variable could be quantitatively described.

## 3.2 Methods

To make it possible to determine and visualize the transport of nano-iron a new setup was constructed. In the following section the setup will be described, the material and used conditions for the different experiments will be given in the succeeding sections.

### 3.2.1 Setup

For the experiments columns were used that were 2000 *mm* long and had a 36 *mm* inner-diameter. They consisted of transparent Plexiglas (Acrylglas XT, Ernst Kienzle GmbH, Stuttgart).

The effect of the wall can be fully neglected for mass transport in a porous media if the diameter of the column is at least 50 times the grain size, which is a common used rule of thumb [Bruining, H., April, 2006]. If a mono grain size of 3 *mm* is to be used, this would already result in an inner diameter of the column of 150 *mm*. For the used diameter (36 *mm*) a maximum mono grain size of 0.7 *mm* would than have to be used at maximum.

There were a few reasons why the diameter of the column was not made as large as the common rule of thumb tells it should be. In order to prevent too large effects of the gravity acting on the particles during movement, the column diameter needed to be kept small. The amount of necessary nano-iron to do several experiments in the column would be huge if a column of 2 *m* length and 15 *cm* length were to be filled. Furthermore the metal detector that was planned to be used could without too many changes, be made applicable for a column with a maximum outer diameter of 45 *mm*.

This resulted in the decision to use a column with an inner diameter of 36 *mm*, in which small boundary effects are likely to occur, but which were expected to be of no significance for the experiment in total.

In the preliminary experiments it was shown that the transport was partly dependent on the gravitation (e.g. fig. 2.9 or section 2.9.2). Because of this, the 1-D flow experiments were also done in a horizontally placed column.

In a horizontal column the gravity force is oriented perpendicular to the mean flow direction. In a 1-dimensional experiment the discharge is constant through the whole set-up, and the packing of the

porous media is assumed to be homogeneous resulting in a flow velocity that is equal at all locations within the column. The flow field is thus assumed to be 1-dimensional. In the preliminary research the test setup with a horizontal column still showed some apparent gravitational influence. This was assumed to be partly related to the large void space between the inlet and the filter gaze, resulting in a sedimentation of the nano-iron before entering the sand packing in the column. For the 1-D transport experiments the inflow and outflow plugs (fig. 3.1) were improved, which minimized this effect.

The plugs used were made of PTFE (fig. 3.1). The plugs were constructed out of two parts that could be tightened together in order to push out a rubber ring, which fixes the plug in the column. A PTFE gauze (Sefar Nyal, PA5-HD225, mesh-opening  $225 \mu\text{m}$ ) was pulled over the front of the plug to create a larger contact area with the sand in the tube and prevent small grains to get into the plugs. The screws, valves and tube-nipples were made of PVC. The whole setup of the column and plugs was thus constructed without any iron parts.

The inner wall of the column was made rough at both sides with coarse sandpaper at a length of  $7 \text{ cm}$  to prevent the in- and outflow plugs from sliding out.

The column was placed vertically on a shaker platform (originally a sand sieve shaker, Frisch Analysette 03 502), with a plug on the bottom side placed. A pipe with a funnel on top was used to fill the column. To create a random ordering of the sand grains in the column a mouthpiece (fig. 3.2) was placed on the bottom of the pipe. The mouthpiece contained two wire gauzes which were placed on a  $45^\circ$  angle to each other, which scattered the sand grains twice.

During the filling the mouthpiece was moved constantly upward such that a  $5 \text{ cm}$  distance was preserved between the sand in the column and the mouthpiece, a reproducible near homogeneous packing could be made in this way. When the column was full, the column was tapped with two woodblocks to create a further compaction of the sand. The top side was closed with a plug and tubes were connected to the bottom and top plugs. From bottom to top  $\text{CO}_2$  gas was pushed through (app. 3 pore volumes), which replaced the air in the pore spaces. Next the column was filled from bottom to top with degassed tap water. The remaining  $\text{CO}_2$  gas dissolved in the water which made it possible to create a fully saturated column. The degassed water was held in a glass reservoir of 300 liters. The water had an oxygen content of approximately  $1 \text{ mg/l}$ . The column was flushed with at least 3 pore volumes to remove the  $\text{CO}_2$  and the finest sand particles.

When the column was saturated and flushed with water, it was placed horizontally in a framework. Since a metal detector was to be used for the measurement of the nano-iron distribution and interference from other iron should be prevented be present, in an radius of at least 1 meter around the metal detector no metal parts should be present.

The framework was made completely from wood and contained no metal parts. The column was now situated  $1.5 \text{ m}$  above the floor (concrete reinforced with metal), this prevented the metal in the concrete floor to interfere with the metal detection. Alongside the framework a carrier could be moved at a constant velocity of  $1 \text{ mm/s}$  on a rails, the carrier held a wooden framework with the metal detector. Within one of the coils of the metal detector the column was placed. The columns outer diameter of  $4.4 \text{ cm}$  fitted within the coil, which was also a reason for using this diameter for these experiments.

The inflow and the outflow end were connected to a constant head tank. The water level between

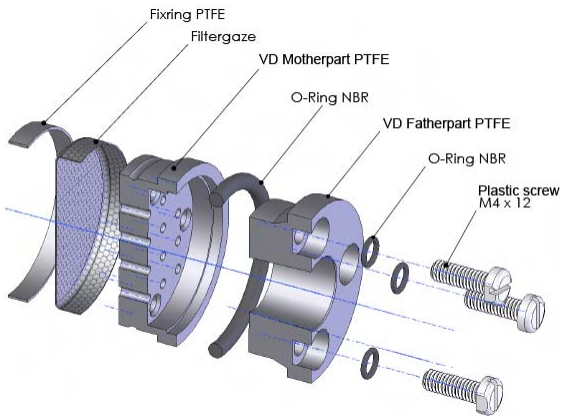


Fig. 3.1: Technical drawing of the plugs used in the 1-D flow experiments

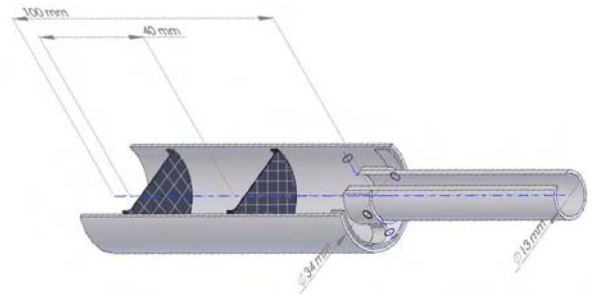


Fig. 3.2: Technical drawing of the mouthpiece, used to homogeneously pack the column

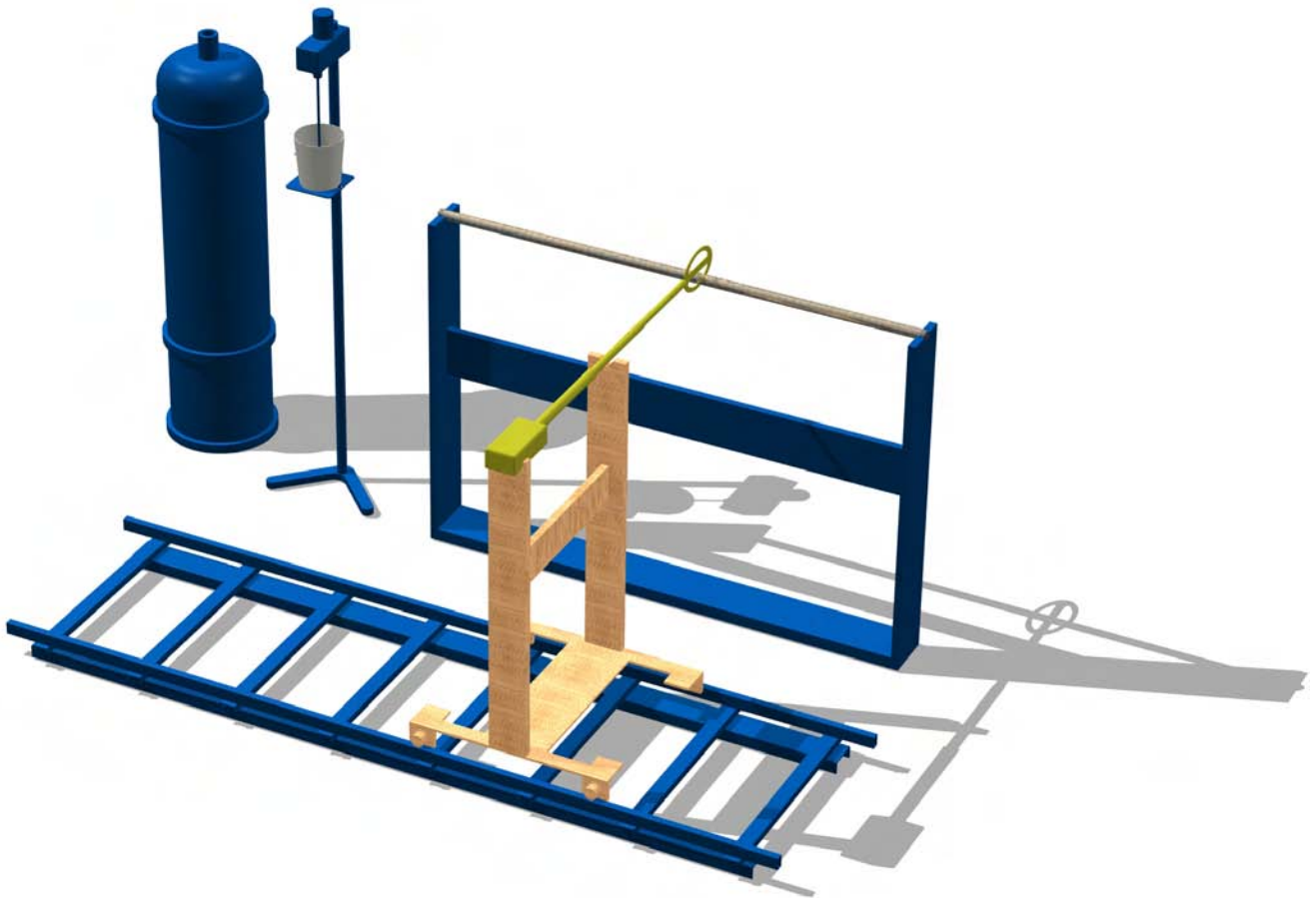


Fig. 3.3: Setup of the 1-D flow experiment. The degassed water container and the nano-iron stand with mixer can be removed to prevent influence on the measurement. The metal detector can move over the rail at a constant velocity. The framework holding the column is made of wood, the column is positioned 1.5 m above the ground, column has a length of 2 m and has an inner diameter of 3.6 mm. The pump was placed on the outlet side, righthand side in the picture

both tanks could be varied 70 cm, creating a head difference and thus a constant flow through the column. Based on the amount of water flown through in a given time at a fixed gradient, the hydraulic conductivity of the column was calculated (see eqn. 2.5). After the determination of the hydraulic

conductivity, the constant head tanks were disconnected.

A set-up overview of the experiment is given in figure 3.3. At the inflow side of the column (left hand side in the picture) a bucket was placed such that the bottom was at the same height as the column inlet. This bucket contained the nano-iron suspension and from this tubes went to a disperger (Kinematica, see fig. 2.16 and section 2.9 for more information). This way the nano-iron suspension could be fully disperged before the injection. In the bucket a mixer rotates at a constant velocity to keep the disperged nano-iron in suspension during the experiment. The frame with the bucket and the mixer and the disperger could be moved aside, such that they would not interfere with the measurement. The degassed water reservoir was also movable because the reservoir contained heavy metal rings, and needed to be further away from the metal detector during measurements.

The nano-iron reservoir was placed close to the inflow side (approximately 10 *cm* of tubing in total between the container and the inlet). A peristaltic pump (Watson Marlow, 323) was placed at the outflow side, creating a constant flow rate in the column. The pump was not placed between the nano-iron reservoir and the inlet because that might obstruct the continuity in the nano-iron concentration and would create a larger distance between the reservoir and the inlet. In the preliminary experiments the placement of the pump at the outlet proved to work satisfactory. The pulsating effect seen in the capillarity tube (see fig. 2.10) was not observed in the column. This was the result of the lower permeability and the higher pressure the pump has to build up, causing less pressure fall-back during pumping.

Different factors were expected to be of direct influence on the transport. These factors were, the age of the suspension, the suspension concentration, flow velocity and the permeability of the aquifer material. Several were done one condition was changed every time. These experiments were compared with each other in four sets, such that each factor was highlighted.

For all experiments the disperged RNIP nano-iron of Toda Kogyo was used (the duration of disperging and the disperging rate was approximately in proportion to the volume of suspension prepared).

Before the start of most runs a Uranine tracer test was done to test the column packing for unwanted heterogeneities. The nano-iron suspension was always mixed with an Uranine tracer to see the differences in velocities of the water and nano-iron front during each experiment.

During each run every 10, 20 or 30 minutes a photograph was taken (depending on the velocity of the nano-iron transport), after each time interval a line was drawn on the column to indicate the visually observable location of the nano-iron and water front at that moment.

### 3.2.2 Initial and Boundary Conditions

The initial and boundary conditions of the base-case experiment were chosen such that they compare to field conditions. The base-case pore velocity was  $5.3 \cdot 10^{-5} \text{ m/s}$  which was created by a constant discharge with the pump at the outflow side. An input nano-iron suspension concentration of 10 *g/l* was used. The hydraulic conductivity was approximately  $1 \cdot 10^{-3} \text{ m/s}$  (this value depended on the chosen sand).

The pore velocity of the base-case experiment was based on the data of a field test of ALSTOM (after Müller et al. [2006b] and provided information through personal communication with ALSTOM). In the field test of ALSTOM a spreading of the nano-iron of at least one meter was determined. At a distance of 0.5 m full transport should thus have been possible based on this information. The velocity at 0.5 m from the injection well was calculated based on a parabolic decrease of pore velocity with increasing distance from the well. This calculated pore velocity was the base-case pore velocity.

The pore velocity at 0.5 m was calculated as following:

At the field test 11 kg of nano-iron were injected at a concentration of 35 g/l, 315 l total suspension was injected on a filter of 1 m length with a diameter of 5 cm at a discharge of 3 l/min, the average porosity in the field test was 0.30 .

$$v = \frac{Q}{An} \quad (v=\text{pore velocity}; n=\text{porosity})$$

$$Q = 3 \text{ l/min} = 5 \cdot 10^{-5} \text{ m}^3/\text{s}$$

$$A = 2 \cdot \pi \cdot r \cdot b \quad (r = \text{distance from well}; b = \text{thickness of aquifer})$$

$$A|_{r=0.5m; b=1m} = 2 \cdot \pi \cdot 0.5 \cdot 1 = 3.1416 \text{ m}^2$$

$$v = \frac{5 \cdot 10^{-5}}{3.1416 \cdot 0.30} = 5.305 \cdot 10^{-5} \text{ m/s}$$

The pore velocity of  $5.3 \cdot 10^{-5} \text{ m/s}$  was used as the base-case velocity.

In the first nano-iron experiments performed at VEGAS and most of the experiments in the preliminary research, an input-concentration of 10 g/l was used. This concentration was the base-case concentration.

In table 3.1 all performed experiments are presented with the set conditions. The four last columns show how the experiments were compared to each other. Some experiments were performed in column that was also used for a previous experiment. The spreading in the previous experiment had then been minimal enough to reuse the column by injecting the nano-iron suspension from the other side (i.e. the column was turned around). In these experiments the spreading of the second injection was expected not to reach the nano-iron injected in the first experiment from the other side. The experiment pairs performed in the same column were #'s 1 & 2 ; 3 & 4 ; 5 & 7 ; 6 & 8 and 10 & 11.

#### Addendum:

The above calculated base-case velocity was to be used for the experiments. In the calculation of the pumprate to achieve the desired velocity in the experiments, an error was made. Unfortunately, this error was discovered after all experiments had been conducted. This incorrect pumprate resulted in a discrepancy of the pore-velocity by a factor  $n^{-2}$ , where n is the porosity. Hence, for porosities of 0.35 and 0.25 the factor was 8.2 and 16, respectively. Therefore, the simulated velocities are higher than those in the chosen field test.

Nevertheless, since the experiments showed that the spreading of the nano-iron depends much more on the concentration of the input suspension than on the pore velocity, the results are applicable.

While in the rest of the thesis, all the velocities have been corrected accordingly, this has no effect on the general result and the conclusion of this experimental work.

Tab. 3.1: Experiments overview. The last four columns show if the experiments were compared with each other by the used (A) concentration, (B) velocity in Dorsilit sand, (C) velocity in Rhine-Valley sand and/or (D) sand type. The experiments with a  $\diamond$  were included for completeness, since they did not have all conditions such that they were fully comparable

Exp. #	Sand type	Pore Velocity (m/s)	Concentration (g/l)	Disperger rate (rpm)	Disperger time (min)	A	B	C	D
1	0.3-0.8 mm Dorsilit	$4.4 \cdot 10^{-4}$	0.01	9 200	6.0	X			
2	0.3-0.8 mm Dorsilit	$4.4 \cdot 10^{-4}$	0.10	8 600	8.0	X			
3	0.3-0.8 mm Dorsilit	$4.8 \cdot 10^{-4}$	1.00	9 000	5.0	X			
4	0.3-0.8 mm Dorsilit	$4.8 \cdot 10^{-4}$	10.00	9 700	6.0	X	X		X
5	0.3-0.8 mm Dorsilit	$1.1 \cdot 10^{-4}$	10.00	8 400	4.0		X		
6	0.3-0.8 mm Dorsilit	$2.1 \cdot 10^{-4}$	10.00	8 800	3.5		X		
7	0.3-0.8 mm Dorsilit	$8.8 \cdot 10^{-4}$	10.00	8 400	5.0		X		
8	0.3-0.8 mm Dorsilit	$1.6 \cdot 10^{-3}$	10.00	8 500	8.0		X		
9	0-4 mm Rhine Valley	$2.1 \cdot 10^{-4}$	10.00	8 400	2.0			X	
10	0-4 mm Rhine Valley	$4.1 \cdot 10^{-4}$	10.00	8 100	2.0			X	
11	0-4 mm Rhine Valley	$9.9 \cdot 10^{-4}$	10.00	8 400	6.0			X	X
12	0-4 mm Rhine Valley	$3.5 \cdot 10^{-3}$	10.00	8 400	6.0			X	
13	2-3.15 mm Dorsilit	$4.1 \cdot 10^{-4}$	9.00	7 300	8.0			X	X
14 $\diamond$	3-5 mm Dorsilit	$3.8 \cdot 10^{-4}$	10.60	10 100	7.0				X
15 $\diamond$	0-4 mm Rhine Valley	$5.9 \cdot 10^{-4}$	10.40	7 300	8.0				X
16 $\diamond$	0.6-1.2 mm Dorsilit	$4.4 \cdot 10^{-4}$	13.30	10 000	6.0				X

### 3.2.3 (A) Nano-iron Suspension Concentration - Dorsilit Sand

The influence of the nano-iron suspension concentration on the transport of nano-iron was compared for four experiments (#'s 1, 2, 3 and 4). For these four experiments all variables except for the concentration were kept constant. The used sand for these experiments was Dorsilit 1/8, 0.3-0.8 mm, which had a very low natural concentration of iron. The concentrations of the experiment numbers 1, 2 and 3 were respectively a factor of 800; 100 and 10 smaller than the concentration of experiment number 4 of 10 g/l which was the base-case concentration.

### 3.2.4 (B) Pore Velocity - Dorsilit Sand

To test the influence of the flow velocity on the transport of the nano-iron five experiments with different flow velocities were compared with each other (#'s 5, 6, 4, 7 and 8). The used sand was Dorsilit 1/8, 0.3-0.8 mm. The velocities of the experiments numbers 5, 6, 7 and 8 were respectively 0.25, 0.5, 2 and 4 times the pore velocity of experiment # 4.

### 3.2.5 (C) Pore Velocity - Rhine-Valley Sand

The influence of the pore velocity on the transport was also compared for a different sand type (#'s 9, 10, 11 and 12). The sand type 0-4 mm Rhine-Valley sand has lower hydraulic conductivity and a wider sand grain size spectrum. The same sand was also used in the 2-D sandbox experiments as described in section 2.3.1. The pore velocities in experiments 9, 10, 11 and 12 were 0.25; 0.5; 1.23 and 4 times the

pore velocity of experiment # 4 respectively. The hydraulic conductivities of these runs were close the  $4 \cdot 10^{-4} \text{ m/s}$  as given by Müller et al. [2006b].

### 3.2.6 (D) Grain Size Distribution / Hydraulic Conductivity - Different Sand Types

Several experiments were performed with different sand types (#'s 4, 11, 13, 14, 15 and 16) The first performed experiments were used to find out how the setup was operated at best and thus did not yet have the conditions set such that they could be used for the previous three comparisons. Though the ones with as much equal conditions except for the sand type, were compared with each other to get an impression of the relation between the sand type and the transport of nano-iron.

### 3.2.7 Nano-Iron Detection

The basic principle of the metal detector is the same as described in section 2.7. Within the metal detector two independent frequencies of  $19.2 \text{ kHz}$  are generated. This alternating current passes through the two coils and produces an alternating magnetic field. With the presence of metal within reach of one of the coils a difference in the measured frequency from the coils is detected. The two frequencies are demodulated into two phase components,  $0^\circ$  and  $90^\circ$ . The 4 phases (2 for each coil) and the difference between the two coils (i.e.,  $\Delta\mu = f_{190} - f_{290}$ , where  $f_{190}$  is the  $90^\circ$  component of the first frequency) are all recorded on a computer. The data that is of interest for the detection of the nano-iron in one of the coils is the phase signal  $f_{290}$ . The change in frequency in one coil is in linear relation to the metal content inside (or in the vicinity of) the coil. This linear relationship can be seen in the calibration curve given in figure 3.5 and described in the section 3.2.9 & 3.3.2.

### 3.2.8 Signal Analysis

As was planned in section 2.7.1.1, the recorded data was expected to require further analysis. The recorded signal was analyzed by the Hydrodynamics Group of the Institute of Physics at the University of Oldenburg.

The signal was analyzed on the possible presence of a signal characteristic for the nano-iron. On the measured response signal a noise was seen. This noise might have contained information about the material or interference that induced the signal. If such a characteristic was present in the signal, it should have been possible to filter the signal such that only the influence of the nano-iron was left over. Other interfering sources, like bypassing cranes or metal in the floor construction could then also be filtered out.

To be able to process the data at least 10 000 data values were needed per measurement. This was obtained by moving the metal detector at  $1 \text{ mm/s}$  along the column. The metal detector recorded the signal at  $25 \text{ Hz}$ , thus 25 values were recorded per  $\text{mm}$  column length. In total on  $2 \text{ m}$  column length, this resulted in 50 000 recorded values.

### 3.2.9 Calibration

For the calibration of the metal detector, different amounts of dry metal powder were mixed with sand. In order to get a good compaction and to ensure a homogeneous spreading of the metal in the column, water with a weight of 10% of the total sandmass was added to the sand. The metal mass was each time completely mixed with 140 g sand, this filled a section of 10 cm in the column. In the column the iron sand mixtures were separated by a section with 10 cm clean sand for the low concentrations and a section with 15 cm clean sand for the higher concentrations. The whole column was measured by moving the detector at a rate of 1 mm/s along the column.

### 3.3 Results & Discussion

In appendix A for each experiment a short comment is given. The comments are based on the notes that were written during the experiments. Each comment is followed by a short discussion.

#### 3.3.1 Signal Analysis

To analyze the recorded signal of the metal detector, the Hydrodynamics Group of the Institute of Physics at the University of Oldenburg interpreted it as a diffusion process. For a diffusion process they developed a method to investigate the dynamics of the signal [Böttcher et al., 2005]. The dynamics in the signal were reconstructed with the coefficients of a Langevin equation. The analysis was performed on the measured data of experiment number 2, with a concentration of 0.1 g/l. For the Langevin equation two Kramer-Moyal terms were determined. The two Kramer-Moyal terms represent a diffusion and noise component of the signal. This was done for the whole dataset as well as for smaller sections.

In the analysis of the whole run only a negative drift was observed. The noise in the recorded data was strongest in the section where the amount of injected nano-iron reduced (i.e. the front of the nano-iron injection). The smaller sections where either metal or no metal was expected to have been measured, showed that the noise seen represented a pure measurement noise and that there was no drift in these sections.

From this analysis there appeared to be no characteristic signal that could be used to distinguish between the nano-iron and other sources that influence the response.

Based on this analysis, it was decided that the amount of data could be reduced and that the recording could be smoothed, by taking average values.

The averaging and smoothing was done by calculating the average of 10 data points, giving each time one new value. Each set of 10 recorded data points (e.g. 1 till 10) were added to each other and divided by 10, this gave one new data point, next the following 10 recorded data points (e.g. 11 till 20) gave the following data point, this procedure was repeated for the whole dataset. This procedure reduced the original dataset by a factor of 10 and thus made the new dataset easier to handle.

The followed procedure for this averaging as well as the subtraction of both measurements is given in appendix C.

#### 3.3.2 Calibration

In figure 3.4, the recorded metal detection curve for the metal detector calibration is given. For the calibration of the metal detector, each section containing metal gave its own frequency response. The signal of the metal detector was a response to the metal content in the vicinity of the location of the measuring coil. Thus the signal was already changing in the clean sand area when it got close to the section containing metal. In the middle of each iron filled section, the signal was at a maximum because on both sides of the measuring coil an equal amount of metal was present.

From the metal detector the signal was recorded with 25 values per second, the detector was moved at a rate of 1 mm/s along the column. Within each 1 mm the metal response signal was thus recorded

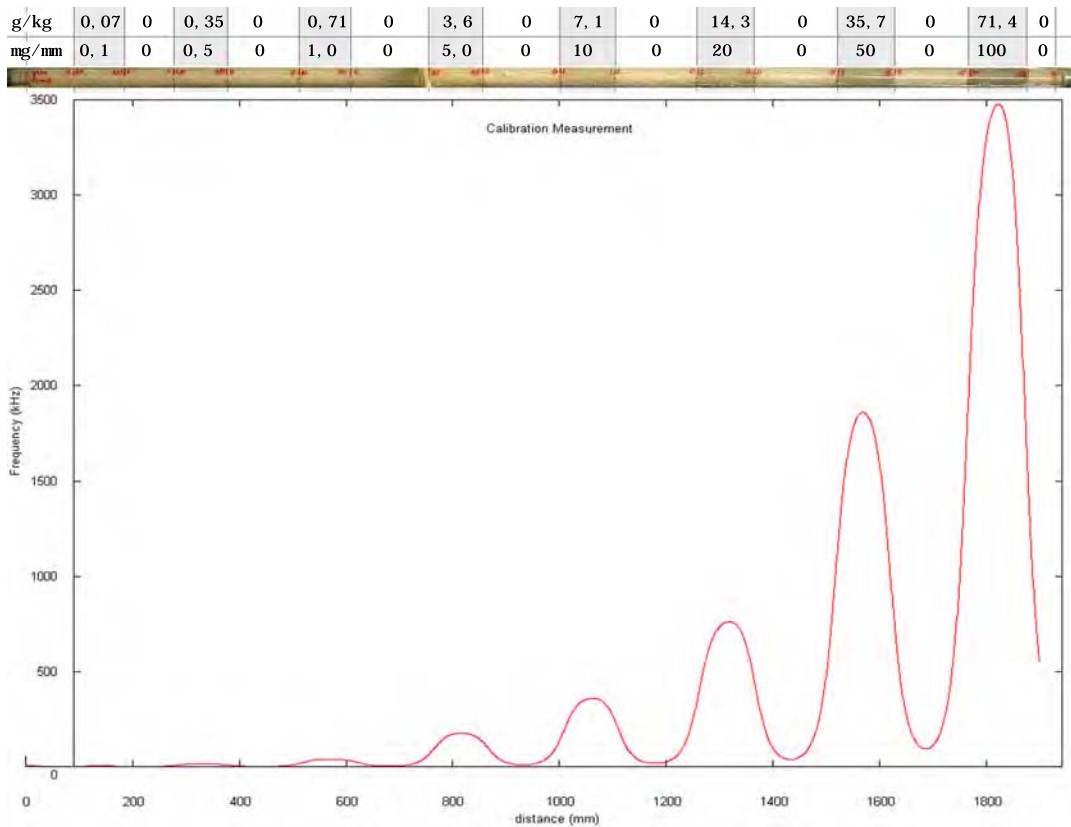


Fig. 3.4: Calibration setup and the recorded frequency response. The upper values above the column present the iron mass ( $g$ ) per  $kg$  sand, the lower values present the iron mass ( $mg$ ) per  $mm$  of column length. Each iron containing section was separated with a section containing no iron

25 times, giving a data value for each  $\frac{1}{25}$ <sup>th</sup> millimeter. After averaging the recorded data, each value represented the average response of  $0.4\text{ mm}$ .

To determine the maximum value for each metal containing section, over a length of  $10\text{ mm}$  around the maximum value (12 data points in each direction, giving 25 data points in total), the surface integral of the response frequency was taken. This integral value was divided by the amount of data point in  $10\text{ mm}$  to get an average response for  $1\text{ mm}$  of column length. Figure 3.5 shows the determined values for each integrated section. This graph was used to determine the slope of the fitted line through these values. Using this slope, all further measurements with the metal detector could be converted into iron content ( $g$ ) per column length ( $mm$ ).

The measured nano-iron concentrations never reached the maximum concentrations used for the calibration (e.g.  $0.1\text{ g/mm}$ , fig. 3.4). The maximum concentration measured in the experiments was  $0.023\text{ g/mm}$  (fig. B.4). Based on these results the calibration could probably be improved by covering more lower concentrations and by leaving out the measured high concentrations. The exact range of influence for the metal detector should also be described for each concentration range.

### 3.3.3 About the Metal Detector

The movement of the metal detector on the rails was nearly constant, but some vibration in the direction of travel at the measure coil was seen. This was one reason for the fluctuations seen in the measured

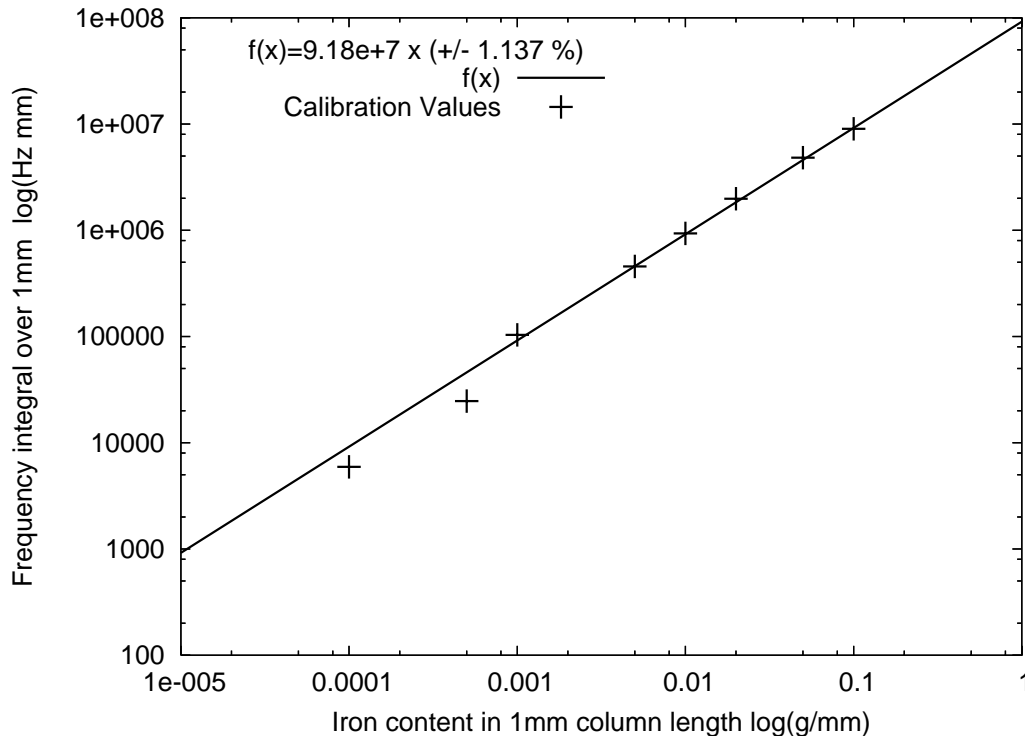


Fig. 3.5: Calibration curve of the metal detector. The measured frequency was integrated over 1 mm and set out against the average iron content in 1 mm column length. The linear fitted relation is:  $f(x) = 9.18 \cdot 10^7 x$  with  $R^2 = 0,9986$

signal. During the measurement the metal detector carrier moves over the rails, this movement induces some vibrations. Improving the setup such that it can move without inducing this vibration would produce a smoother signal. When the detector was not moving, fluctuation in the signal was also observed, though smaller. Which supports the presence of noise in the measurement.

The calibration curve as shown in figure 3.5 shows an accurate fit through the measured data. The problem is that in this calibration setup the iron concentration in the column changed abruptly. This abrupt change resulted in a measured iron concentration before the iron part was exactly reached by the detector. The conversion factor might thus not be fully transferable to the measurements of a continuous changing iron concentration. Probably the conversion factor can be improved with more calibration measurements, of which one in a continuous grading of iron concentration.

The surfaces under the curves presenting the measured concentration distribution in the experiments represent the total mass of nano-iron injected. In tables 3.4, 3.7, 3.10 & 3.13 for each measurement a difference in the 'Injected' mass and the 'Measured' mass can be seen. The injected mass was calculated from the suspension concentration and the total discharge. Whether the difference between the measured and calculated mass was a failure in the measurement is not sure. The input concentration was thought of to be exact, but might have had an inaccuracy as well. This difference can be a result of a not fully known input concentration as well as a not fully applicable calibration constant for the measurement.

A relatively high accuracy was reached with the measurements, especially for the lower concentrations. A chemical determination of the concentrations would not likely be able to give such a high accuracy. In a chemical determination the natural presence of iron in the sand will create a large unknown factor in the

determination. Because the geogenic iron content in the sand is not homogeneously spread within the column, it is not possible to make a reliable difference measurement based on chemical iron detection.

Until now only speculative assumptions about the transport of nano-iron during the injection period can be made based on the visual observation. When possible, in a future research measurements of the nano-iron concentration in the column should be made at several time steps during the injection. Quick measurements during the injection would provide a view on the transport of the nano-iron during the injection. A measurement of the nano-iron concentration in the column took 30 minutes, if this could be minimized to 1 or 2 minutes, it should be possible to create the concentration profiles during the injection. It must be tested if this can be done with the mixer and reservoir in place. In the current research, it is shown that the difference measurement works very well. It is expected that the small changes in the column can be seen, even with a high background signal resulting from nearby metal objects.

#### 3.3.4 Conditions used for the 1-D flow experiments

In the tables 3.2, 3.5, 3.8 & 3.11 the measured and determined conditions of each experiment are given. For each experiment the hydraulic conductivity, the length of the sand packing in the column, the porosity, the duration of nano-iron injection and the total nano-iron injected were determined. The total injected iron was calculated from the input concentration and the total injection duration.

In the large figures 3.7, 3.10, 3.13 & 3.16 the determined nano-iron concentration in the column after four hours of nano-iron injection are given for each of the experiments. Some experiments were not comparable due to errors and their results are given in the appendix in figures B.3 & B.4. The y-axis gives the 'Iron Content per mm of Column Length ( $g/mm$ )' which represents the mass of nano-iron present in 1 mm of column length. This can also be rewritten in ' $g$  iron per  $kg$  sand', which is a notation used more frequently. By plotting it as nano-iron content per mm of column length, the surface below the curve directly represents the total mass of iron injected into the column.

It can be seen that in the first 15  $mm$  an increase in concentration was measured. This was observed for all measurements. The metal detector measured the nano-iron content in the vicinity of the measuring coil. At the beginning of the column the nano-iron was only on one side of the coil and thus resulted in a smaller response. When iron was present on both sides, the measured nano-iron concentration was higher.

#### 3.3.5 Characteristics of 1-D flow experiments

From the curves presenting the nano-iron content in the column (section 3.3.4) several characteristic values were determined. The distance of 50% of the total mass (half of total surface under the curve), 50% of the maximum concentration and the distance where the curve goes below the input concentration (the nano-iron concentration in the column if the injected nano-iron would have been transported as a conservative tracer). These determined characteristic values are given in the first columns of tables 3.3, 3.6, 3.9 & 3.12, the data are graphically presented in the figures at the bottom left of the nano-iron content curves (figures 3.9, 3.12, 3.15 & 3.18).

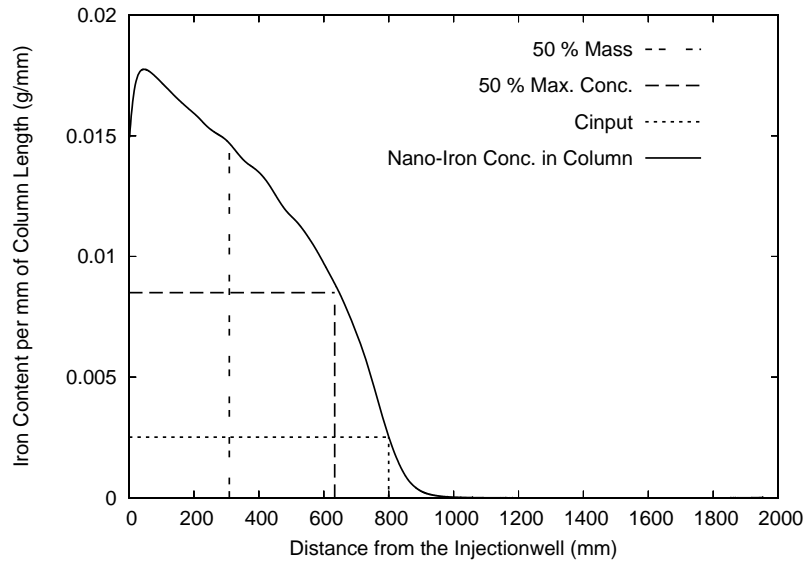


Fig. 3.6: Nano-Iron concentration distribution in an example experiment to demonstrate the locations of the determined characteristic values *50% Mass*, *50% Conc.* and  $C_{input}$

In figure 3.6 an example figure is shown. The determined characteristics of the concentration distribution in the column are shown in this figure.

- The surface under the curve left and right of the *50% Mass* line each represent 50% of the total injected nano-iron.
- The *50% Conc.* lines show the distance where the concentration in the column is at 50% of the maximum reached concentration in the column.
- The  $C_{input}$  line represents the expected concentration in the column for the hypothetical situation that the nano-iron behaved as a conservative tracer.

For some of the experiments this input concentration is also drawn in the graph.

A different presentation made it possible to compare the characteristic values with each of the other experiments, the determined characteristic values were converted into a retardation factor. This is not exactly the same as the retardation seen in solute transport, but a scaled representation of the transported distance. The distances were taken relative to the distance that a conservative tracer would have traveled in the injection time.

A larger retardation factor means that the nano-iron was held back more. A smaller retardation, that the nano-iron got further.

In tables 3.3, 3.6, 3.9 & 3.12 the converted characteristic values are given in the last three columns, they are graphically presented in the figures on the bottom right of the nano-iron content curves.

In these tables and graphs the *50% Mass* values represent the distance from the inlet where 50% of the total nano-iron mass is located. The *50% Conc.* values represent the distance from the inlet upto the location where the nano-iron concentration in the column got below 50% of the maximum measured concentration in the column. The  $C_{input}$  values represent the distance from the inlet upto the location in the column where the nano-iron concentration in the column got below the input concentration,

which is a theoretic concentration that would be build up in the column if the nano-iron behaved as a conservative tracer. The *Rel.* values represent the relative values of each of the three corresponding values in the previous columns.

From the characteristics it can be seen whether a curve is concave or convex. When the '50% Mass' distance is smaller than the '50% Concentration' distance, the curve is convex, otherwise it is concave. A convex curve represents a sharp nano-iron front and a concave a wide spreading of the nano-iron front.

### 3.3.6 Measurement Results Overview

The surface under the measured data curve represents the total mass of nano-iron injected ('Measured' in tables 3.4, 3.7, 3.10 & 3.13). The input concentration multiplied with the discharge and the duration of injection gives the total mass ('Injected' in tables 3.4, 3.7, 3.10 & 3.13). From the difference between the injected and measured data given in these tables, it can be seen that the order of magnitude was for all measurements reached.

### 3.3.7 (A) Nano-iron Suspension Concentration - Dorsilit Sand

The experiments #'s 1, 2, 3 and 4 were compared to each other to show the influence of the nano-iron suspension input concentration on the transport of the nano-iron. The experiments # 3 and # 4 were performed in the same column, by using the outflow side of experiment # 3 as inlet for # 4.

The input conditions, characteristics of the nano-iron distribution and the measurement overview are given in table 3.2, 3.3 and 3.4 respectively. In figure 3.7 the measured nano-iron distribution of each experiment is drawn.

Tab. 3.2: Conditions used for the concentration dependent 1-D flow experiments. A detailed explanation is given in section 3.3.4. \* values were measured, † values were initial conditions, ‡ values were a combination of both

Exp. #	† Concentration (g/l)	* K value (m/s)	* Column Length (mm)	* Porosity (-)	* Duration of Inj. (min)	‡ Total iron inj. (g)
1	0.01	$1.09 \cdot 10^{-3}$	1944	0.347	240.0	0.028
2	0.10	$1.09 \cdot 10^{-3}$	1944	0.347	242.3	0.226
3	1.00	$9.99 \cdot 10^{-4}$	1924	0.334	240.0	2.326
4	10.00	$9.99 \cdot 10^{-4}$	1924	0.334	242.0	23.457

Tab. 3.3: Characteristics of concentration dependent 1-D flow experiments. The *Rel.* values represent the relative values of each of the three corresponding values in the previous columns. Explanation is given in section 3.3.5

Exp. #	Concentration (g/l)	50% Mass (mm)	50% Conc. (mm)	$C_{input}$ (mm)	Rel. 50% Mass (mm/mm)	Rel. 50% Conc. (mm/mm)	Rel. $C_{input}$ (mm/mm)
1	0.01	20.4	34.8	87.2	31.15	18.26	7.29
2	0.10	37.2	69.2	152.8	17.24	9.27	4.20
3	1.00	106.4	210.8	289.6	6.43	3.25	2.36
4	10.00	204.0	422.8	455.6	3.38	1.63	1.51

Tab. 3.4: Overview of the total injected mass and the measured total mass of nano-iron. ( $\diamond$  + values present a higher and - values a lower measured mass). Explanation is given in section 3.3.6

Exp. #	Concentration (g/l)	Injected (g) (=100%)	Measured (g)	Difference $\diamond$ (g)	Difference $\diamond$ (%)
1	0.01	0.028	0.093	+0.065	+230.7
2	0.10	0.226	0.916	+0.690	+304.8
3	1.00	2.326	3.747	+1.421	+61.1
4	10.00	23.457	14.849	-8.609	-36.7

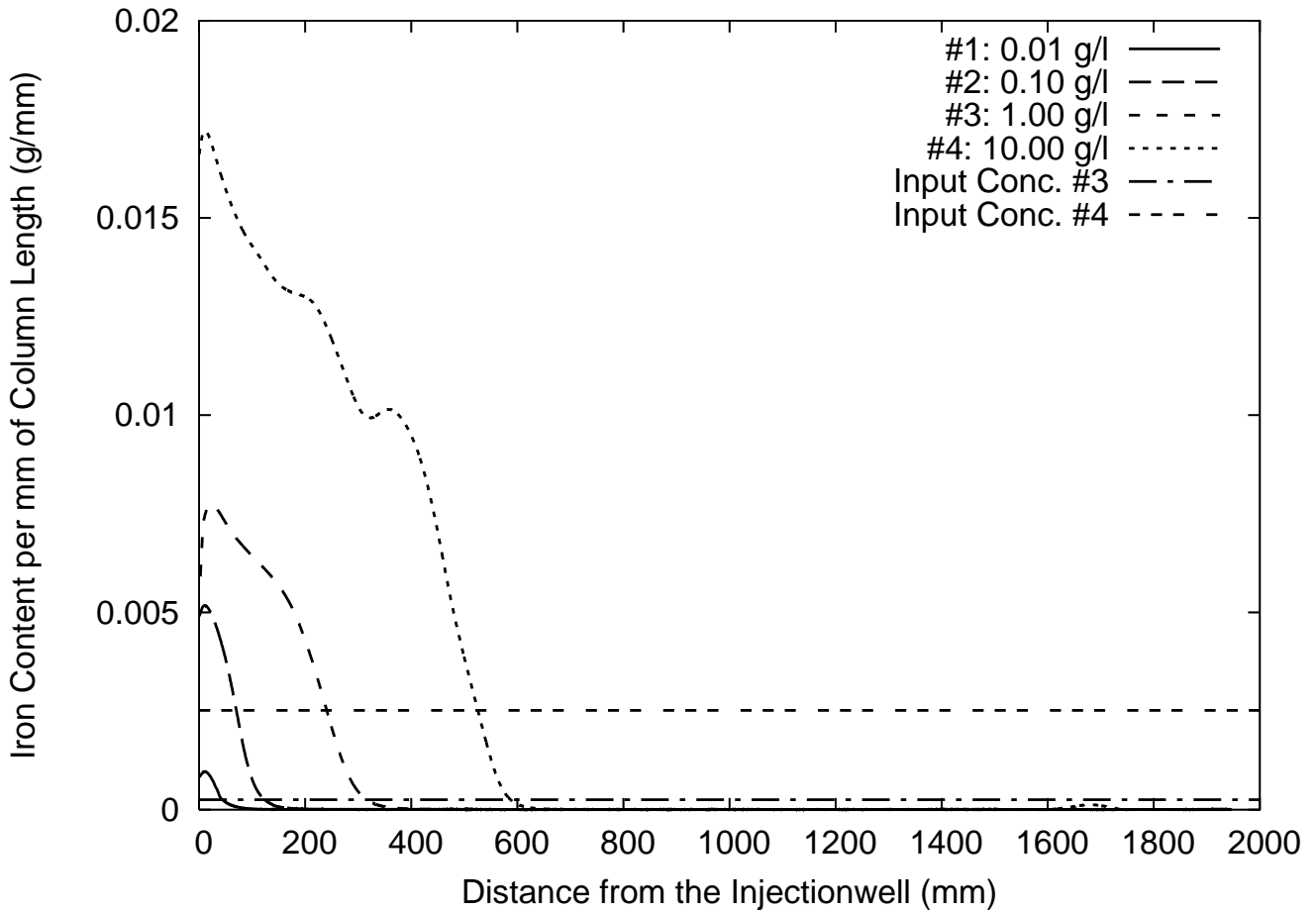


Fig. 3.7: Nano-iron content per 1 mm of column length for experiments #'s 1, 2, 3 & 4 with each a different input suspension concentrations. Each curve represents the nano-iron content after 4 hours of injection. Explanation is given in section 3.3.4

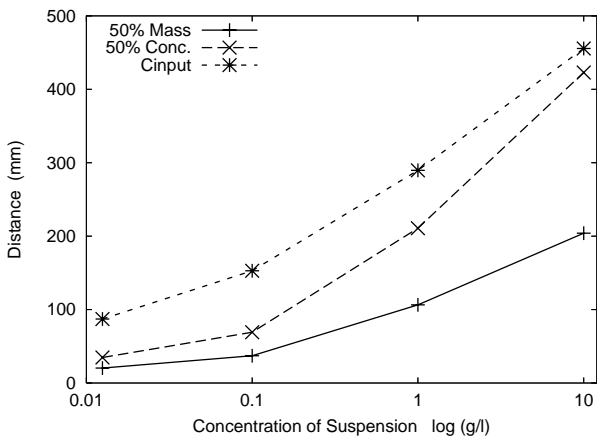


Fig. 3.8: Transport distance characteristics. Explanation is given in section 3.3.5

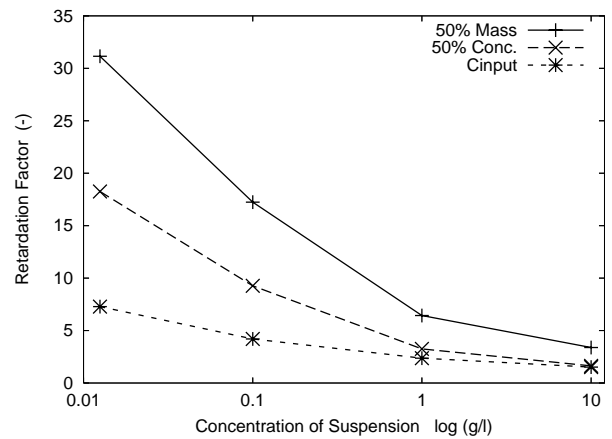


Fig. 3.9: Relative transport distance characteristics. Explanation is given in section 3.3.5

For the two experiments # 3 and # 4 the input concentrations are also given, these lines represent the expected concentration in the column for the hypothetical situation that the nano-iron behaved as a conservative tracer.

For experiment # 2, after the measurement at 4 hours, the injection was continued for another 464 minutes. This result is shown in the appendix in section B.1.

For experiment # 4, after the measurement of iron content at 4 hours, the injection of the nano-iron was continued to see if the front would propagate further after a full stop. In total an extra 290 minutes continuous injection followed. The result is shown and described in the appendix in section B.2.

Each increase in suspension concentration raised the traveled distance of the nano-iron front. The increase also produces a higher peak concentration at the beginning of the column. For a higher input concentration the total injected mass of nano-iron is also increased.

In figure 3.7 it can be seen that a higher concentration resulted in a larger transport distance. From figure 3.8 it becomes clear that the increase in transport distance was not linear related to the increase in concentration. Each increase in concentration also raised the nano-iron concentration in the column.

Based on the results of these experiments, a classic filtration system could not be identified. The transport distance increased with a higher concentration. With the lower concentrations the concentration near the inlet did not show a continuous build up of concentration, i.e. to reach the same concentration in the column as for the higher input-concentrations was reached. It is expected that in the experiments the maximum concentration in the column was not reached. This indicates that pore-plugging could not have been a major mechanism of retarding the transport at these concentrations.

In the curve of experiment # 4 (10.00 g/l) an increase in the concentration at 400 mm is seen, this might have been a result of heterogeneities in the column packing. The heterogeneities will be discussed in more detail in section 3.3.11.

The little peak in the concentration around 1700 mm was a response on moved iron left behind from experiment # 3 (1 g/l), which was performed previously in this column using the other side as inlet. The difference measurement removed most of this iron occurrence but some iron was re-transported during experiment # 4, which resulted in a difference between the measurement before and after the injection.

The characteristic values are given in table 3.3 and plotted in figure 3.8, because of the large differences in concentrations, the concentrations are plotted on a log-scale.

In figure 3.9 it can be seen that from experiment # 1 to 4 the curves becomes more convex because the '50% Mass' and '50% Concentration' distances are getting further from each other.

In table 3.4 it can be seen that the measured total mass of experiments # 1, 2 and 3 should actually have been less. This would result in a lower concentration curve for these experiments. The measured total mass of experiment # 4 was lower, thus a higher concentration curve would have been expected.

It is likely that the input concentration for these very low concentrations was not as exact as assumed. It was difficult to prepare a suspension with these low concentrations. For experiment # 1 with a 0.01 g/l concentration, 0.5 ml of concentrated nano-iron suspension was mixed in 8 liters degassed water. The exact amount of nano-iron particles that get into the syringe was difficult to determine, also the concentration of the delivered base-suspension was uncertain and expected to be not equal for all cases. Sometimes (especially when the suspension was older) part of the nano-iron was attached to the bottom of the bottle and this part could not be used. For the calculation of the injected concentration, still the same average base-concentration of 200 g/l was used. For the larger volumes and higher concentrations, this appears to be acceptable. For the very low concentrations probably a better concentration determination of the injected suspension needs to be done.

If the measured total mass is assumed to be exact, a backward calculation of the input concentration can be done as well.

Based on visual observations during these four experiments, different phases of the transport were seen. First the nano-iron front moved relatively fast (though still strongly retarded), then the propagation stagnated. In the second phase, the concentration in the first section was building up. In the third phase, the front started to propagate again. From the measurements it could be seen that the concentration in the last section was lower. In the two extra long runs as presented in the appendix it was seen that the concentration in the first part still continued to build up.

Within this project there was not enough material and time to perform runs with higher concentrations. The used input concentrations at some field test are higher (e.g. 35 g/l, Müller et al. [2006b]). For a comparison to field test situations, higher input concentrations would thus have been preferable. In further research higher concentrations should thus also be taken into account. There is a chance that higher concentrations would create pore-plugging, as expected from a filtration system. When in future research, computer models are to be written, the mechanism responsible for the retardation must be known and fully described.

An other comparison of these four experiments with different concentrations could also be performed. Experiments with an equal mass of nano-iron could be performed instead. The duration of each injection would then be different. As such, it should be possible to see the influence on the absolute retardation by the total mass of injected nano-iron. As well, it would then be possible to see if the relative transported distance for the lowest input concentration (exp. #1) will increase or will still be the smallest.

## 3.3.8 (B) Pore Velocity - Dorsilit Sand

The experiments #'s 4, 5, 6, 7 & 8 were compared with each other to investigate the influence of the pore velocity on the transport of nano-iron.

The measured conditions of each of the experiments are given in table 3.5. The initial conditions were given in table 3.1.

Tab. 3.5: Conditions of the 1-D flow experiments in Dorsilit 1/8 sand (0.3-0.8mm), compared by their pore velocity. A detailed explanation is given in section 3.3.4. \* values are measured, † values are set, ‡ values are a combination of both

Exp. #	† Pore Velocity (m/s)	* K value (m/s)	* Column Length (mm)	* Porosity (-)	* Duration of Inj. (min)	‡ Total iron inj. (g)
5	$1.1 \cdot 10^{-4}$	$1.48 \cdot 10^{-3}$	1944	0.348	240.0	5.588
6	$2.1 \cdot 10^{-4}$	$1.08 \cdot 10^{-3}$	1918	0.359	240.0	10.805
4	$4.8 \cdot 10^{-4}$	$9.99 \cdot 10^{-4}$	1924	0.334	242.0	23.457
7	$8.8 \cdot 10^{-4}$	$1.48 \cdot 10^{-3}$	1918	0.348	240.0	44.701
8	$1.6 \cdot 10^{-3}$	$1.08 \cdot 10^{-3}$	1918	0.359	240.0	86.443

Tab. 3.6: Characteristics of 1-D flow experiments in Dorsilit 1/8 sand with different pore velocities. ◊ is with errors and is included for completeness. Explanation is given in section 3.3.5

Exp. #	Pore Velocity (m/s)	50% Mass (mm)	50% Conc. (mm)	$C_{input}$ (mm)	Rel. 50% Mass (mm/mm)	Rel. 50% Conc. (mm/mm)	Rel. $C_{input}$ (mm/mm)
5	$1.1 \cdot 10^{-4}$	87.2	125.2	120.0	1.81	1.26	1.32
6	$2.1 \cdot 10^{-4}$	113.2	180.8	274.0	2.61	1.63	1.08
4	$4.8 \cdot 10^{-4}$	204.0	422.8	455.6	3.38	1.63	1.51
7	$8.8 \cdot 10^{-4}$	309.2	633.6	762.4	4.09	1.99	1.66
8◊	$1.6 \cdot 10^{-3}$	844.4	1652.4	1637.2	2.80	1.43	1.44

Tab. 3.7: Overview of the total injected mass and the measured total mass of nano-iron. (◊ + values present a higher and - values a lower measured mass, † present exp. where an unknown part of iron left the system through the outlet). Explanation is given in section 3.3.6

Exp. #	Pore Velocity (m/s)	Injected (g) (=100%)	Measured (g)	Difference◊ (g)	Difference◊ (%)
5	$1.1 \cdot 10^{-4}$	5.588	4.046	-1.542	-27.6
6	$2.1 \cdot 10^{-4}$	10.805	6.413	-4.392	-40.6
4	$4.8 \cdot 10^{-4}$	23.457	14.849	-8.609	-36.7
7	$8.8 \cdot 10^{-4}$	44.701	25.238	-19.463	-43.5
8†	$1.6 \cdot 10^{-3}$	86.443	18.971	-67.472	-78.1

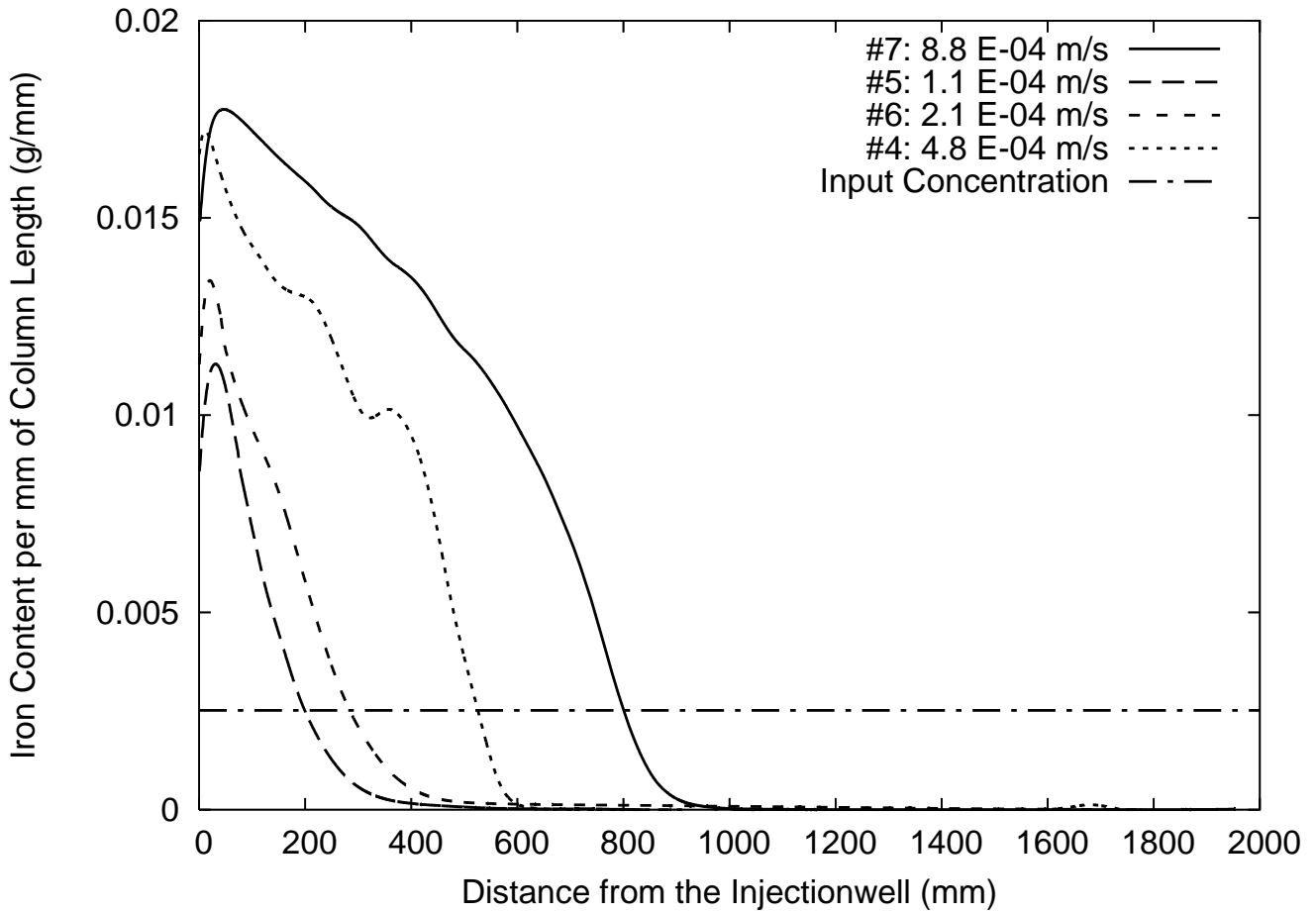


Fig. 3.10: Nano-iron content per 1 mm of column length for different flow velocities in Dorsilit 1/8, 0.3-0.8 mm sand. Each curve represents the nano-iron content after 4 hours of injection. Explanation is given in section 3.3.4

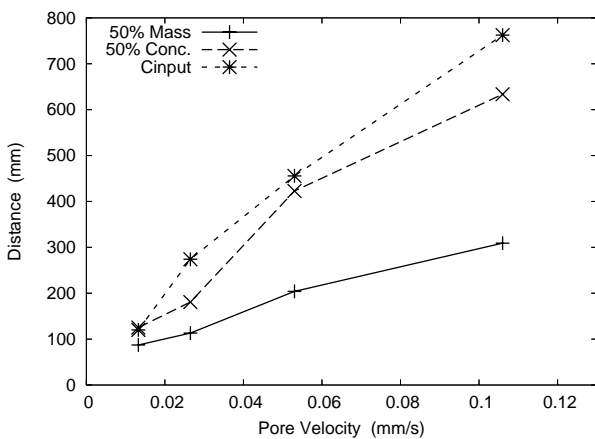


Fig. 3.11: Transport distance characteristics. Explanation is given in section 3.3.5

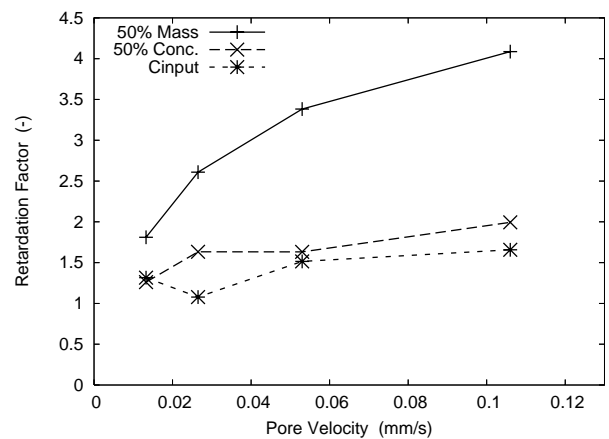


Fig. 3.12: Relative transport distance characteristics. Explanation is given in section 3.3.5

In figure 3.10 the five measured concentration distributions recorded after four hours of injection in the column are presented. The line of 'input concentration' represents the nano-iron concentration in the column if the nano-iron would have behaved as a conservative tracer.

The experiment with the highest pore velocity (# 8) is not shown in the graph. This experiment was not fully representable due to errors in the data recording and the loss of nano-iron due to a breakthrough at the outlet. Because of this the total measured mass and the set mass showed a large difference (table 3.7). The measured curve is presented and discussed in the appendix (app. B.3).

From the doubled pore velocity increase from experiment # 5 to # 6 did not result in a doubled transport distance for 50% of the mass, but the concentration first got below the input concentration at more than the double distance. Also the concentration curve changed from an almost concave to a more convex curve. The nano-iron front thus got sharper.

The used nano-iron suspension of experiment # 5 was one day old. Due to this, the suspension was colored dark brown. Because the mixed suspension is exposed to oxygen, part of the iron oxidized and dissolved in the water. The Uranine tracer was not visible because of this. Due to the dark color of the suspension, it was not possible to visually observe the transport of nano-iron. The detection with the metal detector made it possible to determine the exact concentration distribution in the column. It is thinkable that in field cases based on the color of the suspension it was decided how far the nano-iron was distributed in the subsurface. This experiment shows that the spreading of the darkened suspension is not to be mistaken with the real spreading extend of the nano-iron itself.

During the first 60 minutes of experiment # 4 the propagation velocity was very fast, after one hour the propagation velocity of the front decreased significantly. Several peaks in the concentration can be seen in figure 3.10, these are likely to be caused by heterogeneities in the column packing.

During the pre-injection measurement of the column used for experiment # 7 a metal clip was located on the outflow side, this resulted in a small peak in the pre-injection measurement. After subtracting the measurement taken after the injection, the clip was no longer present in the curve. This showed that the difference measurement can remove metal objects from the signal.

The front of the nano-iron distribution in experiment # 7 showed the sharpest front, as also follows from the large distance between the *50% Mass* and *50% Concentration* locations (fig. 3.11).

The largest velocity (exp. # 8) was unrealistic. It would, e.g. in the described field application used for the base-case conditions, only be reached in the direct vicinity of the injection well

The characteristics of each of the presented curves of figure 3.10 are given in the first columns of table 3.6, they are graphically presented in figure 3.11. From the figure it can be seen that there was an almost linear relationship between the transported distance and the pore velocity.

The calculated retardation factors are given in the last columns of table 3.6 and graphically presented

in figure 3.12. As can be seen in this figure, the retardations did not change much with an altered pore velocity. The *50% Mass* distances did increase, but the relative differences were much smaller (retardations between 1.1 and 4.1, table 3.6) when compared to the retardation difference seen for the experiments with different concentrations (table 3.3, retardations between 1.5 and 31).

Changing the velocity and keeping the injection duration the same created an unequal mass of injected nano-iron between the runs. The retardation curve of the injection though showed that no significant change was observed. The mass of nano-iron thus appears to have been of little influence on the transport. In a future research it would be useful to confirm this observation by changing the velocity while keeping the total injected mass equal.

As can be seen in figure 3.11, the  $C_{input}$  increases faster than *50% Mass* indicating that the concentration distribution became more convex with an increasing pore velocity.

The increase of the retardation of the *50% Mass* factor with higher pore velocities indicates that most of the nano-iron will be taken out of suspension in the near vicinity of an injection well, where the pore velocity is higher. Leaving less nano-iron in suspension further away from the well. The retardation of the nano-iron at lower pore velocities (further from the injection well) decreases slightly, but the retardation due to a decrease in concentration increases fast at the same moment.

Combining the results of section 3.3.7 and 3.3.8, it would probably be best to use a suspension with a high concentration and to use a low injection rate for an optimized spreading of the nano-iron in the column.

## 3.3.9 (C) Pore Velocity - Rhine-Valley Sand

Four experiments with different pore velocities were performed in Rhine-Valley sand, which has a grain size ranging between 0 and 4 mm. The initial conditions for these experiments are given in table 3.1, the measured conditions for each of the experiments are given in table 3.8. The determined hydraulic conductivities of the Rhine-Valley sand ( $10^{-4}$ ) compare to those of many field situations in sandy aquifers [Schwartz and Zhang, 2003].

Tab. 3.8: Conditions used for the 1-D flow experiments in Rhine-Valley sand (0-4 mm) with different pore velocities. A detailed explanation is given in section 3.3.4. \* values are measured, † values are set, ‡ values are a combination of both

Exp. #	† Pore Velocity (m/s)	* K value (m/s)	* Column Length (mm)	* Porosity (-)	* Duration of Inj. (min)	‡ Total iron inj. (g)
9	$1.3 \cdot 10^{-5}$	$1.69 \cdot 10^{-4}$	1942	0.247	240.0	3.224
10	$2.7 \cdot 10^{-5}$	$1.76 \cdot 10^{-4}$	1944	0.257	240.0	6.350
11	$6.5 \cdot 10^{-5}$	$1.76 \cdot 10^{-4}$	1944	0.257	240.0	15.460
12	$2.1 \cdot 10^{-4}$	$2.00 \cdot 10^{-4}$	1420	0.251	240.0	52.392

Tab. 3.9: Characteristic of 1-D flow experiments in Rhine-Valley sand with different pore velocities. († present exp. where an unknown part of iron left the system through the outlet). Explanation is given in section 3.3.5

Exp. #	Pore Velocity (m/s)	50% Mass (mm)	50% Conc. (mm)	$C_{input}$ (mm)	Rel. 50% Mass (mm/mm)	Rel. 50% Conc. (mm/mm)	Rel. $C_{input}$ (mm/mm)
9	$1.3 \cdot 10^{-5}$	57.6	98.0	153.2	5.26	3.09	1.98
10	$2.7 \cdot 10^{-5}$	131.6	160.8	342.4	4.43	3.62	1.70
11	$6.5 \cdot 10^{-5}$	200.8	399.6	464.0	7.06	3.55	3.06
12†	$2.1 \cdot 10^{-4}$	153.6	1516.8	1920.0	32.54	3.30	2.60

Tab. 3.10: Overview of the total injected mass and the measured total mass of nano-iron. (° + values present a higher and - values a lower measured mass, † present exp. where an unknown part of iron left the system through the outlet). Explanation is given in section 3.3.6

Exp. #	Pore Velocity (m/s)	Injected (g) (=100%)	Measured (g)	Difference° (g)	Difference° (%)
9	$1.3 \cdot 10^{-5}$	7.739	4.419	-3.320	-42.9
10	$2.7 \cdot 10^{-5}$	15.240	7.789	-7.451	-48.9
11	$6.5 \cdot 10^{-5}$	37.104	13.061	-24.043	-67.8
12†	$2.1 \cdot 10^{-4}$	125.740	30.177	-95.563	-76.0

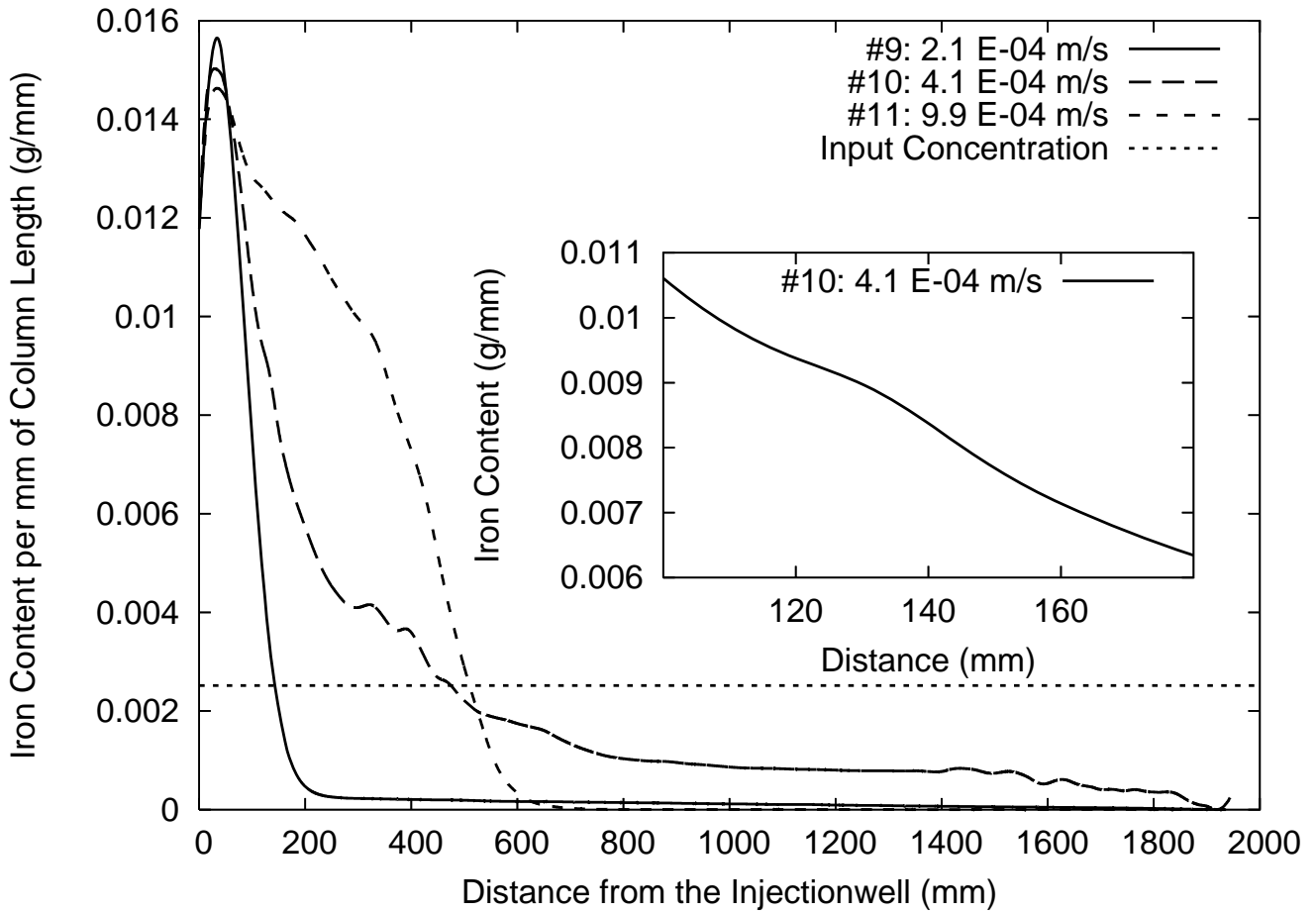


Fig. 3.13: Nano-iron content per 1 mm of column length for different pore velocities in Rhine-Valley sand, 0-4 mm. Each curve represents the nano-iron content after 4 hours of injection. Explanation is given in section 3.3.4

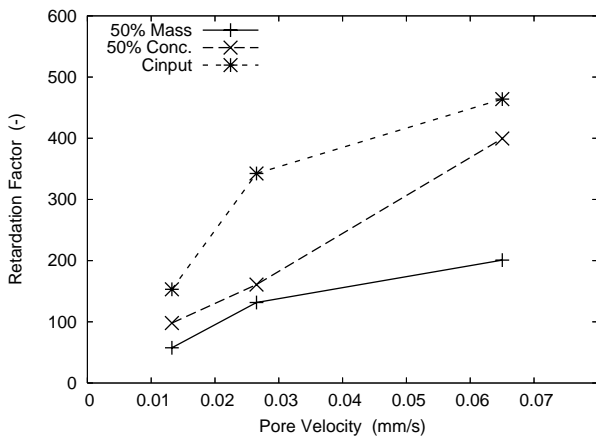


Fig. 3.14: Transport distance characteristics. Explanation is given in section 3.3.5

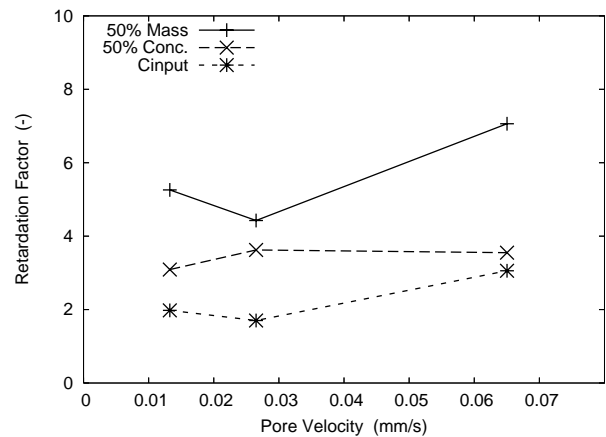


Fig. 3.15: Relative transport distance characteristics. Explanation is given in section 3.3.5

In figure 3.13, the concentration distribution measurement of experiment # 9 shows that a small amount of nano-iron was transported much further than the rest. A low concentration was measured between 20 and 100 *cm*. This low concentration of nano-iron could not be seen in the column by visual observation. It can be expected that these particles were more mobile and could thus be transported over a greater distance. The rest of the injected nano-iron was all positioned in the first 20 *cm* of the column.

It was difficult to create a near homogeneous packing with the Rhine-Valley sand, it could not be prevented that a few finer and coarser layers developed during the packing. In experiment # 10 a coarse grained layer was positioned around 14 *cm*. In the detail inset in figure 3.13 this section is shown. As can be seen, the nano-iron concentration in this coarse layer was higher.

Experiment # 10 further showed a concentration distribution that differed from other experiments. From 200 *mm* on it did not drop further to zero, but a wide spreading of the nano-iron front was created. The peaks seen between 200 *mm* and 500 *mm* were visible in the column as dark sections, these must have been heterogeneities that were not observed during the packing of the column with sand.

In experiment # 11 then again the front was very sharp and dropped to zero concentration in a short distance. The spreading of the nano-iron created a much more convex curve in comparison to experiments # 9 and 10, as is visualized by the larger distance between  $C_{input}$  and 50% *Mass* in figure 3.14. The low permeability of the column in these experiments resulted in combination with the higher pore velocity of experiment # 11 that the expected pore velocity was not reached. The pump was as for all other experiments located at the outlet side of the column. At the pump rate needed for this pore velocity the water at the end of the column degassed, resulting in a lower pore velocity. The initial goaled pore velocity was a factor 1.2 higher than was reached in this experiment.

For the even higher pore velocity of experiment # 12 the pump was placed between the nano-iron suspension reservoir and the inlet of the column. In that way the degassing problem was overcome. Experiment # 12 is further described in the appendix (app. A.3 & B.3)

In figure 3.15 it can be seen that the retardation in the Rhine-Valley sand also did not change much with an altered pore velocity, as also was seen in the Dorsilit sand. The 50% *Mass* of the Rhine-Valley sand showed an increase for higher pore velocities, but still all the retardation factors were between 1 and 7 (table 3.9). The retardation thus changes much less due to a changed pore-velocity than due to a change in concentration (table 3.3).

Changing the velocity and keeping the injection duration the same created an unequal mass of injected nano-iron between the runs. The retardation curve of the injection though showed that no significant change was observed. The total mass of injected nano-iron thus appeared to have been of no direct influence on the transport. In a future research it would be useful to confirm this observation by changing the velocity while keeping the total injected mass equal.

## 3.3.10 (D) Grain Size Distribution / Hydraulic Conductivity - Different Sand Types

To see how the transport of nano-iron is influenced by the grain size distribution (and with that the hydraulic conductivity of the porous media), several experiments performed in different sand types were compared with each other. The input conditions for those experiments can be found in table 3.1. The measured hydraulic conductivities, and other measured conditions are given in table 3.11.

The different sand types were compared with each other by their different hydraulic conductivities, which is a variable depending on the grain size as well as the grain size distribution and the compaction of the sand which all together define the pore size and pore connectivity.

Tab. 3.11: Conditions used in the experiments compared for the dependencies on the grain size and grain distribution. A detailed explanation is given in section 3.3.4. ‡ values are a combination of measured and set values, \* are runs with errors and are included for completeness

Exp. #	† Sand Type	◊ K value (m/s)	◊ Column Length (mm)	◊ Porosity (-)	◊ Duration of Inj. (min)	‡ Total iron inj. (g)
11	0-4 mm Rhine-Valley	$1.76 \cdot 10^{-4}$	1944	0.257	240.0	37.104
4	0.3-0.8 mm Dorsilit	$9.99 \cdot 10^{-4}$	1924	0.334	242.0	23.457
13	2-3.15 mm Dorsilit	$6.16 \cdot 10^{-3}$	1943	0.361	170.0	13.714
14*	3-5 mm Dorsilit	$9.84 \cdot 10^{-3}$	1959	0.373	592.9	54.404
15*	0-4 mm Rhine-Valley	$5.75 \cdot 10^{-4}$	1938	0.299	661.0	74.592
16*	0.6-1.2 mm Dorsilit	$2.40 \cdot 10^{-3}$	1948	0.348	87.9	10.916

Tab. 3.12: Characteristics of sand dependent 1-D flow experiments. \* values are runs with errors and included for completeness, † values can not be estimated. Explanation is given in section 3.3.5

Exp. #	Sand Type	50% Mass (mm)	50% Conc. (mm)	$C_{input}$ (mm)	Rel. 50% Mass (mm/mm)	Rel. 50% Conc. (mm/mm)	Rel. $C_{input}$ (mm/mm)
11	0-4 mm Rhine-Valley	200.8	399.6	466.0	7.06	3.55	3.06
4	0.3-0.8 mm Dorsilit	204.0	422.8	455.6	3.38	1.63	1.51
13	2-3.15 mm Dorsilit	147.6	313.2	338.0	2.81	1.32	1.22
14*	3-5 mm Dorsilit	474.8	836.0	1441.2	2.85	1.62	0.94
15*	0-4 mm Rhine-Valley	477.6	749.2	1311.2	4.93	3.14	1.79
16*	0.6-1.2 mm Dorsilit	48.4	94.8	†	4.78	2.44	†

Tab. 3.13: Overview of the total injected mass and the measured total mass of nano-iron. (◊ + values present a higher and - values a lower measured mass). \* values are runs with errors and included for completeness. Explanation is given in section 3.3.6

Exp. #	Sand Type	Injected (g) (=100%)	Measured (g)	Difference◊ (g)	Difference◊ (%)
11	0-4 mm Rhine-Valley	37.104	13.061	-24.046	-64.8
4	0.3-0.8 mm Dorsilit	23.457	14.849	-8.609	-36.7
13	2-3.15 mm Dorsilit	13.714	12.362	-1.352	-9.9
14*	3-5 mm Dorsilit	54.404	54.741	+0.336	+0.6
15*	0-4 mm Rhine-Valley	74.592	41.773	-32.820	-44.0
16*	0.6-1.2 mm Dorsilit	10.916	2.324	-8.592	-78.7

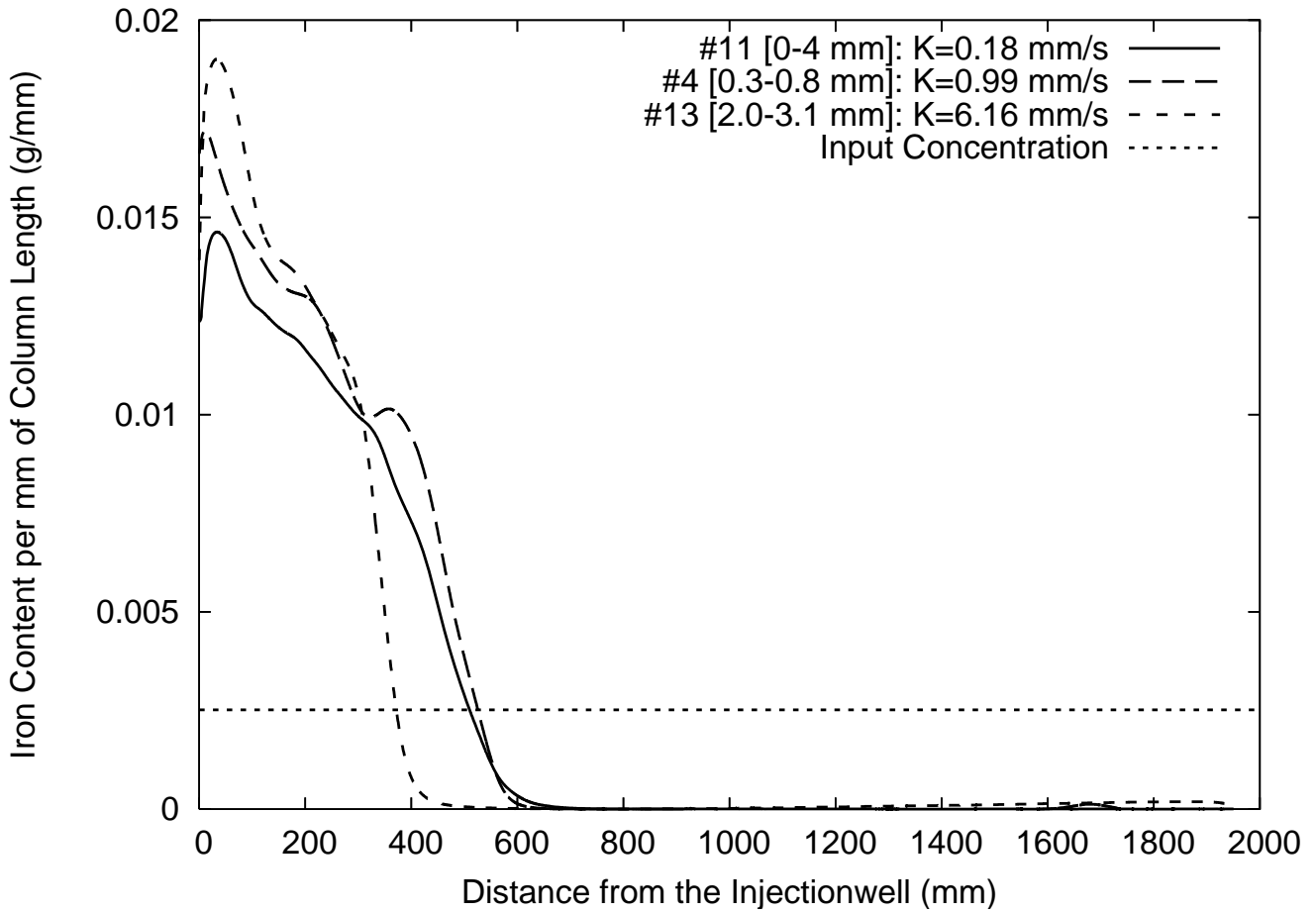


Fig. 3.16: Nano-iron content per 1 mm of column length for sand types with different hydraulic conductivities. Each curve represents the nano-iron content after 4 hours of injection. Explanation is given in section 3.3.4

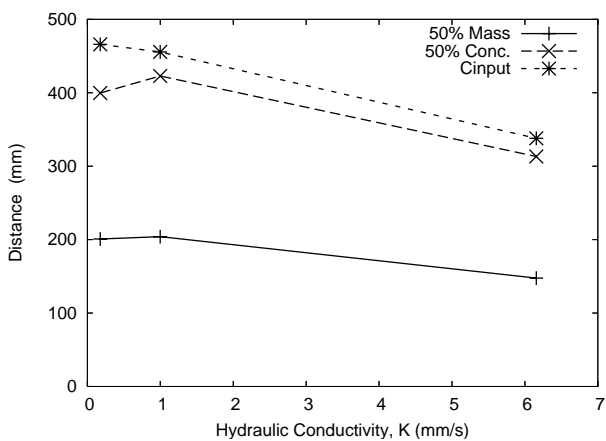


Fig. 3.17: Transport distance characteristics (K=0.18 mm/s: # 11; K=0.99 mm/s: # 4; K=6.16 mm/s: # 13). Explanation is given in section 3.3.5

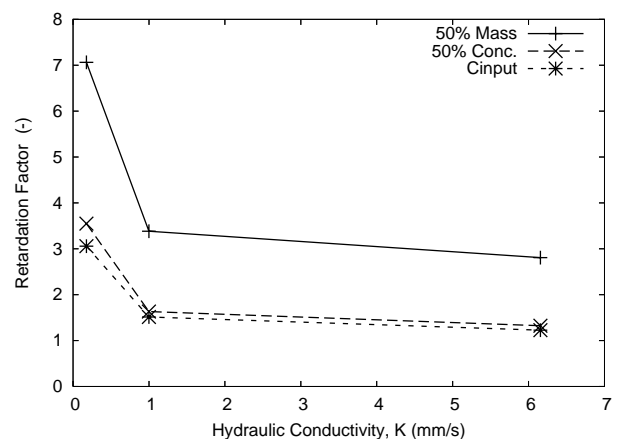


Fig. 3.18: Relative transport distance for sand types with different K-values (K=0.18 mm/s: # 11; K=0.99 mm/s: # 4; K=6.16 mm/s: # 13). Explanation is given in section 3.3.5

The experiments #'s 13-16 belonged to the first experiments done during this research, it was at that time expected that abundant time would be available to create enough good comparable experiments. Though this was not possible within the time available for this project. In a following research a systematic comparison of the influence of the porous medium will have to be performed.

The injection durations of the experiments were not equal for all experiments. Also the input suspension concentration was not equal for all experiments (table 3.1). Only the three experiments with an almost equal injection duration and comparable input concentrations are presented in figure 3.16. The results for all the experiments that were performed in different sand types are given in tables 3.11-3.13. The three experiments that are not presented in figure 3.16 are described and presented in the appendix (app. A.4 & B.4)

Experiments # 4 & 11 were already described in sections 3.3.8 & 3.3.9. The nano-iron front of in the coarser material of experiment # 4 came approximately 20 *cm* further. 50 % of the mass though reached the equal distance.

From the three compared experiments # 13 had an unequal injection duration. In # 11 & 4 240 *min* of injection were used where for # 13 only 170 *min* were used (table 3.11). Because of this only the retardation values given in table 3.12 can directly be compared with each other, since these values are converted relative to the total traveled distance of a conservative tracer.

From figure 3.18 it could be concluded that in coarser material with equal pore-velocity less retardation occurred, even though the difference is small. This means that the mobility of the nano-iron increased with increasing permeabilities.

In future research more well comparable experiments should be performed to get a better view on the dependency of the material of the porous media on the nano-iron transport.

### 3.3.11 Homogeneous Packing

In many runs a fluctuation in the concentration over distance was seen. This could in some cases be related to inhomogeneities. During the filling of the column sometimes small finer or coarser layers were build up. When there were too much of these, or if they were too big, the column filling was redone (fig. 3.19).

In some of the earlier runs the column bended through before the injection started. It happened that the column accidentally bended through by 10 *cm*, resulting in a compaction of the lower part in the middle of the column and a widening in the upper part. Giving a large preferential flow field in the upper part (fig. 3.20). When this was seen (e.g. during the tracer test) the column was re-compacted by placing it on the shaker plate and tapping it with wood logs. In later runs the columns were stabilized by gluing Plexiglas plates vertical on both sides of the column, which resulted in a maximum bend through of 5 *mm*. This was enough to keep the packing unchanged.

### 3.3.12 Retardation

For the retarded transport there could have been several mechanisms responsible. A low concentration could, with equal velocity, result in less retardation since the influence of filtering and coagulation can



Fig. 3.19: Small heterogeneities that can occur during packing with material of a large grain-size distribution, here a small coarse and fine grained layer are visible



Fig. 3.20: Preferential flow path resulting from a bend through of the column before injection

be smaller. Less particles in suspension could reduce the absolute amount of very mobile particles (expected to be the really nano-sized particles). On the other hand, for higher concentrations the distances between the particles should be smaller and thus the coagulation of the particles should take longer, resulting in a slower sedimentation rate. Whether this was of a large influence, is difficult to say. Since the sedimentation experiments done during the preliminary experiments were done in large vessels ( $\approx 0.5\text{ l}$ ) and a capillarity tube (diameter  $3.6\text{ mm}$ ). In the column a particle is much sooner sedimented because of the small cross-sectional area of a pore space, and the influence of the coagulation during the sedimentation in this short time period might be insignificant.

For a correct determination of the retardation coefficient, a full retardation curve should be created. For this it is necessary to take measurements at different stages of the injection. The retardation as determined now only includes the final stage after 4 hours of an injection. This way it was not possible to determine the type of retardation.

It is most likely that the observed retardation was a combination of different retardation principles. Most likely the main mechanism was a filtration combined with a small amount of electrical attachment to the sand grains. The filtration might be caused by straining and subsequent clogging [Saleh et al., 2006] as well as by gravitational settling of the coagulated (and subsequently gelled) particles. The nano-iron particle collisions resulting in filtration may be a result from Brownian diffusion, interception and gravitational settling [Tratnyek and Johnson, 2006].

The gravitational influence was observed in most of the experiments. Most transport was located in the lower part of the column. Also in the preliminary experiments, gravitational influence on the transport

was observed. Single colloidal particles between 10 *nm* and 10 *micron* should not be influenced by gravitational settling and can thus not be removed by convectional filtration alone [EPA, 1999]. The particles can though settle when they are coagulated. The observed gravitational influence on the transport of the nano-iron might thus be an indicator for the existence of coagulated and gelled particles. Though, it should be determined if the common guidelines for colloidal transport apply on the transport of colloidal iron particles. The density of iron is much higher than that of other colloidal particles. Most of the literature describing colloidal transport describes this for soil minerals, organic matter or biotic material. The wide range of 10 *nm* till 10 *micron* should actually cover the density difference. In other words, a nano-iron colloid of 60 *nm* will not be heavier as a carbon colloid of 1 *micron*.

Pore-plugging due to too high concentrations was not identified in this research. At the suspension concentration of 10 *g/l*, the maximum concentration reached in the column was approximately 18 *mg/mm* column length, which corresponds to 0.9 % or 1.2 % of occupied pore space volume in this 1 *mm* of column length for  $n = 0.33$  and  $n = 0.25$  respectively. It represents 10.4 *mg Fe/kg* sand and 9.3 *mg Fe/kg* sand respectively. The used average density of nano-iron was 6150 *kg/m<sup>3</sup>* as reported by Toda Kogyo for RNIP.

In other experiments on particle transport of for example Al-Abduwani et al. [2005], a concentration of 400 *mg/l* Hematite ( $Fe_2O_3$ ) could lead to pore-plugging, the particle diameter used was between 0.1  $\mu m$  – 5.0  $\mu m$  where 65% of the particles were less than 1.0  $\mu m$  in diameter. The particles used in the presented research were expected to be smaller, 60 *nm* – 100 *nm* (based on data provided by Toda Kogyo), but particle size analysis was not performed, and the size of the dispersed particles was thus not exactly known.

During several experiments it was visually observed during the injection that three phases of transport were present.

- In the first phase, the nano-iron front moved relatively fast until at some moment it stopped moving any further.
- In the second phase, the concentration in the section between the inlet and the nano-iron front was increasing, a darkening of the column was observed during this phase.
- During the third phase, the nano-iron front started moving again.

### 3.4 Summary

A set-up was developed to systematically perform transport experiments with nano-iron. To get a non-destructive determination of the nano-iron distribution a new detection technique was developed and tested. It showed good and promising results.

It was shown that the mobility of nano-iron was influenced by (I) the age (and with that the aggregation stage) of the particles, (II) by the pore velocity in the porous media and (III) the concentration of the suspension during injection, by the grain size distribution, and with that (IV) the permeability and (V) heterogeneity of the porous media.

To be able to compare the different permeabilities (IV) to each other more experiments are needed that are better comparable with each other. When it is prevented that more than one variable is altered or when a factor analysis is used, it should be possible to relate all runs to one base-case.

From the results it could be concluded that an increased pore velocity (II) could transport the nano-iron further when the injection duration was kept the same, and that at the same moment the retardation of the nano-iron particles was not significantly influenced.

## 4. DISCUSSION

### 4.1 2-D Experiments

The project started as planned with the reproduction of the 2-D experiments performed in 2003. To get a good impression of the flow fields in the container a numerical model was set up. The model was used to simulate different well locations and pumping rates in the wells to generate a flow inside the container perpendicular to the background flow direction. When the 2-D experiment in the container was built, the model outcome was tested with a conservative tracer. The first results were not exactly as modelled. The main problem was the capacity of the pumps used to produce the pumping rates and to keep the constant head at the inflow side constant. The numerical model then was adjusted to the limits of the pumps. This created a flow field that was slightly wider but still perpendicular to the background flow. Hence anisotropy was included in the numerical model to calibrate it with the physical setup. This improved the results and the simulated flow paths closely resembled the tracer tests in the container.

At this point the nano-iron of FZK was injected. The result though was far from expected. The spreading of the nano-iron was limited to a small area around the injection well. For the same conditions the conservative tracer reached in the same injection time the extraction wells. A spreading perpendicular to the background flow was at least expected for the nano-iron. From these results it was concluded that the new and improved nano-iron of FZK still needs to be further improved to achieve the transport required in a field application. Most likely the individual particles had already created aggregates that were too big to be transported. This is likely because the nano-iron was delivered without any additives to prevent the particles from aggregation in degassed and deionized water. In the literature it can be found that surfactants can prevent a great part of this aggregation in the time between the production and application. Hence, it was decided to test a different nano-iron suspension formulation for the following experiments.

The same container setting was used, to test the nano-iron delivered by ALSTOM, which was the RNIP of Toda Kogyo. This suspension contained a surfactant. And the base concentration of the delivered suspension was much higher, 200 *g/l* for RNIP as compared to 10 *g/l* for the suspension of FZK. The suspension was diluted to 10 *g/l* with degassed tap water before the injection. The spreading of RNIP was better, but the extend was radial and not elliptical as expected from the flow paths in the container. However, the RNIP suspension did not reach the extraction wells, which would have been expected based on the set conditions.

The conditions were similar to those of the field test of ALSTOM, where a much better spreading was reported. The larger spreading in a field situation can be due to heterogeneities, resulting in preferential flow paths that transport the nano-iron further. They might as well be a misinterpretation of the

geophysical measurements. The RNIP used had probably, like the FZK particles, build aggregates that made the particles bigger and less suitable for transport. But also other mechanisms should have been at work, limiting the transport distance. With increasing distance from the well, the velocity decreases hyperbolically. The nano-iron moved in the first part of the injection but then stopped to propagate any further. Hence, it was expected that there is a minimum velocity below which the nano-iron particles no longer can be transported.

## 4.2 *Small Scale Experiments*

Several small experiments were performed to get a better understanding of the behaviour of nano-iron under different circumstances. The production and development of better nano-iron at FZK could not be accomplished during this project. The remaining nano-iron of FZK appeared to be less stable than RNIP. Due to aging the particles became too aggregated and the amount of nano-iron was not enough for the remaining experiments that were planned. RNIP could be delivered in larger amounts and the rest of the experiments were thus performed with RNIP. Because the nano-iron of FZK was not further developed, parts of the research planned for this project were not performed. The electrostatic stabilization, the effects of surfactants on the particles and the upscaling in the production are some of these.

### 4.2.1 *Minimum Velocity and Drag Force*

To find out if there is a minimum velocity at which nano-iron can be transported an experiment in a glass tube was performed. The velocity was constant through the length of the pipe. At very small velocities some transport was still visible, but the nano-iron was not kept in suspension too long. Even at a constant velocity within a glass tube there appeared to be a maximum transport distance. Most of the nano-iron was grouped in aggregates which increased the size and weight of the particle that needed to be transported. The aggregates were pulled to the bottom of the tube by the gravity and deposited. It was hardly possible to get it back into movement by increasing the flow velocity. Within the tube the flow field was parabolic, at the boundaries the velocity went to zero and in the center the velocity was twice the average velocity. This resulted in a very small drag force close to the boundaries and a large one in the center. The particles in the upper part would thus move vertically down and reach the higher velocity field which could keep them in suspension. At some velocities it was seen that in the upper part no particles were visibly moving, in the middle most were moving and in the bottom part a sedimentation bed was developing. With increasing distance from the inlet the amount of particles in suspension decreased and the visible particles appeared smaller. At the end of the tube a fine sedimentation bedding occurred that indicates that nano-iron was transported that far, but it was not seen in the tube as transported particles. Indicating that a small part of the particles was still very small and invisible for the bare eye. From this experiment it was concluded that gravity indeed plays a large role during the transport. The drag force should to be large enough to compensate for the gravity and keep the particles in suspension. In a porous media the gravity is not always perpendicular to the flow direction, which means that the gravity can improve or reduce the transport.

Without a determination of the particle size, it is impossible to calculate the forces acting on the

particles. The size of the individual particles at the moment of production is known to be approximately 60 nm. Calculating the sedimentation velocity of these particles, it should be almost impossible for them to settle when transported at the velocities used in the glass tube. Only a small portion of the particles close to the boundary of the glass will be transported with such a low velocity that they will settle. If it can be achieved that the particles are smaller, either the size as given by the producers (60 nm) or the favorable size for transport of 400 nm as given by Tratnyek and Johnson [2006], the gravity will play less of a role in the transport.

#### 4.2.2 Chemical Detection of Nano-Iron

To chemically determine the amount of nano-iron in a soil probe the iron in the probe needs to be dissolved with an acid. This procedure can not distinguish between natural iron and the added nano-iron. The concentration of iron in sand can highly fluctuate between two samples taken at the approximately same location. The small amount of nano-iron is thus hard to identify, because it is never known, if the increased amount of iron is due to the nano-iron or natural iron. This created a problem for the research on the transport of nano-iron in a column. First it was thought that a column can be parted and that for each part the iron content could be determined to create a nano-iron concentration distribution. The idea that this could be measured with a metal detector seemed promising. The simple metal detector that was build though was highly instable and the recorded signal drifted strong. Several producers of metal detectors were contacted to find a detector that was very stable and that from the producer was thought of to be suitable for this application. Most of the detectors can not distinguish the extremely low concentrations that were expected in the column experiments. Most of the metal detectors do not have the possibility to record the signal and often they filter out even a continuously changing background metal content. This filtering is very nice for a field situation finding single occurrences of metal in a changing background, but in the column a continuous changing of the concentration is exactly what is needed to be recorded. The metal detector of Institute Dr. Foerster finally was able to give an almost raw signal of the frequencies in the two coils. This signal could be recorded and a measurement before and after the injection of iron gave two datasets that could be subtracted from each other to discriminate the injected nano-iron from background changes.

#### 4.2.3 Disperged Nano-Iron

The use of a disperger to break up the aggregates of nano-iron particles showed improving results. The distance that the nano-iron could be transported in a glass pipe and a column was significantly larger after disperging the nano-iron suspension. The particle size was not determined, but based on the improved transport and reduced sedimentation velocities it could be concluded that they had to be smaller. Less aggregation of the particles was also observed in the glass tube. The disperged nano-iron suspension did look more flaky than the round particles of the original suspension. Most of the particles were well visible, thus the nano-size region was on average not yet reached by disperging the nano-iron. In the column experiment to compare the disperged nano-iron with the original suspension the front was much steeper for the disperged one. This speaks in favour of less gravitational settling. In this experiment a void space between the inlet and the filter caused a settling of nano-iron before entering

the filter. The velocity in the part is much lower and thus the drag force is smaller. In later experiments the inlet plugs were improved to minimize this void space. During the whole period of injection the disperger was turned on. This resulted in small air bubbles in the suspension, this air also entered the column and accumulated in the upper part of the column. Later it was found out that a short disperging was enough to break up the particles and that a continuous gentle stirring of the suspension would keep the particles from settling and creating new aggregates within the time needed for the injection.

Both the original and the disperged suspension were tested on the sedimentation velocity. The difference between both was large. The disperged particles settled almost 10 times slower. Comparing the curve of the disperged suspension with the findings of Saleh et al. [2006], it shows much resemblance. The sedimentation occurs in well distinguishable phases. First the sedimentation is slow, then the nano-iron settles relatively fast and in the last phase the remaining particles settle slowly. The increase in sedimentation is described by Saleh as a result of mainly magnetic attraction between the particles creating aggregates and gelating these aggregates together to form large structures of attached aggregates.

The disperger breaks up the aggregates into smaller pieces. To see if this influences the reactivity of the nano-iron to reduce PCE a batch experiment was done. The results showed that on the short term the disperged suspension was as effective as the original suspension. Next to the reduced concentration of PCE, byproducts were seen in the chemical analysis. For both suspensions different byproducts were seen. What these byproducts were, was not determined. The long time reactivity of a disperged suspension was not tested, this and the full analysis of the chemical reduction of PCE should be done before it is applied in the field. The break up of the aggregates could cause exposure of the bare zero-valent iron since the surrounding shield of magnetite might be broken. Then it would be expected that the suspension is more reactive and would reduce the PCE faster and that corrosion processes would be accelerated, but this was not seen in this batch experiment. It thus might be that only the aggregates are broken up and the nano-iron particles themselves are preserved, or still together but in smaller aggregates.

### 4.3 *The use of a Metal Detector for Nano-Iron detection*

The response of the metal detector of Institute Dr. Foerster to the occurrence of nano-iron was much better than expected in the beginning. A very clear signal was seen that indicated the presence of nano-iron. On the signal a noise was seen, but not so large that this influenced the detection of the nano-iron. Some of the recorded data was send to the Hydrodynamics Group of the University of Oldenburg to see if there is more information in the noise of the signal. It was thought of that a certain characteristic in the noise could be present to distinguish between nano-iron, natural occurring iron and metal objects. Also small drifts in the signal could perhaps be identifiably, removing these would then further improve the data. The results though showed that it was only a pure measure noise in which no characteristics could be seen. A drift that occurs in all measurements could also not be identified. Because the signal did not contain any further information, it was decided that the recorded signal could be averaged by a factor 10 to reduce the noise and data. Which made it easier to process and analyze the data.

After all experiments were done, it appeared that a calibration of the metal detector to the amount

of iron in the column could not be made from the measured data. A special calibration experiment was done to get a transfer factor from the recorded frequency response into iron amount per column length ( $g/mm$ ). The calibration of the metal detector was done by mixing each time 190 g of sand (representing a filling of 10 cm in the column) with a certain amount of dry metal dust (it was expected, that the water content in the column would not affect the metal detector signal). Between the metal containing parts pure sand was located. The metal detector already detects the metal before it was positioned exactly at the metal containing part. The measured curve was thus very smooth and the calibration might not be fully transferable to a situation where the content in the column changes gradually. Only the response between the beginning and the end of the metal containing part was taken into account for the calibration. This might be the reason that most of the measured values in the experiments were under-determined. Different calibration setups should perhaps been made to get a better approximation of the iron content in the column. The metal detector had a small drift in the first hour after starting the device. A warming up of the components was the main source of this drift. Because of this drift, the frequency response was set to zero at the start of each measurement. Also when at the start of the measurement the metal detector already was positioned above the nano-iron containing section of the column. This was at that time thought of to be a good approach, but it would have been better to either not change the output or perhaps even better to set the metal detector to zero on a fixed and known concentration before starting the measurement. Especially in the experiments where the whole column was filled with nano-iron, no zero iron value could be estimated in the recorded data. Most likely resulting in an underestimation of the nano-iron content. The determinations of the nano-iron content was in all cases within the same order of magnitude and less than a factor 4 from the injected amount. An improved calibration curve and a better starting value of the detector will probably produce even better determinations of the nano-iron content.

#### 4.4 Column Experiments

The 1-D experiments were performed in a horizontal column of 2 meter and a inner diameter of 3.6 centimeter. The idea was that the influence of gravitation was minimal in a horizontal orientation. In most of the experiments, especially with coarser grained fillings, there was still some influence of gravitation visible, resulting in a long stretched front. In the finer materials the front was sharper and more vertical. It would have been useful to have ran a few experiments during the final column experiments, with a top-to-bottom and bottom-to-top injection in a vertical column orientation. The time to do these experiments was though not available and the exact influence of the gravitation was thus not further quantified. In the preliminary research a horizontal column experiment was also performed, the large void space that was present before the filter of the column resulted in a settling of the colloids before entering the sand. The new in- and outlet plugs did not contain these void spaces. The injection could thus occur over the whole surface of the filter.

Several sets of experiments with each time one changing variable, were performed. In the experiments with different sand types there was though more than one variable changed. Not only the grain size also the grain size distribution and the pore connectivity changed. Since these experiments were the first 1-D experiments performed in this research, it was not yet known how long the injection should be continued

resulting in experiments that have different injection durations, which made it almost impossible to compare their results. To be able to really say something about the influence of the permeability of the porous media on the transport more experiments with equal injection durations should have been performed.

In the first experiments it also happened occasionally that the column bended through, resulting in large heterogeneities in the packing. Later the column was strengthened with two plastic plates, this made the column much better handleable and reduced the chance of introducing heterogeneities during the experiment. To keep the column straight, in the middle a pole held the column at height. During the measurement before and after injection the pole needed to be removed such that the metal detector can pass. This was done by placing a second pole just behind the metal detector and removing the one in front, letting the metal detector continue it's measurement of the column without interruption. A small vibration could in most cases not be prevented. In the recorded signal this resulted in a small fluctuation, but not significant in the cases where there was nano-iron present at this position. In the other cases where the nano-iron did not reach the middle of the column, this was also of less importance. Since this small fluctuation occurred in both the pre-measurement and the after-measurement, it could also be expected that they would extinct each other when the measurements were extracted from each other. This showed to work very well when the data were processed.

#### 4.4.1 Pump Location

In all runs except for one, the pump was positioned at the outlet of the column. This was done to minimize the distance between the nano-iron container and the inlet. A constant flux could be reached in almost all runs. Except for the 0 – 4.0 mm sand, where the permeability was too low for the higher discharges to be reached. Though the water used was degassed, this does not mean that all the oxygen is removed from the water, the pump at the outlet created a vacuum that further degassed the water in the column, and no continuous flow could be established. In the following run where even a higher velocity was wanted, the pump was placed at the inlet side and then this degassing problem did not exist and the flow could be kept constant. These high velocities would only be found in a 2-D or 3-D setup very close to a injection well.

#### 4.4.2 Theory and Practice

Since no experience for these experiments was present, the quality of experiments was improved as more experiments were done. This also resulted in a better comparison of the later experiments than the ones performed at the beginning (which were the experiments with different sand types). The problems in the first experiments took much time but also showed where the setup needed to be improved and how the measurements needed to be recorded. The experiments took more time than planned, during the development of the setup it was thought that two or even three experiments could be performed on one day. It showed very soon that this was not possible, and it took about two to three days to perform one experiment. The large amount of tests as thought of in the beginning (app. 50) was not possible within the maximum time available and needed to be reduced. In the end about 16 of the performed runs were

usable for comparison.

#### 4.4.3 Base-Case

It was planned to create one base-case to which all experiments could be compared. This was not possible with the small amount of runs. It was then decided that three sets of 4 to 5 runs were performed that could be compared with the others of this set. In one set the concentration of the injection was changed. In two other sets the pore velocity (by changing the discharge) in two different sand types was changed. As stated before, the comparison of the different sand types as planned was not really possible since most of these runs had more than one variable altered.

#### 4.4.4 Influence of Injection Concentration - About the Results

In the experiments where the concentration was altered, the retardation reduced with an increasing concentration. In the literature the system that retards the nano-iron described is a filtering. A filtering would increase the retardation with an increase of the concentration. It could be that this increase in retardation first occurs when the concentration is further increased. Then also the pressure should increase and the discharge should decrease. As long as the discharge can be kept constant and the nano-iron continues to move forward in the column, a filtering and complete pore-plugging can not be the main mechanism of retardation. The injected volume of suspension was kept constant in these runs, resulting in a difference of total mass of injected nano-iron. During each run it was observed that in the beginning a fast spreading occurred that stagnated and some time later continued. For each concentration there appeared to be some concentration in the column that was first to be reached before the front continued to move. Since this concentration in the column was different for each injected concentration, it could also be expected that filtering and pore-plugging is not the main cause for the retardation. The gravitational settling of the colloids might be the main reason.

#### 4.4.5 Stages of Movement - About the Results

In most of the experiments several phases of transport were observed during the injection. First the front moved quite fast and then stopped moving any further. Next the concentration in the occupied part was increasing until at some moment the front started moving again. This might have been the case in the 2-D experiments as well. There the injection though was stopped when no further propagation of the front was observed. It should be tested with this knowledge of transport-phases, if in a 2-D experiment the nano-iron will start propagating again after some time.

#### 4.4.6 Influence of Pore Velocity - About the Results

In both sand types the nano-iron flew through the whole length of the column at the highest velocity set. In the Dorsilit sand the measured concentration though showed a very smooth spreading whereas in the Rhine valley sand the concentration showed strong fluctuation. The packing in the Rhine valley sand might not have been very homogeneous, resulting in the strong fluctuations. For the fastest run in the Rhine valley sand the pump was placed at the inlet side of the column, whether this had a consequence

on the continuity of the injected concentration is unknown. The retardation in both the sand types was quite constant for both sand types. The 50% mass curve of the Dorsilit sand showed an increase for the middle flow velocities, but all the retardation factors were between 1 and 4. In comparison, the retardation factors for the different concentrations were between 1 and 30. These results thus showed that with an decreasing velocity the retardation stays the same.

Translated to a injection well, this means that the retardation based on the velocity does not change with an increasing distance from the well. It is still such that with an increasing distance from the well continuously nano-iron is left behind, resulting in a reduction of the concentration in the suspension at the front. Also the surface of the front increases in 2-D and 3-D situations, meaning that the total available nano-iron is continuously reduced per area. In the concentration experiments it was seen that a reduced concentration increased the retardation. The amount of nano-iron left behind in the suspension during an injection will then influence the retardation of the nano-iron with respect to the distance from the well.

Increasing the velocity further transformed the concentration curve from concave into convex. The front of the nano-iron in the column was thus getting sharper at higher velocities. At very high velocities, the maximum concentrations reached in the columns were not as high as those of the lower velocities. At these velocities the drag force on the colloids was larger than the gravity and friction force that would at lower velocities keep the colloids from moving and thus the high concentrations could not be reached. Which would be preferable when injecting nano-iron in most field situations. Since in the vicinity of a injection well the velocities will be relatively high, these results show that the accumulation of nano-iron in this area then might not be that large resulting in less reduction of the nano-iron concentration in the suspension.

#### 4.5 *Obstacle for Further Research?*

During the literature research a statement was found of Gillham and Burris [1992], which represents my own feeling at this moment toward the use of nano-iron in a remediation technique. The statement of them was presented as an obstacle to implementation of permeable in situ treatment walls for remediation of contaminated groundwater.

It is remarkable that after 15 years this statement still holds ground.

In general the results of field tests with nano-iron performed by the industry show good and promising results, whereas the results of most research institutes show that the method is far from field ready.

Gillham and Burris [1992]:

Through enthusiasm or motivated by profit, new technologies are commonly over-promoted, falling short of expectations when applied at contaminated sites. Pervasive scepticism is therefore a major cultural impediment to the early implementation of new technologies.

## 5. CONCLUSIONS

To test the applicability of reactive nano-iron for in-situ remediation several small scale experiments were performed. These included 2-D, 1-D and batch scale experiments. From these experiments it became clear that the injection of nano-iron in a porous medium is strongly retarded, and in the 2-D experiments appears to have a maximum transport distance. One main mechanism responsible for the poor inject-ability could not easily be pointed out.

Several mechanisms were thought of to be of possible influence and were further investigated. An experimental setup was constructed to test the influence of various factors on the transportability of nano-iron during the injection.

It could be shown that the transport was influenced by (I) the age of the nano-iron prior to injection, (II) the pore velocity, (III) the input concentration, (IV) the grain size, grain size distribution and the hydraulic permeability and (V) the heterogeneity of the porous media. Most of these could only be described qualitative or partly quantitative within this feasibility study. More research is needed to further quantify the results.

A new method to measure and visualize the concentration distribution of nano-iron in a column at high resolution (mm-scale) was developed. This new method based on a metal detector originally designed for mine detection, has given good results and made it possible to get a real-time and non-destructive measurement of the distribution of nano-iron injected in a column.

Qualitatively it can be concluded that: (I) The age of the suspension influences the size of aggregations, for old suspensions the individual particles are no longer of nano-size. Larger particles result in larger retardation and faster sedimentation during the injection. Partly this process of aggregation can be reversed by application of high shear force on the suspension with a disperger device. The long time stability and chemical behaviour of this alteration needs further research. The behaviour of the disperged nano-iron suspension was in close comparison with the described behaviour by the supplier for a fresh suspension, and greatly improves the transportability. (II) Gravitational settling is a major mechanism acting on the particles due to their high density. An increase in the pore velocity changes the drag force (in horizontal flow acting perpendicular to gravitation) and will keep the particles longer in suspension. With a higher level of agglomeration of the particles, the influence of the gravitation increases. (III) Higher input concentrations showed a greater transport distance. When there are more particles, also more real nano-sized particles are available, which can travel much further. The total amount of nano-iron needed for the injection is then also increased, which is a less favorable situation. Based on a possible constant flux through the column, during and after injection of nano-iron, and a continuous propagating nano-iron front, pore-plugging is assumed to be of minor importance. (IV) The mobility of nano-iron is dependent on the pore-sizes and pore-connectivity. In a large grained sand packing with a large hydraulic conductivity the nano-iron can move freely through the column after

the injection stopped. In contrast, in a sand packing with a low hydraulic conductivity (e.g. due to a large particle size distribution or a small grain size) the spreading is strongly retarded, and the nano-iron almost can not be moved after injection, not even when the column is flushed with fresh water at higher velocities. (V) A negative effect of heterogeneities is that strong fluctuations of the concentration can occur and that in low permeable areas the nano-iron can be absent. Heterogeneities can also have a positive effect on the transport distance. In larger pores the transport is less retarded, thus the nano-iron will be transported further.

From this research it has become clear that there are many factors that can prevent the use of nano-iron for in-situ remediation to be successful. At this moment it is not yet possible to determine the extend of nano-iron injected in the subsurface. A well known injection extend is necessary for success of the technique. Because the transport is influenced by many factors, which could not yet be quantified, the extend can not be calculated or approximated a priori. Due to the absence of trustful methods to determine the presence of nano-iron in the subsurface of a field situation, the extend also can not be determined a posteriori. The developed measure technique in this research can not yet determine the extend in a field situation, but already works very well in a 1-D experiment.

## 6. OUTLOOK

This feasibility study shows a strong need for further research to make the remediation with nano-iron possible and predictable. Listed below are the main topics that need further research.

- Long term (several years) reactivity test of the nano-iron, with both fresh original and aged dispersed suspensions
- Continuation of the 1-D transport experiments to quantify the effects, with a factorial designed planning
- Upscaling of the transport experiments to 2-D and 3-D
- The measure technique will have to be further developed to make it suitable for a large scale experiment and field applications
- Development of a mathematical model and implementation in a flow and transport model
- Chemical behaviour of the colloids in an aquifer (e.g. side reaction, occurrence of unwanted by-products)
- Influence of the groundwater chemistry on the colloid behaviour in an aquifer
- Physical-chemical modifications toward mobility
- Economical feasibility (which was not performed within the presented research)

For a real comparison of all experiments, all should be based upon the one base-case. Each run should if possible have only one variable changed. In some cases this will not be possible and factor analysis should make it possible to find the relations. Ways to improve the results of the experiments and better compare them with each other can be:

- Run the transport experiments with an equal total suspension volume or total nano-iron mass, instead of a equal injection duration
- Test more different sand types, also the much finer materials with lower hydraulic conductivities
- Run the experiments in glass pebbles of different sizes to get to the basic factors influencing the transport
- A good quantitative description can only be given when more runs are performed
- Speed up of the measurements in order to be able to get a real-time analysis
- Measurements of the nano-iron distribution during the injection will help to create a detailed description of the transport behaviour
- Particle size analysis of the dispersed nano-iron, to be able to compare the results with other experiments

With the quantification of the influences of the different mechanisms acting on the nano-iron during injection, it will be possible to create a mathematical model to describe the transport (e.g. as done by

Al-Abduwani et al. [2005]). This model can then be implemented in an existing flow- and transport model for porous media (e.g. MUFTE [Helmig et al., 1998]). Giving the possibility to calculate the injection extend a priori.

It is expected that the measuring technique can be adapted for a 3-dimensional situation. This way a reliable method can be developed to visualize the extend of nano-iron during and after the injection. From the measurements after the injection it should be possible to decide when or whether a next injection of nano-iron is necessary.

The presented experiment set-up can be used to test the transport behaviour in location specific sand, e.g. obtained from probe cores. The obtained data from the experiments can then be used to calibrate the computer model for the field situation. As well different types of nano-iron or alterations (e.g. comparing several surfactants) can be tested in a controlled setting.

Focus of this project has been on the use of nano-iron for plume remediation by creating an in-situ reactive barrier. Early in the project it became clear that the delivery of nano-iron at a specific location is difficult. From a chemical point of view, at least as much nano-iron as contaminants (i.e. chlorinated hydro compounds) in weight is needed to fully remediate them. If a part of the nano-iron is consumed by other materials (which is often the case in a field situation), there even needs to be a larger amount of nano-iron injected.

In a source zone with pure phase present, it is unlikely that this amount of nano-iron can be injected, resulting in an incomplete remediation. Either by an incomplete chemical reduction, or by remediating only a part of the contamination.

In a plume remediation, the concentration of nano-iron in the subsurface needs to be much lower. A demand for success in a plume remediation is that the injection extend is large and a closed barrier is constructed. Also the barrier should not have a significant change in the permeability, otherwise the plume will find a way around the barrier. For a field situation a larger injection extend results in less injection wells, which is economically preferable.

At the required concentrations for a typical plume remediation no significant changes in the permeability are observed in the experiments.

From the presented results it can not be determined whether the injection of lower concentration will be able to reach the distances in a porous media which are needed to create a reactive barrier. In future research the use of nano-iron for source or plume remediation should be investigated.

In several field tests the transport distance of the nano-iron is determined solely by the reduced concentration of the contaminants in observation wells. Dilution effects are often not noted or seen of less importance in the reports. Though large amounts of fresh water are injected in order to get the nano-iron in place. Which will dilute the concentration in the direct surrounding of the injection well significantly. After the injection, this low concentration plume will flow with the groundwater flow downstream. The developed method to measure the concentration of nano-iron in a column might be able to identify the nano-iron in a field situation as well. Therefore it will have to be adapted to a 3-dimensional system. It is expected that this will be possible. With detection probes installed in wells around the injection wells a visualisation of the nano-iron in the subsurface is expected to be possible. Natural occurring metal in the subsurface is expected to be of no large influence, since difference

---

calculations can be made from measurements before, during and after the injection. A high content of metal in the subsurface might though reduce the accuracy. On a larger time-scale it is expected to be able to provide information about the amount of reactive nano-iron left in the target zone. Giving the possibility to decide when a next injection of nano-iron is necessary.

Throughout the preliminary researches a better understanding of the behaviour of nano-iron was developed. Based on this, it can now be expected that the performed 2-D experiments, will give better results when the used nano-iron is dispersed and the duration of the injection, and with that the volume of the suspension, is increased.

Pore-plugging was not observed in this research. There might have been some pore-plugging, but water transport through the column was possible in all cases. A determination of the permeability after the injection should be able to indicate the level of pore-plugging. A pressure measurement at the inlet and outlet during the injection should also give information about possible pore-plugging.

## 7. ACKNOWLEDGEMENTS

Nano-iron showed to be a fascinating material, that more than once did not behave as was expected. This made it difficult but above all challenging to work with it. It also created the need for much in-detail research of different aspects that were unplanned for this project. In total more time than planned was used for the project, which though created the possibility to get more information from the experiments and gave the time to work around and interpret the results.

I would like to thank all who helped me with my experiments, the process of writing, the German language and all those other things that were so important for me and my work in the past year in Stuttgart. They know my gratitude and should read their names in this acknowledgement.

The funding for this research was provided through "Baden-Württemberg Programms Lebensgrundlage Umwelt und ihre Sicherung (BWPLUS)" under the project number "BWR25001"

## BIBLIOGRAPHY

- F.A.H. Al-Abduwani, P. Bedrikovetsky, R. Farajzadeh, W.M.G.T. van den Broek, and P.K. Currie. External filter cake erosion: Mathematical model and experimental study. In *SPE 6th European Formation Damage Conference*, SPE 94635. Society of Petroleum Engineers Inc., Scheveningen, The Netherlands, 25-27 May 2005.
- G. Bartzas, K. Komnitsas, and I. Paspaliaris. Laboratory evaluation of  $fe^0$  barriers to treat acidic leachates. *Minerals Engineering*, 19:505–514, 2006.
- F. Böttcher, J. Peinke, and M. Siefert. A generalized method to distinguish between dynamical and measurement noise in complex dynamical systems. *unknown*, 2005.
- Bruining, H. personal communication, April, 2006.
- K.J. Cantrell and D.I. Kaplan. Zero-Valent Iron Colloid Emplacement in Sand Columns. *Journal of environmental engineering*, may:499–505, 1997.
- Y.A. Çengel and J.M. Cimbala. *Fluid Mechanics, Fundamentals and Applications*. Graw-Hill, New York, 2006.
- W.-H. Chiang and W. Kinzelbach. *Processing Modflow (PM), Pre- and postprocessors for the simulation of flow and contaminant transport in groundwater system with MODFLOW, MODPATH and MT3D*. Scientific Software Group, Washington, DC, 1993.
- P. D'Andrea, K.C.K. Lai, P. Kjeldsen, and I.M.C. Lo. Effect of groundwater inorganics on the reductive dechlorination of TCE by zero-valent iron. *Water, Air and Soil Pollution*, 162:401–420, 2005.
- H. Darcy. *Les Fontaines Publiques de la Ville de Dijon*, 1856.
- D.S. Dunford and S.A. Lorentz. *Tests of hydraulic and leaching properties of the vadose zone and groundwater*. Department of Agricultural and Chemical Engineering, 1994. Laboratory Manual.
- D.W. Elliott and W-X. Zhang. Field assessment of nanoscale bimetallic particles for groundwater treatment. *Environ. Sci. Technol.*, 35:4922–4926, 2001.
- EPA. *Guidance Manual, Turbidity Provisions, Chapter 8*. EPA, 1999.
- C.W. Fetter. *Contaminant Hydrogeology, Second Edition*. Prentice Hall, NJ, 1999.
- A. Gavaskar, L. Tata, and W. Condit. Nanoscale zero-valent iron technologies for source remediation, cost and performance report, 2005.

- R.W. Gillham and D.R. Burris. Recent developments in permeable in situ treatment walls for remediation of contaminated groundwater. In *Subsurface restoration conference, 3rd International conference on Ground Water Quality Research*, Dallas, Texas, 21-24 June 1992.
- R.W. Gillham and F. O'Hannesin. Metal-Catalysed Abiotic Degradation of Halogenated Organic Compounds. In *IAH Conference "Modern trends in Hydrogeology"*, Hamilton, Ontario, Canada, 10-13 May 1992.
- R. Glazier, R. Venkatakrishnan, F. Gheorghiu, L. Walata, R. Nash, and W-X. Zhang. Nanotechnology Takes Root. *Civil Engineering*, 73(5):64–67, 2003.
- R. Hahn. Personal Communication, Mai 2006. Landesanstalt für Umwelt, Messungen und Naturschutz Baden-Württemberg (LUBW).
- A.W. Harbaugh, E.R. Banta, M.C. Hill, and M.G. McDonald. MODFLOW-2000, the U.S. Geological Survey modular ground-water models. Open-File Report - U. S. Geological Survey, 2000.
- R. Helmig, H. Class, R. Huber, H. Sheta, R. Ewing, R. Hinkelmann, H. Jakobs, and P. Bastian. *Architecture of the Modular Program System MUFTE-UG for Simulating Multiphase Flow and Transport Processes in Heterogeneous Porous Media*, volume 2 of *Mathematische Geologie*. unknown, 1998.
- Y.H. Huang, T.C. Zhang, P.J.S. Shea, and S.D. Comfort. Effects of oxide coating and selected cations on nitrate reduction by iron metal. *Journal of Environmental Quality*, 32:1306–1315, 2003.
- Manual for MEGATRON MT 36-48, TB-Nr. 2005 10 17*. Kinematica AG., 2005.
- H.F. Lecoanet, J-Y Bottero, and M.R. Wiesner. Laboratory assessment of the mobility of nanomaterials in porous media. *Environ. Sci. Technol.*, 38:5164–5169, 2004.
- H-L. Lien and W-X. Zhang. Nanoscale iron particles for complete reduction of chlorinated ethenes. *Colloids and Surfaces*, 191:97–105, 2001.
- Y. Liu, S.A. Majetich, R.D. Tilton, D.S. Sholl, and G.V. Lowry. Tce dechlorination rates, pathways, and efficiency of nanoscale iron particles with different properties. *Environ. Sci. Technol.*, 39:1338–1345, 2005.
- C. Müller, E. Löbel, and P. Rissing. Sanierung mit Nano-Eisen - Stand der Technik. *Altlasten Spektrum*, 2:75–83, 2006a.
- C. Müller, P. Rissing, F. Widmayer, and M. Wischott. Nano-Eisen Feldversuch: Strategie, Durchführung, Ergebnisse und Auswertung. *Altlasten Spektrum*, 3:137–147, 2006b.
- J.T. Nurmi, P.G. Tratnyek, V. Srathy, D.R. Baer, J.E. Amonette, K Pecher, C. Wang, J.C. Linehan, D.W. Matson, R.L Penn, and M.D. Driessen. Characterization and properties of metallic iron nanoparticles: spectroscopy, electrochemistry, and kinetics. *Environ. Sci. Technol.*, 39:1221–1230, 2005.
- T. Phenrat, N. Saleh, K. Sirk, R. Tilton, and G. V. Lowry. Aggregation and Sedimentation of Aqueous Nanoiron Dispersions. *In press at Environ. Sci. Technol.*, June 2006.

- J. Quinn, C. Geiger, C. Clausen, et al. Field demonstration of DNAPL dehalogenation using emulsified zero-valent iron. *Environmental Science & Technology*, March 1(39):1309–1318, 2005.
- E. Ruzin. Reduktion organischer Schadstoffe in Grundwässern mit aquatischen  $Fe^0$ -Kolloiden. Master's thesis, Forschungszentrum Karlsruhe, Institut für Technische Chemie Bereich Wasser- und Geotechnologie, 2003.
- N. Saleh, K. Sirk, Y. Liu, T. Phenrat, B. Dufour, K. Matyjaszewski, R. Tilton, and G. V. Lowry. Surface Modifications Enhance Nanoiron Transport and DNAPL Targeting in Saturated Porous Media. *Environ. Eng. Sci.*, in press, 2006.
- B. Schrick, B.W. Hydutsky, J.L. Blough, and T.E. Mallouk. Delivery Vehicles for Zerovalent Metal Nanoparticles in Soil and Groundwater. *Chem. Mater.*, 16:2187–2193, 2004.
- F.W. Schwartz and H. Zhang. *Fundamentals of Ground Water*. John Wiley & Sons, Inc., New York, 2003.
- J. Solc. In situ site remediation, Integrated Environmental Services. handout - short course - University of Utrecht, 2006.
- P.G. Tratnyek and R.L. Johnson. Nanotechnologies for environmental cleanup. *nanotoday*, 1(2):44–48, 2006.
- C.-B. Wang and W.-X. Zhang. Synthesizing Nanoscale Iron Particles or Rapid and Complete Dechlorination of TCE and PCBs. *Environ. Sci. Technol.*, 31(7):2154–2156, 1997.
- Wikipedia. the free encyclopedia, jan. 2007. URL [http://en.wikipedia.org/wiki/Metal\\_Detector](http://en.wikipedia.org/wiki/Metal_Detector).
- W.X. Zhang. Nanoscale iron particles for environmental remediation: An overview. *Journal of Nanoparticle Research*, 5:323–332, 2003.

# APPENDIX

## A. COMMENTS ON 1-D TRANSPORT EXPERIMENTS

For each experiment a short summary is given, based on the comments noted down during the experiment and the presented measurements in section 3.3. The comments are given here and discussed.

The comments are not presented in a chronological order, but sorted by compared altered initial conditions. Changes made in the set-up during the experiments can sometimes be described for one experiment where in the next described experiment this change did not take place yet.

### *A.1 (A) Nano-iron Suspension Concentration - Dorsilit Sand*

- **# 1: 0.01 g/l**

The nano-iron suspension was prepared 3.5 hours before injection start, no visual change of the suspension could be seen at the start of the injection.

After 1 hour of injection, very little transport was visible. What was seen, was mainly in the upper part of the column.

After 2 hours the nano-iron was settling in the tubing between the reservoir and the column inlet. To reduce the chance that the iron was settling due to agglomeration in the reservoir, the nano-iron suspension was dispersed a second time. At 9 200 *rpm* for 5 minutes.

After 3.5 hours, the front of the nano-iron did not move for 0.5 hours. The concentration in the iron containing part did rise, based on the visually observed darkening of this part.

In the last hour of the experiment the main transport area was changed into the lower section of the column. The front was moving forward again, where the front was more vertical and covered the whole cross sectional area of the column.

#### *Discussion*

In a later experiment the mixer was modified to make sure that also the bottom portion of the suspension was mixed and preventing a higher concentration of nano-iron in the bottom part, from which the suspension was taken to inject. This way the nano-iron concentration was kept more stable during the injection. In research done by others sometimes the suspension was set to rest for a short period and the suspension used was from the upper part. Making sure that only the most stable particles were used for the injection (e.g. Phenrat et al. [2006]).

In most experiments performed in this research the nano-iron suspension was prepared shortly before the experiment was started. In a few experiments the suspension was more than a day old, which did show visual changes, e.g. brownish color of the suspension and nano-iron settled at the bottom of the container.

- **# 2: 0.10 g/l**

During the first 20 minutes a front was moving forward but then stopped moving further.

After 2 hours the front did not move any further, a more dense iron filling was building up.

The iron did not get much further in the whole experiment, but an almost vertical front was developed which was located approximately at the location of the front seen at 20 minutes after start.

After the measurement at 4 hours, the injection was continued for another 464 minutes. In this time the nano-iron front reached 30 *cm*, which was approximately 20 *cm* further. This result is shown in appendix figure B.1.

#### *Discussion*

In the four hours the column appeared to be filling with nano-iron until the position of the front from 20 minutes. In the 8 hours of continued injection after the measurement the front did get further. The concentration in the last 10 and 20 *cm* though was less. Some of the nano-iron was left behind in the first part and thus the amount of nano-iron available for the front was less. If the injection was continued for a longer period, the front did get further but would not be able to reach the same concentration as was reached in the first part.

- **# 3: 1.00 g/l**

The Uranine tracer test showed a higher velocity in the upper part of the column. In the middle of the column the velocity in the upper part increases and after 55 minutes the Uranine broke through at the outlet. The flow in the upper part was at that moment approximately 40 *cm* ahead of the Uranine in the lower part.

The column was re-compacted by placing it vertically on the shaker and tapping it with woodblocks (app. 2 *cm* further compacted). The new Uranine tracer test showed no preferential flow paths.

#### *Discussion*

The problems induced by inhomogeneities is described in section 3.3.11. In this experiment the second Uranine tracer test showed no significant high or low velocity regimes. In the curve no strong fluctuations were seen. Indicating that the re-compaction did not lead to unequal compaction.

- **# 4: 10.00 g/l**

In the first 60 minutes the propagation of the front was very fast. Then the propagation velocity decreased.

A large angle of the front was visible, with most iron and transport in the bottom part. The concentration decreased from bottom to top. The curve shows fluctuations in the concentration. The little peak in the concentration around 1700 *mm* was a response on moved iron left behind from the 1 *g/l* experiment which was performed previously in this column, using the other side

as inlet. The difference measurement removed most of this iron occurrence but some iron moved and thus resulted in a difference between the measurement before and after the injection.

After the measurement of iron content, the injection of the nano-iron was continued to see if the front would propagate further after a full stop. In total an extra 290 minutes continuous injection followed. The nano-iron front propagated further. Based on the extra 50 minutes the front should have moved 15 cm further, but moved in total 40 cm further. The large gradient was still visible in the front but over the whole length iron is present. The nano-iron concentration in the column was increased over the whole section where before the continued injection nano-iron was present. This result is shown in figure B.2.

### *Discussion*

As for the rest of the experiments also in this experiment the fastest spreading was in the first period. In this experiment some fluctuations were seen in the concentration in the column. Probably some inhomogeneities were present in this packing. This fluctuation was still present in the last measurement after 530 minutes. The larger change in the concentration appears to be in accordance with the location where the front in the first 60 minutes stagnated.

## A.2 (B) Pore Velocity - Dorsilit Sand

- **# 5:**  $1.3 \cdot 10^{-5} \text{ m/s}$

The nano-iron suspension was one day old, because of this the suspension was coloured dark brown, the Uranine tracer was not visible anymore. The water front was first only drawn on the column because the nano-iron was not visible, later in the photos with flashlight the nano-iron was visible, and was as with the other experiments, moving slower forward.

### *Discussion*

Due to the age of the suspension, it was dark brown. This was a result of oxidation products of nano-iron, giving dissolved iron. The visual observation of the transport did not tell much about the real concentration in the column, but was useful to identify the different transport phases and to get a rough impression of the concentration distribution. The measurement of the nano-iron content showed to be very useful in this case.

- **# 6:**  $2.7 \cdot 10^{-5} \text{ m/s}$

The mixer was modified with rubber plates that reach till the bottom of the container. Which made it also possible to mix smaller amounts of nano-iron suspension. For small velocities less suspension was needed and if a larger amount was prepared this would either become unusable or coloured dark brown, when used one or two days later for a next experiment.

The velocity was doubled, but the nano-iron was not transported twice as far.

### *Discussion*

The modified mixer was not only for smaller volumes of suspension more suitable, also in larger

volumes the iron particles would get less chance in the lower part to settle at a slower rotation. Reducing the chance of air bubbles mixed into the suspension.

- **# 4:**  $5.3 \cdot 10^{-5} \text{m/s}$

This experiment was included from the concentration dependent experiment, see for more details section 3.3.7 experiment 10 g/l.

The front was developing to a more convex curve, compared to the lower velocities.

#### *Discussion*

The fluctuations seen in the concentration curve were most likely be a result of inhomogeneities in the packing.

- **# 7:**  $1.1 \cdot 10^{-4} \text{m/s}$

A little metal tube clip was still on the tube at the outlet, a small increase in metal content in the last cm's was observed in the zero-iron measurement before the injection start. It was kept exactly there, such that with the difference measurement it would be removed. Which worked very well. The Uranine tracer was at 100 cm at 20 minutes, the Uranine breakthrough at the outlet was at 38 minutes.

At 195 minutes, a little stream of nano-iron reaches 100 cm, in the lower part of the pipe.

#### *Discussion*

After taking the difference of the two measurements, the metal clip indeed was no longer present in the curve. This showed again that the difference measurement is a powerful tool to visualize the change in iron content, even if there is a higher amount of iron already present before the injection.

- **# 8:**  $2.1 \cdot 10^{-4} \text{m/s}$

The column used was previously used for the  $2.7 \cdot 10^{-5} \text{m/s}$  experiment, with the other side as inlet side. Fast and wide spreading was observed. The iron was after 5 minutes at the position where at  $2.7 \cdot 10^{-5} \text{m/s}$  it needed 4 hours for. Though the velocity difference was a factor of 8. The spreading was much faster in the beginning, later the transport decreased in velocity.

The same large front tailing was visible as for  $2.7 \cdot 10^{-5} \text{m/s}$ , so also here a larger transport velocity in the lower part of the column was present.

At 80 minutes the first iron reached the tailing of the previous injection. The spreading was wider then expected and so the iron will partly add to the iron that was still there from the previous experiment. It was expected that this effect could be removed with the difference measurement.

The pre-injection measured data files were not exported correctly. This meant that no good difference measurement could be made. The second measurement of the previous experiment was used in reversed order. In that one there was more iron because partly this was pumped out during the flushing and hydraulic permeability measurement of the column before starting the injection at  $2.1 \cdot 10^{-4} \text{m/s}$ . At least the last 50 cm will be unreliable.

In the following experiments the recorded data will need to be checked after each measurement

to prevent the loss of data.

### *Discussion*

Because the data of the pre-injection measurement was lost, the exact amount of iron that left the system was difficult to determine. A chemical analysis of the effluent was done to determine its iron content. Unfortunately the iron got attached to the glass bottle in which it was collected. This iron could not be fully removed and the chemical analysis and the surfactants that were present in the nano-iron suspension complicated the measurement, resulting in unusable data. An other problem was that the chemical determination can not distinguish between dissolved  $Fe^{2+}$  or suspended  $Fe^{3+}$  and  $Fe^0$  nano-iron colloids.

If the effluent needs to be chemically analyzed a next time, the effluent must be conserved in a narrow-necked volumetric flask.

The measured and set total mass were due to this not presenting the same total mass (see table 3.7).

## A.3 (C) Pore Velocity - Rhine-Valley Sand

- **# 9:**  $1.3 \cdot 10^{-5} \text{m/s}$

A very narrow peak in the beginning is seen. Between 20 *cm* and 100 *cm* a really small amount is seen in the measured data.

### *Discussion*

In the measured data between 20 *cm* and 100 *cm* a low concentration of iron was seen. This was likely to be the result of a small amount of nano-iron that was more mobile and could be transported to greater distance. This low-concentration could not be seen by visual observation of the column.

- **# 10:**  $2.7 \cdot 10^{-5} \text{m/s}$

The first few mm's of the column at the inlet side contained more coarse grained sand, also a little coarser grain vertical layer was located at 14 *cm* from the inlet.

At 12 minutes the Uranine tracer was at 40 *cm*. After 30 minutes the tracer was at 75 *cm*.

At 145 minutes the average discharge was calculated based on the volume of effluent, this was 6.4 *ml/min*, the set discharge was 6.35 *ml/min*, thus the discharge was as set.

In the measured data some peaks are visible, they are mainly located at places where the column was coloured darker. This indicates small inhomogeneities that were not visible before the injection.

### *Discussion*

Because of the low permeability of the column, the discharge was checked to be sure that the set discharge was reached.

- **# 11:  $6.5 \cdot 10^{-5} \text{m/s}$**

In the first 4 minutes only transport in the lower part was seen. The rest of the columns cross section was in the following minutes occupied as well.

At 20 minutes the Uranine tracer was at 140 *cm*. The set flow velocity was incorrect by using two Tygoon WM229 tubes. At 32 minutes Uranine breakthrough was seen, which was slower than expected. The wanted velocity of  $1.1 \cdot 10^{-4} \text{m/s}$  was not reached.

Due to the much lower permeability of the column, the pump could probably not create the discharge as expected.

For these low permeabilities this would have to be measured before starting the injection of nano-iron. The pump curves (created without a low permeable column connected) used till now are not fully applicable in these sands. The determined velocity based on the breakthrough time of the Uranine tracer is:  $v = 6.5 \cdot 10^{-5}$ , instead of the wanted  $1.1 \cdot 10^{-4} \text{m/s}$

#### *Discussion*

In the following experiments performed the discharge was checked during the injection (as described for  $2.7 \cdot 10^{-5} \text{m/s}$ ). Since the reached velocity of  $6.5 \cdot 10^{-5} \text{m/s}$  was very close to  $5.3 \cdot 10^{-5} \text{m/s}$  no experiment at  $5.3 \cdot 10^{-5} \text{m/s}$  was performed. This creates an error in later comparison with experiments from other experiments, where the velocity was  $5.3 \cdot 10^{-5} \text{m/s}$ .

- **# 12:  $2.1 \cdot 10^{-4} \text{m/s}$**

The total volume of nano-iron suspension needed for this experiment could not be contained in the reservoir. At 80 minutes another 7 liters was added and dispersed at 8 500 *rpm* for 6 minutes. This large velocity can not be established with the pump connected at the outlet, the pump was thus placed between the reservoir and the inlet. After 4 minutes the Uranine tracer was at 90 *cm* and the nano-iron front was at 30 *cm*. At 8 min 45 sec the Uranine tracer breaks through at the outlet.

After 30 minutes the nano-iron front was at 100 *cm*, and broke through at 65 minutes at the outlet. The nano-iron was thus moved through the complete column.

#### *Discussion*

The water used was degassed, but still contained a small amount of gas which was withdrawn due to the vacuum created by the pump. An unknown part of the nano-iron left the system through the outlet, a sample was taken to determine chemically the concentration of the effluent. Due to the same reasons as described in the last experiment of Dorsilit sand ( $2.1 \cdot 10^{-4} \text{m/s}$ ), this determination failed.

This resulted in a large difference between the total injected mass and the measured mass, (76% difference) given in table 3.10.

#### A.4 (D) Grain Size Distribution / Hydraulic Conductivity - Different Sand Types

The comments are for each experiment given and discussed below. The three experiments with a  $\diamond$  refer to the corresponding data in tables 3.11, 3.12 & 3.1.

- **# 11: 0-4 mm Rhine-Valley**

This experiment is included from the velocity dependent experiment, see for more details section 3.3.8 experiment Rhine-Valley sand  $6.503 \cdot 10^{-5} m/s$ .

##### *Discussion*

The velocity was close to that of the other experiments, but not exactly the same. This makes the comparison not completely satisfied.

- **# 4: 0.3-0.8 mm Dorsilit**

This experiment is included from the concentration dependent experiment, see for more details section 3.3.7 experiment 10 g/l

##### *Discussion*

The transported distance in comparison to the 0–4 mm sand is almost the same. The retardation for both experiments differ approximately a factor two. Which will partly be a result of the small difference in the velocity.

- **# 13: 2-3.15 mm Dorsilit**

The prepared nano-iron suspension was two days old and because of this, the fluid was dark brown to black, the Uranine could not be seen clearly anymore. The transported distance of the nano-iron could only follow from the measurement afterwards. The brownish water broke through at 86 minutes. In total 2 pore volumes were injected in 170 minutes. The density of the effluent was 998 g/l so the colour was dark brown, but the density did not change. The brown colour was a result of oxidation products (dissolved iron) not of suspended nano-iron.

##### *Discussion*

The duration of this experiment was unequal to the above two. It is likely that the nano-iron would get further if the injection duration was 4 hours as well.

- **# 14: 3-5 mm Dorsilit**

The nano-iron suspension used was 17 days old. It had been dispersed every day for several minutes. The column was first flushed with fresh degassed water, the nano-iron suspension was dispersed again before injection. After the nano-iron injection stopped, the nano-iron settled in the column and could be moved through the column by rotating the column. After placing the column vertical, the nano-iron freely moved to the lowest point.

##### *Discussion*

The total duration of this experiment was 6 hours longer, making it impossible to compare the result with the other experiments. This experiment showed that with such large pores and high connectivity of the pores (large hydraulic conductivity), the nano-iron was highly mobile. This indicates that in a field situation where coarse material is dominant and a large hydraulic conductivity is present, the nano-iron will after the injection move vertically downward until it reaches a less permeable layer in the aquifer.

- **# 15: 0-4 mm Rhine-Valley**

Large preferential flow paths were present in the top part of column, the packing was changed due to bending of the pipe when the support pole in the middle fell away before injection. At the start of the injection air bubbles came inside, these were extracted with a syringe through the inlet side, this partly destroyed the pathways and nano-iron distribution in the column by doing so.

After 11 hours switched to fresh degassed water. At 110 *cm* there was a well developed front visible. After injecting fresh water, this did not move any further. In the first 100 *cm* mainly flow in top part was observed. In this part also vertical movement from top to bottom was visible, most likely gravitation induced. The vertical movement was not from the beginning visible, but started in a later stage. The fresh water injection was stopped at 26 *h*, total of 15 *h* water equals to 9.72 liters.

A large amount of gas was observed in the column in the two days after the injection had stopped, which was not there during the injection.

Some densities were measured during and after the experiment. The water that first came out of the column and where no nano-iron is visible had a density of 998 *g/l*. The water that contained nano-iron that has flown through the column has a density of 1000 *g/l*. The density of the fresh water that was drawn through the column after the nano-iron injection had a density of 998 *g/l*, which was the same as before entering the column.

### *Discussion*

The column used was not yet stabilized with the plastic plates on the sides, so a large preferential flow path was build in the upper part of the column after it bended through.

The gas in the column seen in the following two days could have been  $H_2$  gas, which is a product of the oxidation process of  $Fe^0$  with  $H_2O$ . It is though more likely that it was oxygen entering through a leaking valve, because this was observed in an other experiment as well. The vertical movement was not seen in the beginning, first the nano-iron was transported through the large pores and void space in the top part of the column. After a while this would settle and could then move vertically into the smaller pores of the rest of the column.

- **# 16: 0.6-1.2 mm Dorsilit**

Due to little amount of mixed suspension (1.5 *l*) the mixer could not mix it and thus the disperger needed to function as a mixer as well, this created tiny air bubbles in the suspension which entered and stayed in the column after injection.

In the last 7 minutes, air entered the column because the reservoir was empty.

In total one pore-volume was injected, so all the eluted water was from before the injection.

*Discussion*

The duration of the experiment was much shorter and thus it was not possible to use this experiment for comparison with the other experiments.

## B. EXTRA FIGURES

### B.1 Continued Injection of Experiment # 2

For experiment # 2, after the measurement at 4 hours, the injection was continued for another 464 minutes.

Over the whole distance where after the first injection nano-iron was positioned, the concentration was increased. In the second injection, the nano-iron front reached 30 cm, which was an increase of approximately 20 cm, showing approximately a linear relation between time and nano-iron front distance.

The corresponding information of this experiment can be found in section A.1 and section 3.3.7, the initial conditions for the experiment are given in table 3.1.

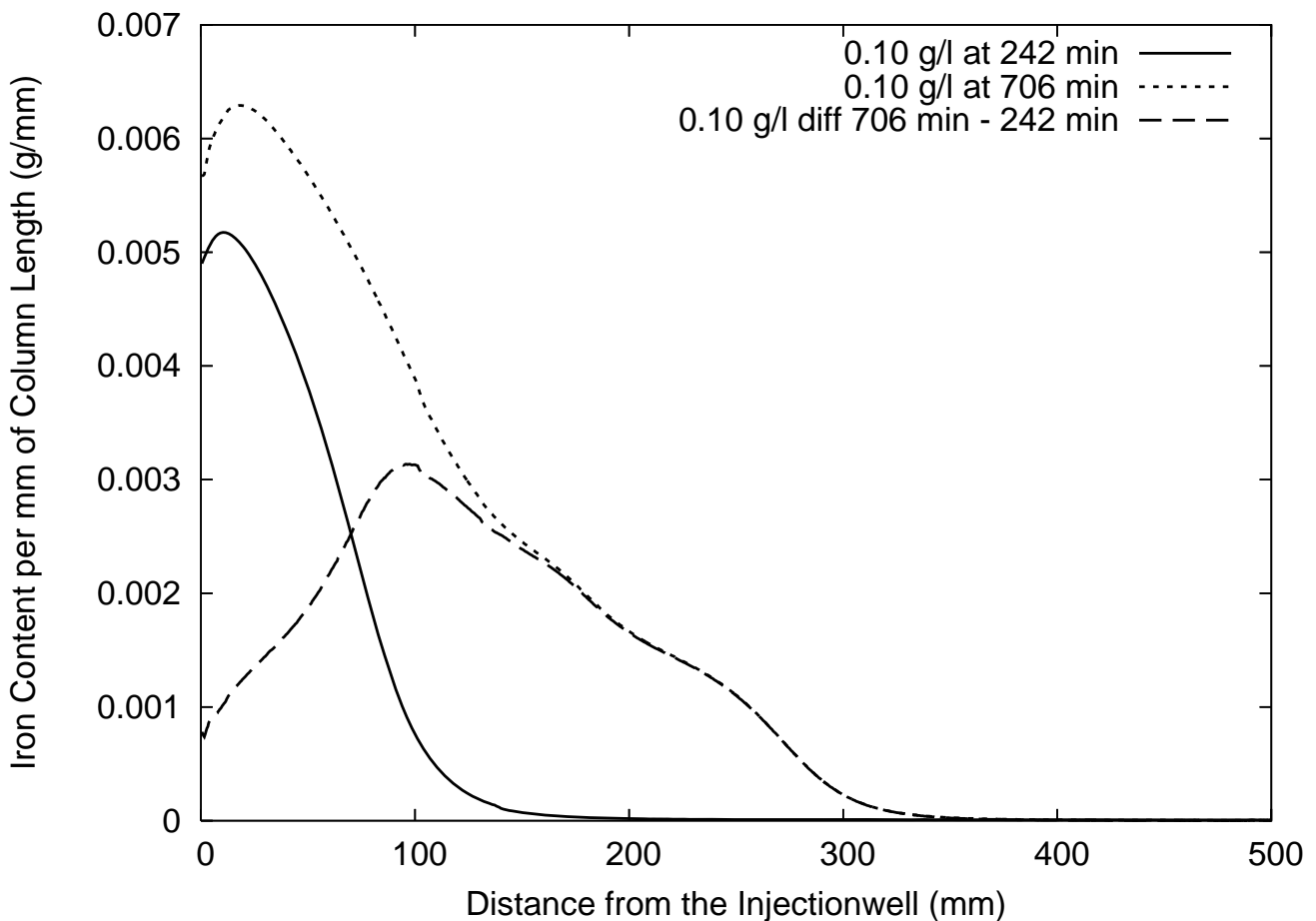


Fig. B.1: # 2: 0.1 g/l injection continued for an extra 464 min after 240 min. The plot shows only first 50 cm of the column, and the difference of both concentration distributions is also given.

### B.2 Continued Injection of Experiment # 4

For experiment # 4, after the measurement of iron content at 4 hours, the injection of the nano-iron was continued to see if the front would propagate further after a full stop. In total an extra 290 minutes continuous injection followed.

Over the whole length of the previously injected nano-iron the concentration was increased. As well the front of the nano-iron moved further forward.

The corresponding information of this experiment can be found in section 3.3.7 and section A.2, the initial conditions for this experiment are given in table 3.1.

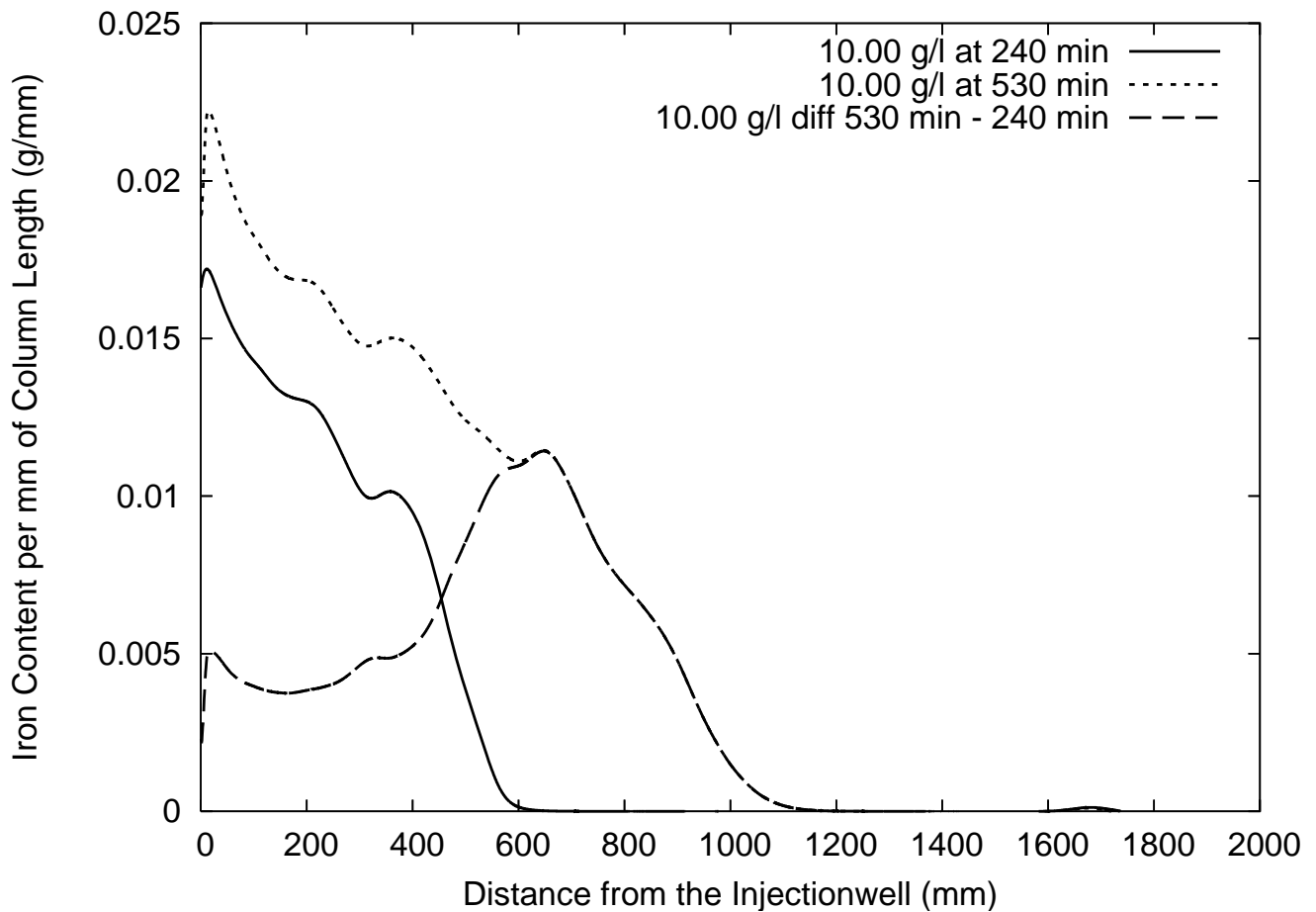


Fig. B.2: # 4: 10 g/l injection continued for 290 min. Both the 240 min and 530 min concentrations are given, the third curve shows the difference between both concentration distributions.

### B.3 Experiments with Errors - B # 8 & C # 12

Experiment # 8 was the fastest experiment and is not fully representable due to errors in the data recording and the loss of nano-iron due to a breakthrough at the outlet. The pre-injection measured data files were not exported correctly. This means that no good difference measurement could be made. The second measurement of the previous experiment performed in this column (experiment # 6) was used in reversed order. Between that recording and the start of experiment # 8 there was a difference in iron content, because partly the nano-iron of experiment # 6 was pumped out during the flushing and hydraulic permeability measurement of the column. At least the last 50 *cm* is be unreliable due to this.

Because the data of the pre-injection measurement in experiment # 8 was lost, the exact amount of iron that left the system was difficult to determine. A chemical analysis of the effluent was done to determine it's iron content. Unfortunately the iron got attached to the glass bottle in which it was collected. This iron could not be fully removed and the chemical analysis and the surfactants that were present in the nano-iron suspension complicated the measurement, resulting in unusable data. An other problem was that the chemical determination can not distinguish between dissolved  $Fe^{2+}$  or suspended  $Fe^{3+}$  and  $Fe^0$  nano-iron colloids.

If the effluent needs to be chemically analyzed a next time, the effluent could better be conserved in a narrow-necked volumetric flask.

The measured and set total mass were due to this not presenting the same total mass (table 3.7), resulting in a relatively large difference between the 'Measured' and 'Injected' total mass (difference of 67.5 *g*).

The characteristics and retardations of the two experiments given in table 3.6 (# 8) & 3.9 (# 12) are not graphically presented because they both have the same velocity and would mainly be overlapping each other.

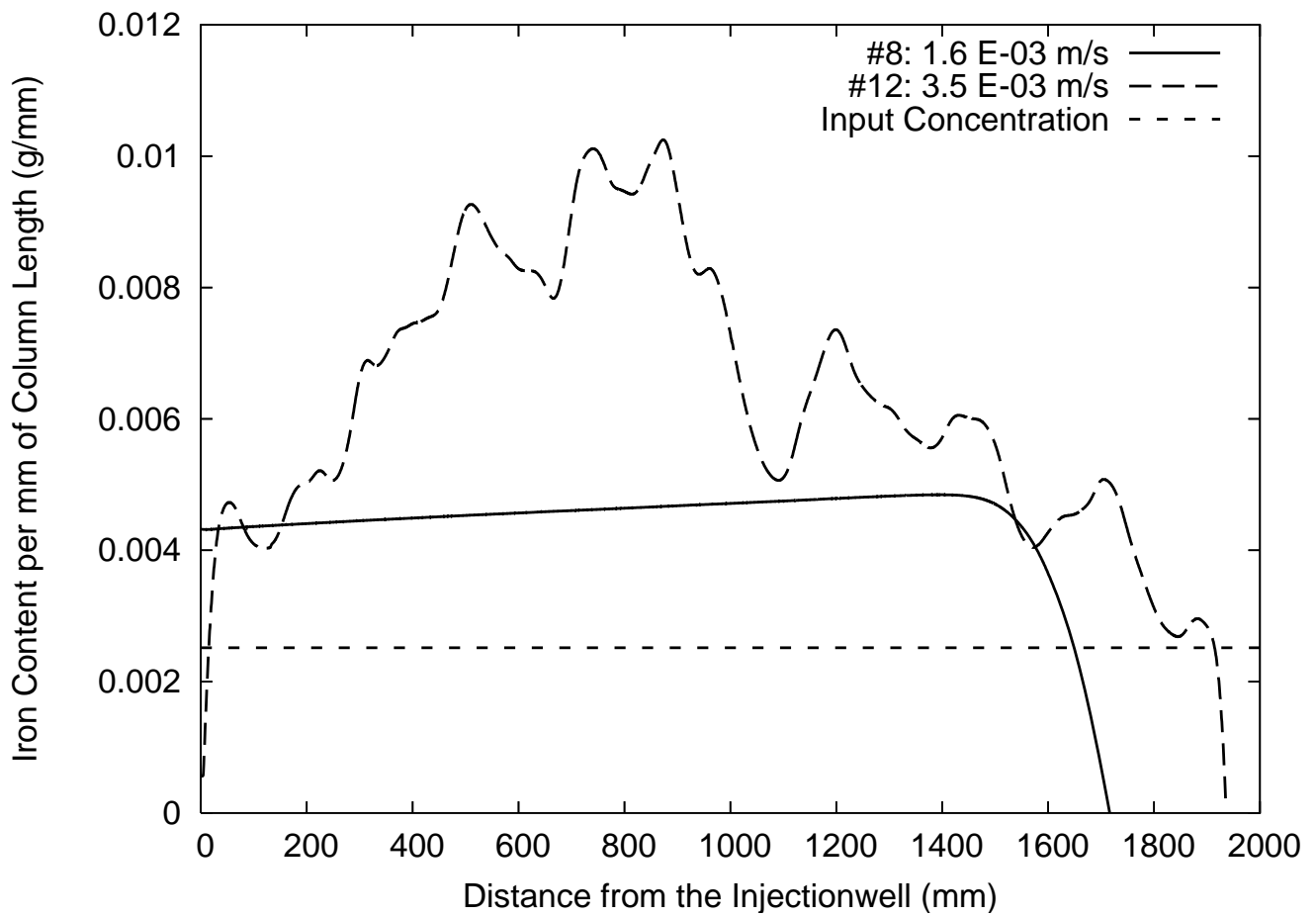


Fig. B.3: Nano-iron content per 1 mm of column length for different velocities in Rhine-Valley sand, 0-4 mm for the experiments with errors. Each curve represents the nano-iron content after 4 hours of injection. Explanation is given in section 3.3.4

B.4 Experiments with Errors - D #'s 14, 15 & 16

The corresponding information of this figure can be found in section A.4 and section 3.3.10, the initial conditions for this experiment are given in table 3.1.

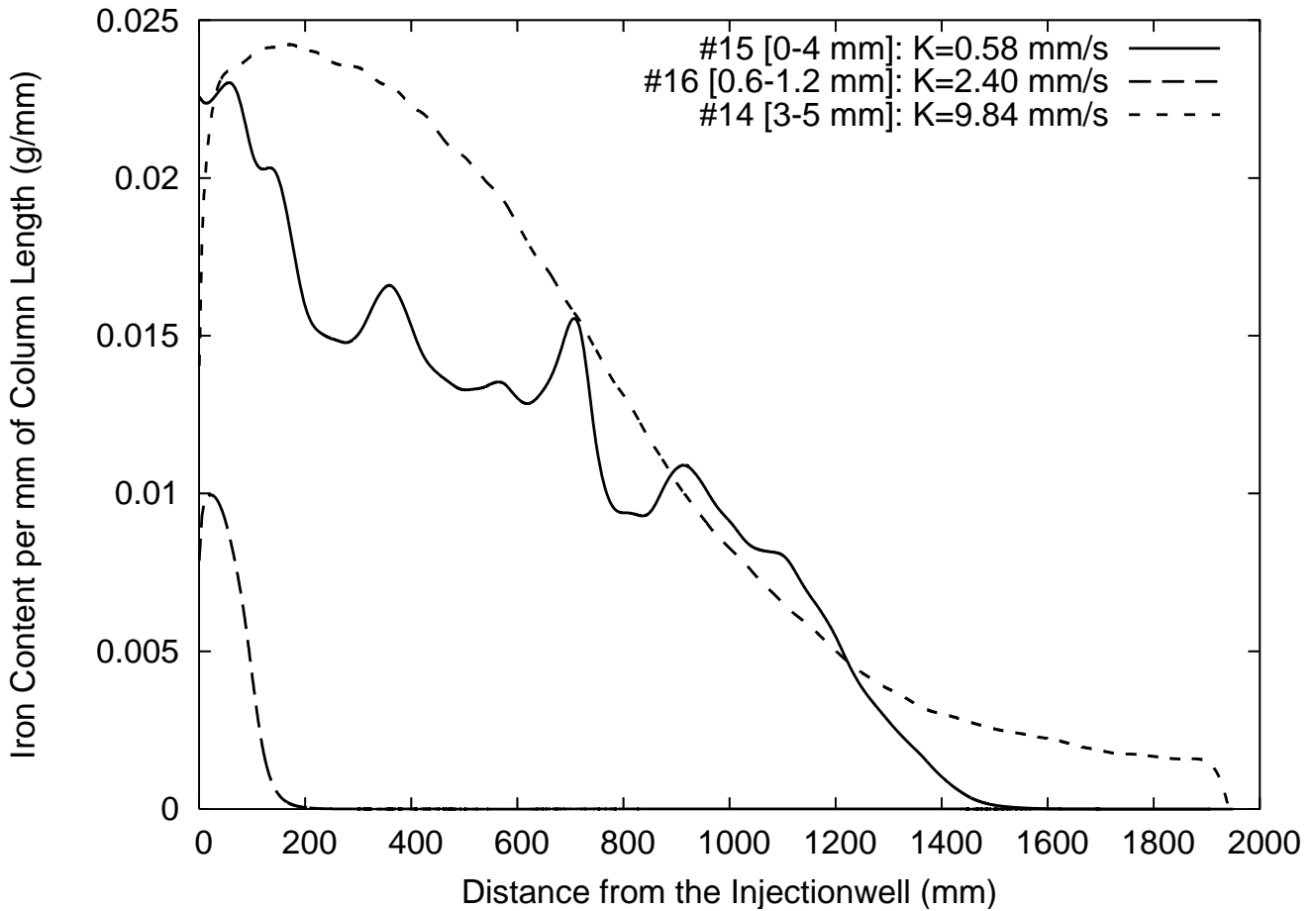


Fig. B.4: Nano-iron content per 1 mm of column length for sand types with different hydraulic conductivities for the experiments with errors. Each curve represents the nano-iron content after 4 hours of injection. Explanation is given in section 3.3.4

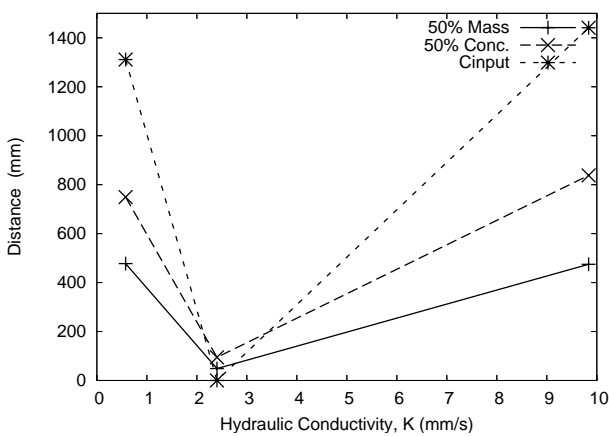


Fig. B.5: Transport distance characteristics (K=0.58mm/s: # 15; K=2.40mm/s: # 16; K=9.84mm/s: # 14). Explanation is given in section 3.3.5

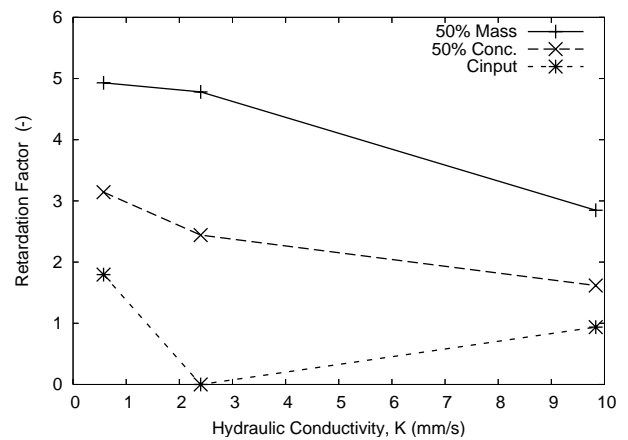


Fig. B.6: Relative transport distance for sand types with different K-values (K=0.58mm/s: # 15; K=2.40mm/s: # 16; K=9.84mm/s: # 14). Explanation is given in section 3.3.5

## C. SIGNAL PROCESSING CODE

```
// Used software: scilab-2.6 Copyright (C) 1989-2001 INRIA

// From the recorded data only the columns 'counter' and 'MEA_VAL_2' are
// used and exported to a ascii file.

// Within Scilab the following code is used:

clear;
chdir 'd:\datalocation';
A=read('datafile_sub1.dat',-1,2); //fill in name of first measurement
B=read('datafile_sub2.dat',-1,2); //fill in name of second measurement
Asize=size(A)
Bsize=size(B)

counter=A(:,1); //put 'counter' in a variable

plot2d(counter(1:length,1),A(1:length,2),style=2); //print A in blue, and B in red
plot2d(counter(1:length,1),B(1:length,2),style=5); //fill in length of A and B

A=A(start:end,2); //crop data as given in the base-case table
B=B(start:end,2);
Asize=size(A) //Print size of A and put into variable Asize
Bsize=size(B) //Print size of B and put into variable Bsize

//average over 10 points, the new data variables are C en D; Fill in A- & Bsize manual
a=0; b=0; g=0; D=[]; T=[]; m=0;
for i = 1:Asize, a=a+1; g=a/10;
    if g-int(g)==0
        then
            m=mean(T); C(g,1)=m; T=[]; b=0;
        else
            b=b+1; T(b)=A(i);
        end;
end;

a=0; b=0; g=0; D=[]; T=[]; m=0;
for i = 1:Bsize, a=a+1; g=a/10;
    if g-int(g)==0
        then
            m=mean(T); D(g,1)=m; T=[]; b=0;
        else b=b+1; T(b)=B(i);
    end;
end;
```

```

end;
end;

Cmin=min(C)           //Set lowest values of C and D to zero
Dmin=min(D)
C=C-Cmin;
D=D-Dmin;

Csize=size(C)        //Print size of C and D
Dsize=size(D)

plot2d(counter(1:Csize,1),C(1:Csize,1),style=2); //print A/C in blue, and B/D in red
plot2d(counter(1:Dsize,1),D(1:Dsize,1),style=5); //fill in length of Csize and Dsize

C=C(start:end,1); //The graphs can be slightly shifted
D=D(start:end,1); //Find a common point in the graphs, and calibrate on that

//Subtract C from D (after-before)
E=D(1:length,1)-C(1:length,1); //fill in shortest length, Csize or Dsize
Emin=min(E)
E=E-Emin; //If Emin is var below zero, then do not run this line
Esize=size(E) //Print size of E

plot2d(counter(1:Esize,1),E,style=1); //Print result in black, fill in Esize

// Gather all data in one variable
// A = sub1 cropped; B = sub2 cropped; C = sub1 averaged and min moved up to zero
// D = sub2 averaged and min moved up to zero; E = sub2 - sub1 (min moved up to zero)
Asize=size(A) //print all sizes, Esize can also be used for Csize and Dsize
Bsize=size(B)
Esize=size(E)

F=counter(:,1); //Put all data of variable 'counter' in the first column of F
F(1:length,2)=A(:,1); //Fill in all lengths manually
F(1:length,3)=B(:,1);
F(1:length,4)=C(1:length,1);
F(1:length,5)=D(1:length,1);
F(1:length,6)=E(1:length,1);
write('alldata.txt',F); //Print all data into a file; fill in a new name

//import data in excel or other data editor
//

```